Mechanisms Regulating Target Selection and Degradation by Selective Autophagy

Mechanisms Regulating Target Selection and Degradation by Selective Autophagy

A dissertation presented

by

Roarke Alexander Kamber

to

The Division of Medical Sciences

in partial fulfillment of the requirements

for the degree of

Doctor of Philosophy

in the subject of

Biological and Biomedical Sciences

Harvard University

Cambridge, Massachusetts

August 2016

Dissertation Advisor: Professor Vladimir Denic Roarke Alexander Kamber

Mechanisms Regulating Target Selection and Degradation by Selective Autophagy

Abstract

Selective autophagy eliminates protein aggregates, damaged organelles, and other targets that otherwise accumulate and cause disease. A class of proteins called autophagy receptors is known to select targets for degradation, but it has remained unclear 1) whether target recognition by autophagy receptors is mechanistically coupled with autophagy initiation and 2) how autophagy receptors select individual organelle targets.

We found that autophagy receptors activate the autophagy master kinase, Atg1, upon target detection. Specifically, we found that in nutrient-rich conditions, Atg1 is active only in a multisubunit complex comprising constitutive protein aggregates, their autophagy receptor, and a scaffold protein, Atg11. Development of a cell-free assay for Atg1-mediated phosphorylation enabled us to activate Atg1 with purified receptor-bound aggregates and Atg11. Another target, damaged peroxisomes, also activated Atg1 using Atg11 with a distinct receptor, Atg36. This work revealed a key piece of signaling logic: receptor-bound targets drive selective autophagy locally by activating Atg1, thereby coupling the rate of autophagy initiation with the rate of target appearance.

To understand how autophagy receptors are themselves regulated by phosphorylation to enable selection of individual targets, we studied Atg36 phosphoactivation by the cytosolic

kinase Hrr25, which is known to drive Atg36-Atg11 binding. Biochemical isolation of Atg36 in complex with its peroxisome anchor protein, Pex3, revealed that Pex3 and Atg36 exist in a multisubunit complex with the peroxisomal Pex1/6/15 AAA-ATPase complex, which had previously been shown to extract ubiquitinated Pex5 from the peroxisome membrane. We found that Pex5 is not involved in Atg36 regulation, whereas loss of Pex1/6/15 causes Atg36 to become constitutively active, suggesting the peroxisomal AAA-ATPase complex has a second function in pexophagy regulation. By retargeting these proteins to an orthologous cellular location, the mitochondrial outer membrane, we showed that Pex1/6/15 are sufficient to inhibit Atg36 independent of other peroxisome proteins. This work uncovered a novel mechanism by which an autophagy receptor is regulated by target-localized factors to enable organelle-specific autophagy decisions.

Table of contents

Dedication

For my grandmother

Acknowledgments

It would be impossible to adequately express my gratitude for Vlad's mentorship over the past six years. More than anything, I am grateful that Vlad has always taken a farsighted view of his students' maturation as scientists. Though I had no real experience in biochemistry, Vlad let me take the reins of a new research direction in his lab, giving me the freedom to choose my own projects and follow my interests. Throughout my time in his lab, Vlad has always seemed always to know the right type of guidance to provide. I feel very lucky to have been able to train under such a brilliant and kind scientist.

I am very thankful for the scientific guidance I've received from faculty members at Harvard, in particular the members of my dissertation advisory committee: Dr. Tom Rapoport, Dr. Tim Mitchison, and Dr. Andrew Murray. It was humbling to have the opportunity to regularly present my work to such brilliant scientists. Each meeting inspired me to think more deeply and critically about my work. I also want to thank Dr. Connie Cepko and Dr. Sheila Thomas for their mentorship and support at the beginning my graduate studies, when I was still deciding what to study during my PhD. I would like to express my gratitude to the members of my exam committee: Dr. Tobias Walther, Dr. Michael Laub, and Dr. Daniel Finley (who also provided useful early guidance as the chair of my qualifying exam committee). I am especially thankful to Dr. Thomas Bernhardt for being willing to step in as my exam chair and thus allow my defense to proceed as scheduled. Looking back further, I am forever grateful for the mentorship that my undergraduate advisor, Dr. Anne Brunet, provided throughout my time at Stanford and for her encouragement to pursue a scientific career.

It has been my great honor to work alongside many talented graduate students and post-docs during my time in the Denic Lab. In particular, Fei Wang has been an inspiration throughout my entire time in the lab. I have to thank Nick Weir not only for significantly improving lab morale but for single-handedly ensuring that expensive lab equipment did not fall apart, and thanklessly fixing it when it did. I am deeply indebted to Chris Shoemaker for invigorating my approach to science midway through my PhD and being an always reliable and cheerful benchmate and teammate as we pushed to the end of our paper. I also would like to thank the undergraduate, masters, and rotation students I have had the opportunity to work over the past few years, in particular Ben Phillips and Sarah Ward, whose excitement about science re-energized me at key points during my graduate work.

The last seven years would have been much less enjoyable without friendship. I'm particularly thankful to Andrew and Sebastian for persistently getting me to enjoy life outside the lab and that I could always count on Ania and Charlene keeping me company during the many late nights in lab.

The second half of my PhD was ultimately much happier than the first half, not just because things started to work in lab, but because I met Ritchie. I'm forever grateful for your patience and constant thoughtfulness, and for the joy and love you've brought into my life the last three years.

Finally, this wouldn't have been in any way possible without the love and support of my family.

List of Figures

List of Tables

Chapter 1: General Introduction

Attributions

RAK wrote the text with input from VD.

1.1 Summary

Quality control is a defining feature of living systems. Defective components are generated constantly in all cells, both through the introduction of errors during macromolecular synthesis and from damage sustained from environmental insults. Damaged components perturb homeostasis not only by failing to perform their functions but by interfering with other vital cellular activities. To survive these ongoing hazards, cells have evolved quality control mechanisms that detect and neutralize (i.e. repair, sequester, or destroy) damaged components. The quality control of proteins – the most diverse and abundant class of macromolecules – in eukaryotic cells (with their more complex proteomes and cytoplasmic organization) is effected by a particularly diverse set of mechanisms, ranging from basal folding assistance to adaptive transcriptional responses. Central to the effectiveness of the cell's protein quality control (PQC) arsenal are sophisticated regulatory mechanisms that ensure timely deployment of the proper response(s) capable of defusing a particular threat.

Here, we examine the regulation of selective autophagy, a quality control pathway conserved in all eukaryotes that enables elimination of wide variety of large cytotoxic subcellular structures. Because of this unique function, selective autophagy is critical for cellular homeostasis, particularly in non- and slowly-dividing cells (Komatsu et al., 2006; Mizushima et al., 2008). Despite increasing evidence over the past decade that selective autophagy is employed in a variety of cellular contexts to combat a diverse set of proteotoxic threats, our understanding of how selective is regulated remains rudimentary. Selective autophagy is thus often commonly described as a housekeeping function that proceeds at a "basal" rate in the absence of major stressors (Eisenberg-Lerner and Kimchi, 2009; Hara et al., 2006).

We begin by critically assessing our current knowledge of selective autophagy, focusing on what has been learned about two key signaling nodes implicated in autophagy regulation. We then outline two fundamental unresolved questions regarding the regulation of selective autophagy. In Chapters 2 and 3, we detail our experimental efforts to address these questions, and conclude in Chapter 4 with a discussion of the significance of our findings.

1.2 Selective autophagy overview

Cellular functions of autophagy

Autophagy[1] is required for survival of two types of stress: 1) nutrient limitation and 2) the presence of a large cytotoxic structure in the cytosol. These two types of stress are dealt with using two different types of autophagy: *Non-selective* autophagy allows survival of nutrient limitation by mediating the recycling of large portions of cytoplasm to sustain catabolism, whereas *selective* autophagy allows cellular survival upon appearance of internal cytotoxic structures – such as intracellular pathogens, damaged organelles, and protein aggregates – by sequestering them and targeting them to the lysosome. Selective autophagy is also used to remodel cells during developmental transitions (Novak et al., 2010; Al Rawi et al., 2011; Zhang et al., 2009) and to deliver structures to the vacuole for biosynthetic (Scott et al., 1997) purposes and for the mobilization of certain nutrient stores (Dowdle et al., 2014; Mancias et al., 2014; Singh et al., 2009). Though our interest here is in the regulation of selective autophagy, given

[1] The term "autophagy" comprises three processes that mediate protein transport to the lysosome: microautophagy (direct engulfment by the lysosome membrane), chaperone-mediated autophagy (transport of individual proteins across the lysosome membrane), and macroautophagy, which involves the enwrapment of portions of cytosol with autophagosomes and is the predominant mechanism of organelle degradation. In this thesis, we use the term "autophagy" to refer exclusively to "macroautophagy", as is typical in the field. Note that the multivesicular body pathway is not considered an autophagic pathway for historical reasons even though it mediates the delivery of cytosolic proteins to the vacuole for degradation.

that non-selective autophagy is mediated by largely the same protein machinery and is much better studied, we integrate knowledge of its regulation in our discussion below.

Mechanisms of autophagosome formation

The evolutionary innovation underlying both non-selective and selective autophagy is the formation of the autophagosome, a large (~1μm-diameter) double-membrane vesicle that enwraps portions of cytoplasm and mediates their transport to the lysosome (Baba et al., 1994). Unlike most other organelles, the autophagosome is not created via growth and division of pre-existing copies. It is instead constructed *de novo* via the re-shaping and assembly of multiple pre-existing membrane sources into a cup-shaped precursor structure (Mizushima et al., 2001) called a phagophore, which expands and ultimately fuses with itself to seal its contents (Figure 1.1) (Noda et al., 2009). The identities of the contributing membrane sources have been notoriously difficult to pinpoint (Hamasaki and Yoshimori, 2010; Juhasz and Neufeld, 2006; Tooze, 2013) but appear to minimally include fragments of the endoplasmic reticulum (Axe et al., 2008; Hayashi-Nishino et al., 2009) and a specialized class of small vesicles containing the transmembrane protein Atg9 (Yamamoto et al., 2012). The membrane remodeling events that drive autophagosome biogenesis are executed by a dedicated machinery of AuTophaGy-related (Atg) proteins in concert with several canonical membrane trafficking proteins, including several SNARE (Itakura et al., 2012; Nair et al., 2011) and tether protein (Lynch-Day et al., 2010; Takáts et al., 2014) complexes. By and large, the mechanisms by which these proteins re-shape membranes remain largely opaque, with our current knowledge reviewed extensively elsewhere (Noda and Inagaki, 2015). Though the molecular functions of most Atg proteins remain unclear, we know that most of the proteins that build autophagosomes are present in cells constitutively,

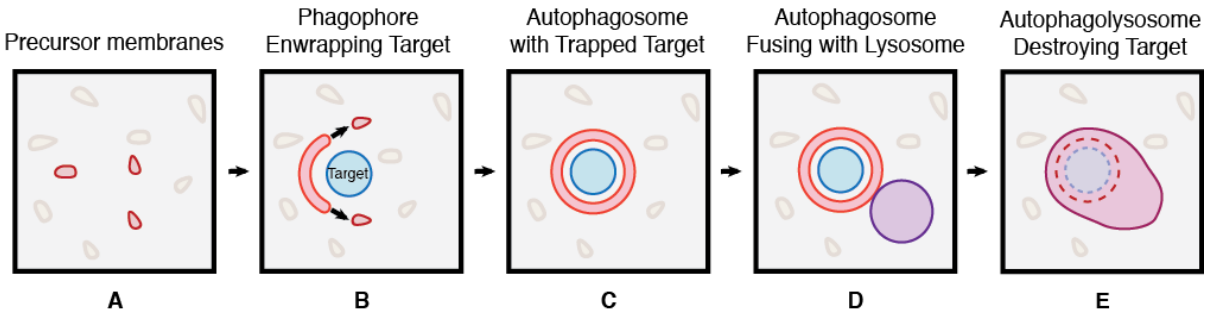

Figure 1.1. The Stages of Selective Autophagy.

(A) Precursor membranes (red), which may be derived from the endoplasmic reticulum and other sources, are present prior to the formation of the autophagosome. Other cellular membranes not relevant to autophagy are shown in beige in all panels.

(B) Autophagosome formation is initiated by the fusion of precursor membranes into a cup-shaped structure called a phagophore (red). The phagophore expands, closely enwrapping the target (blue), with additional lipids derived from further precursor membranes. (The autophagy receptor and Atg8 molecules that mediate this close enwrapment (Sawa-Makarska et al., 2015) are not shown).

(C) Autophagosome (red) formation is complete upon homotypic fusion of the edges of the phagophore to form a sealed sphere trapping the target (blue).

(D) Within minutes, the outer membrane of the autophagosome (red) fuses with the lysosome or vacuole (i.e. yeast lysosome) (purple).

(E) The outer membrane of the autophagosome becomes contiguous with the lysosome membrane, and the inner membrane of the autophagosome as well as the target are digested (indicated by dotted lines) by resident proteases and lipases.

but are inactive and diffusely cytosolic[2] until recruited to construct an autophagosome, at which point they localize (in yeast) to a perivacuolar domain called the pre-autophagosomal structure (PAS) (Suzuki et al., 2001). Approximately 20-60 copies of each Atg protein localize to the PAS (Geng et al., 2008), but are not triggered to begin constructing an autophagosome unless the Atg1 kinase is active (Cheong and Klionsky, 2008) (see below). Autophagosome formation takes approximately 10 minutes (Geng et al., 2008); upon completion of the final closure step some Atg proteins are released from the PAS (Mizushima et al., 2001) whereas others, including Atg1 (Kraft et al., 2012) and the autophagy receptors (Pankiv et al., 2007; Scott et al., 2001), are degraded upon fusion of the autophagosome with the vacuole.

1.3 Regulation of autophagy

Control points during autophagy

Our current understanding of how autophagy is regulated in response to cellular needs has largely been derived from the study of two signaling nodes: (1) the class of proteins called autophagy receptors and (2) the Atg1 kinase complex. The former governs decision-making about which cellular structures are degraded by autophagy, whereas the latter induces the initiation of autophagosomes and is thus capable of modulating the rate at which substrates can be degraded.

[2] Atg9 and certain SNARE proteins that contain transmembrane domains do not strictly exhibit a "diffuse cytosolic" localization. However, Atg9 is present in approximately 30 highly-mobile vesicles per yeast cell; approximately 3 localize to the PAS for each round of autophagosome formation (Yamamoto et al., 2012). At least one transmembrane SNARE, syntaxin-17, exists in a soluble form until recruited to closed autophagosomes to drive fusion with lysosomes (Itakura et al., 2012).

Autophagy receptors: regulation of target capture

Despite relying on the largely same protein machinery, selective and non-selective forms of autophagy are distinguished genetically by the unique dependence of the former on one or more autophagy receptor proteins. Autophagy receptor proteins connect target structures with the autophagosome membrane via their dual interactions with targets and with Atg8-family proteins (Rogov et al., 2014), which are covalently linked to autophagosomes (Ichimura et al., 2000; Kabeya, 2000). Autophagy receptors are defined primarily by this shared function and harbor little sequence or structural homology outside of short, linear Atg8-binding motifs (Noda et al., 2010a). In yeast, autophagy receptors also contain short, linear motifs that bind Atg11 (Farré et al., 2013), a factor required for all yeast selective autophagy events but dispensable for non-selective autophagy (Kim et al., 2001).[3]

How do autophagy receptors regulate target destruction? The current textbook model, largely derived from studies of a small number of mammalian target-receptor systems[4], posits that soluble autophagy receptors induce selective autophagy of their targets upon recruitment from the cytosol to the surface of target structures (Rogov et al., 2014; Stolz et al., 2014). In this scheme, receptors are selectively recruited to organelles that present molecular determinants that distinguish target from non-target structures; the most commonly proposed binding target determinant is ubiquitin (Khaminets et al., 2015; Kim et al., 2008; Kirkin et al., 2009; Lazarou et al., 2015).

[3] Though candidate Atg11 mammalian homologues have recently been proposed (Rui et al., 2015), none has been extensively functionally characterized.
[4] In particular those that control the degradation of depolarized mitochondria and bacterial pathogens.

Many autophagy receptors, however, are clearly not regulated at the level of subcellular localization. In fact, in yeast, most autophagy receptors contain transmembrane domains or are constitutively present on the surface of the structures they target for degradation (Table 1.1). In mammalian cells, several autophagy receptors contain transmembrane domains (Khaminets et al., 2015; Liu et al., 2012; Novak et al., 2010). How, then, is target degradation limited to the specific conditions when organelle turnover is desirable? Recent studies of the post-translational modifications of autophagy receptors suggest that the critical regulatory event for many receptors is phosphorylation by cytosolic kinases. In several cases, these phosphorylation events are tightly correlated with the induction of a target-specific selective autophagy signal (Aoki et al., 2011; Farré et al., 2008; Liu et al., 2012; Tanaka et al., 2014). The function of these phosphorylation events, in yeast, appears to be to promote binding between the receptor and the C-terminal domain of Atg11 and possibly with Atg8 (Farré et al., 2013; Tanaka et al., 2014). The mechanistic function of receptor-Atg11 interactions, however, despite being essential for selective autophagy and subject to regulation, remains unclear; their primary proposed function – tethering targets to the site of autophagosome formation – would seem be redundant with receptor-Atg8 interactions.

Atg1 kinase: regulation of autophagic flux

The Atg1 (ULK1 in humans) kinase is the most upstream identified factor involved in the construction of autophagosomes (Itakura and Mizushima, 2010; Suzuki et al., 2007), and is thus is a natural target for the regulation of autophagic flux. Indeed, during starvation, cessation of Tor signaling causes Atg1 to become highly active via a mechanism that involves the removal of several phosphates from the Atg1 binding partner Atg13 (Kamada et al., 2000). These

Table 1.1. Yeast Autophagy Receptors and Current Knowledge of their Regulation.

Receptor	Target	Constitutively at target?	Phospho-rylated?[3]	Binds Atg11?	References
Atg19	Ape1 aggregates[1]	Yes	Yes (Hrr25)	Yes	Scott et al., 2001 Shintani et al., 2002 Tanaka et al., 2015
Atg32	Mitochondria	Yes (TMD)[2]	Yes	Yes	Kanki et al., 2009 Okamoto et al., 2009 Farre et al., 2013
Atg34	Ams1 complex	Yes	Yes (Hrr25)	Yes	Watanabe et al., 2010 Mochida et al., 2014
Atg36	Peroxisomes	Yes	Yes (Hrr25)	Yes	Motley et al., 2012 Tanaka et al., 2015
Atg39	Peripheral ER	Yes (TMDs)[2]	Yes	Yes	Mochida et al., 2015
Atg40	Nuclear ER	Yes (TMDs)[2]	unknown	unknown[4]	Mochida et al., 2015
Cue5	Ubiquitinated protein aggregates	No	unknown	No[4]	Lu et al., 2014

[1] Ape1 aggregates comprise the vacuolar aminopeptidases Ape1 (which interacts directly with Atg19 via its propeptide), Ape4, Lap3 and Ams1, as well as Ty1 retrotransposon virus-like particles.
[2] TMD indicates the presence of a transmembrane domain.
[3] i.e. is known to be specifically phosphorylated under conditions that induce target degradation. If the kinase is known, it is indicated in parentheses. Note that Atg19 is constitutively phosphorylated by Hrr25 and mediates constitutive transport of Ape1 aggregates to the vacuole.
[4] "unknown" indicates the interaction has not yet been examined; "No" indicates that no interaction was detected by co-IP.

phosphates normally block association of the Atg1-Atg13 subcomplex with Atg17 (Kabeya et al., 2005). Upon binding to Atg1, Atg17, in complex with two other proteins, Atg29 and Atg31 (Kabeya et al., 2009), induces Atg1 autophosphorylation and activation (Yeh et al., 2010) via an unknown mechanism. Active Atg1 phosphorylates several other Atg proteins involved in building autophagosomes, including Atg6 and Atg9 (Papinski et al., 2014; Russell et al., 2013). Some light has recently been shed on the mechanisms by which these Atg1-mediated phosphorylation events drive autophagosome formation. Atg1 phosphorylation of Atg6 stimulates the phosphatidyl-inositol-3 kinase activity of its binding partner, Vps34 (Russell et al., 2013); the ensuing local synthesis of phosphatidyl-inositol-3-phosphate is proposed to recruit other Atg proteins (Noda et al., 2010b). The function of Atg9 phosphorylation is less clear, but appears to regulate the dynamics of Atg9 vesicle trafficking (Papinski et al., 2014).

Though Atg1 is particularly well-characterized for its ability to drive the formation of a large number of non-selective autophagosomes during starvation, Atg1 kinase activity is essential for all types of autophagy, including those forms of selective autophagy that occur in fed cells. Thus, paradoxically, Atg1 activity is required under conditions in which it has been observed to exhibit low or undetectable activity (Kamada et al., 2000; Yeh et al., 2010). A key question is whether this low Atg1 activity is representative of a low level of regulated activation – related to those selective autophagy events that occur during nutrient-rich conditions – or if Atg1 simply has a low, “basal” activity (Nagy et al., 2014; Rui et al., 2015) that drives the formation of a small number of selective autophagosomes.

Other potential control points

Though we have focused on how autophagy receptors and Atg1 kinase activity are used to regulate selective autophagy, other possible control points have been proposed. Chief among these is the lipid kinase complex mentioned above, comprising Vps34, Vps15, Atg14, and Atg6 (Itakura et al., 2010; Liang et al., 1999). Activation of this complex in mammalian cells has been proposed to be sufficient to drive autophagy (Shoji-Kawata et al., 2013) even in cells lacking a functional ULK1 kinase complex (Russell et al., 2013). These findings are inconsistent with a model that Atg1-mediated phosphorylation of multiple substrates (including Atg9) is critical for autophagy initiation (Papinski et al., 2014), and may indicate that the requirement for Atg1/ULK1 activation can be experimentally bypassed in certain contexts by direct activation of a subset of Atg effector proteins.

Transcriptional regulation of several Atg and lysosomal biogenesis genes has also been proposed to be important to sustain ongoing autophagy during starvation and other stresses (He and Klionsky, 2009). However, given that certain selective autophagy events have been shown to proceed normally even in the presence of cycloheximide (Abeliovich et al., 2003), post-translation regulation is likely to be pre-eminent in the regulation of selective autophagic flux and target selection.

1.4 Questions about autophagy regulation

In this thesis we aimed to discover novel mechanisms that regulate selective autophagy, which was previously known to be governed by only one passive regulatory mechanism: receptor-mediated tethering of targets to pre-existing phagophores. We describe below two questions about how autophagy might be regulated that initiated our investigations, and briefly summarize our experimental findings.

Is selective autophagosome formation regulated to match target abundance?

Unlike other PQC degradation pathways, such as the ubiquitin-proteasome and AAA-proteases, that re-use the same proteolytic machine to destroy numerous substrates, each round of autophagy-target destruction necessitates the degradation of thousands of Atg proteins upon fusion of the autophagosome with the lysosome. We hypothesized that the relative expense of this process argues for the existence of regulatory mechanisms that restrict the initiation of autophagosomes to the precise time and subcellular location at which they are needed.

In Chapter 2, we test this hypothesis, beginning our investigations with a study of the activity and physical interactions of Atg1 in the context of a model selective autophagy pathway. We find that Atg1 is tightly regulated by receptor-bound targets via direct physical interactions mediated by the scaffold protein Atg11. Via this mechanism, selective autophagosome formation is controlled in space and time to allow for rapid sequestration of detected targets. This mechanism also resolves the paradox described above regarding the role of Atg1 kinase activity in selective autophagy: receptor-bound targets overcome global inhibition of Atg1 activity in fed cells by locally activating a subset of Atg1 molecules at the site they are needed.

Is receptor phosphorylation used to regulate target selection?

The majority of PQC pathways discern properly folded and functional proteins from damaged proteins using a single distinguishing feature: the exposure of hydrophobic residues (Wickner et al., 1999). Organelle quality control potentially involves a much more complex decision, as a single organelle contains thousands of constituent molecules, each of which can become damaged; organelle "function" can likewise be perturbed in myriad ways, many of which might be reparable. Though it has been proposed that autophagy receptors make decisions about organelle quality by binding to molecular determinants of organelle damage, it remains unclear whether this model is plausible for the majority of autophagy receptors, which (at least in yeast) reside constitutively at the surface of their targets.

Autophagy receptor phosphorylation, which drives the degradation of certain targets, is a possible control point for the integration of local information about the functionality of a given organelle, though it has remained unclear how receptor phosphorylation might be regulated to serve this purpose. In Chapter 3, we scrutinize a model receptor phosphorylation event – activation of the peroxisome autophagy receptor, Atg36, by the cytosolic kinase Hrr25 – to identify mechanisms that control target degradation. We find that Atg36 forms a multimeric complex with its anchor Pex3 and with a peroxisomal AAA-ATPase comprising Pex1/6/15. We find that both of these binding partners regulate Atg36 activation: Pex3 promotes Atg36 phosphoactivation by Hrr25, whereas Pex1/6/15 constitutively inhibit Atg36 activation in the absence of pexophagy-inducing signals. As Pex1/6 are also used to surveil and extract ubiquitinated proteins from the peroxisome membrane, the mechanism we uncovered provides a

plausible explanation for how information about peroxisome protein quality is used to regulate peroxisome autophagy decisions.

Chapter 2: Receptor-Bound Targets of Selective Autophagy Use a Scaffold Protein to Activate the Atg1 Kinase

Attributions

RAK and Christopher Shoemaker contributed equally to this work; RAK, Christopher Shoemaker, and VD designed and analyzed the experiments. This work was published, under the same title: *Molecular Cell* 59.3 (2015): 372-381.

2.1 Introduction

Selective autophagy promotes the survival of non-dividing cells, such as neurons, by preventing the accumulation of cytotoxic structures (Hara et al., 2006; Komatsu et al., 2006). Targets of selective autophagy are first detected in the cytosol by receptor proteins (Behrends and Fulda, 2012). Once bound by receptors, targets are sequestered in autophagosomes, double-membrane vesicles that subsequently fuse with lysosomes resulting in target destruction. The vesicle membrane is the product of a cup-shaped, double-membrane that grows around receptor-bound targets until it fuses with itself. Each round of target elimination turns over an autophagosome precursor, but no mechanistic link connecting target detection with precursor biogenesis has been identified.

Though the primary described role of autophagy receptors is to bridge targets to autophagosome-tethered Atg8-family proteins (Ichimura et al., 2000; Rogov et al., 2014; Schreiber and Peter, 2014; Wild et al., 2011), autophagy receptors also bind Atg11-like proteins in both yeast (Yorimitsu and Klionsky, 2005) and higher organisms (Lin et al., 2013; Rui et al., 2015). The function of the interactions between autophagy receptors and Atg11 family proteins is unknown. Intriguingly, Atg11-like proteins also interact with the autophagy kinase (Atg1 in yeast (Yorimitsu and Klionsky, 2005) and ULK1/2 in metazoans (Hara et al., 2008; Rui et al., 2015)), which is required for both selective and non-selective forms of autophagy. Studies of non-selective autophagy in yeast have shown that nutrient depletion causes Atg1 autoactivation by a mechanism dependent on inhibition of Tor kinase signaling (Kamada et al., 2000; Stephan et al., 2009). Once Atg1 phosphorylates its activation loop it becomes catalytically active (Yeh et al., 2010) and able to drive formation of non-selective autophagosome membranes by mechanisms dependent on substrate phosphorylation (Papinski et al., 2014). This regulatory logic enables

coordination of nutrient deprivation with nutrient replenishment by cytoplasmic turnover. By contrast, the possibility that Atg1 kinase activity is also regulated in nourished cells to couple target detection with selective autophagosome formation has not been explored. We hypothesized that receptor-bound targets can activate Atg1 using Atg11 as a scaffold for signal transduction (Figure 2.1A).

2.2 Results

2.2.1 Atg11 bridges the Atg1-Atg13 subcomplex with Atg19-bound targets

The first key prediction of our hypothesis is that Atg11 scaffolds interactions between receptor-bound targets and Atg1. Budding yeast cells deliver newly-synthesized aminopeptidase precursor pApe1 to the vacuole (yeast lysosome) by a selective autophagy process that depends on the autophagy receptor Atg19, Atg11, Atg1, and Atg13 (an Atg1-binding protein required for Atg1 kinase activity) (Kamada et al., 2000; Kim et al., 2001; Scott et al., 2001). To detect any pApe1 interactions with Atg1, we affinity-purified FLAG-Atg1 from crude, detergent-solubilized extracts using anti-FLAG magnetic beads. Following elution with FLAG peptide, we analyzed the purified material by protein staining (Figure 2.1B), immunoblotting (Figures 2.1B and Figure A1.1A), and quantitative mass spectrometry (Figure A1.1B). pApe1 co-immunoprecipitated with wild-type Atg1, as well as with kinase-dead Atg1 (*kd*-Atg1; D211A mutant) and autoactivation-dead Atg1 (*ad*-Atg1; T226A) (Figure A1.1A), which is missing a critical phosphorylation site in the activation loop of the kinase domain (Lazarus et al., 2015; Yeh et al., 2010). In addition to pApe1, three other proteins were abundantly associated with Atg1: Atg13, Atg11, and Atg19. By purifying *kd*-Atg1 from cell extracts lacking individual Atg1-associated proteins, we made three

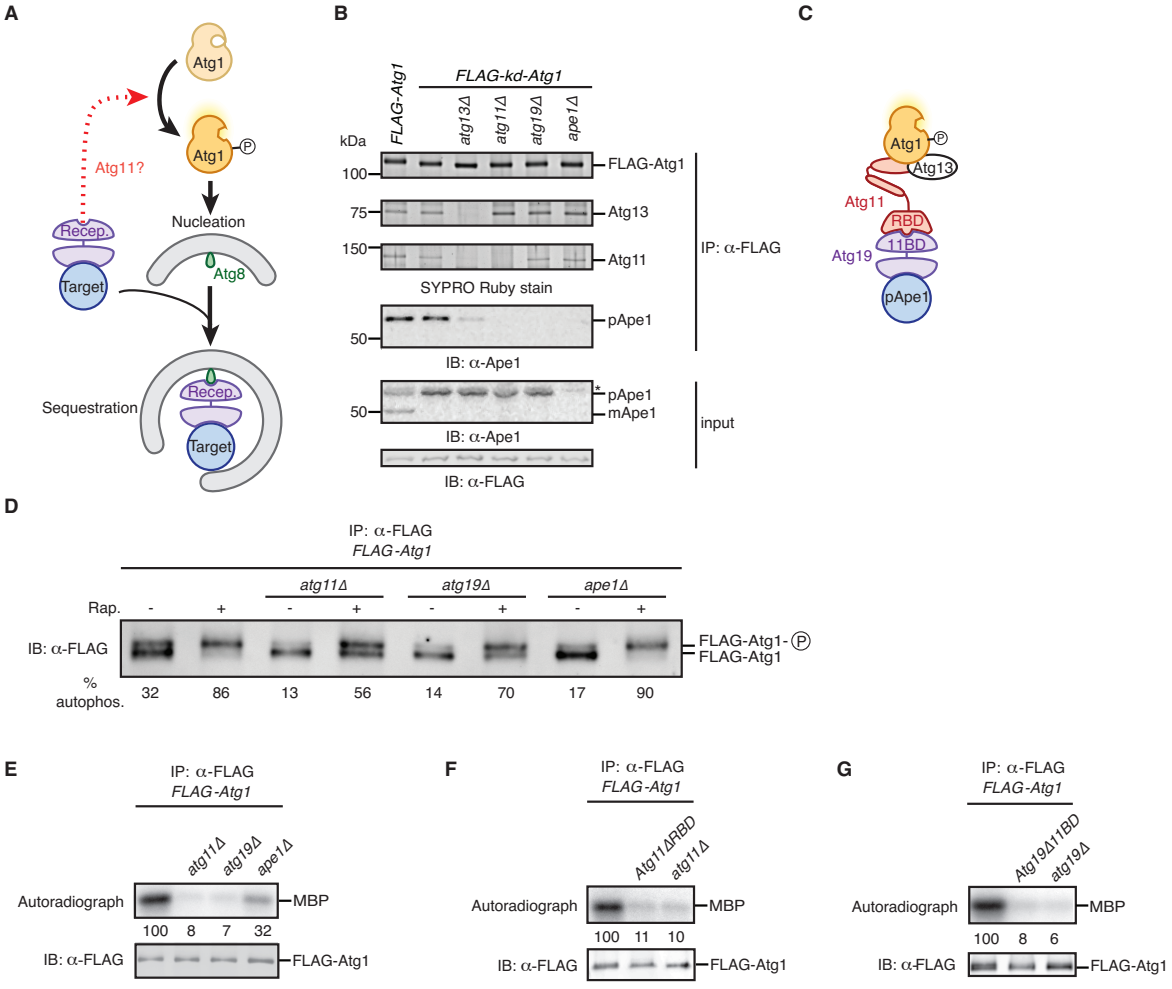

Figure 2.1. Identification of Ape1, Atg19, and Atg11 as Activators of Atg1 Kinase Activity

(A) Schematic depicting possible role (dotted red arrow) of receptor-bound targets in inducing autophagosome nucleation by converting Atg1 from an inactive state to an active, autophosphorylated state in an Atg11-dependent manner. Also indicated is the ability of targets to associate with autophagosome precursors via receptor-mediated interactions with Atg8 proteins. Recep., receptor.

(B) Extracts derived from logarithmically growing cells with indicated genotypes were immunoprecipitated (IP) with anti-FLAG magnetic beads. Eluates and extract (input) samples were resolved by SDS-PAGE followed by either SYPRO Ruby staining or immunoblotting (IB) with indicated antibodies. *kd,* kinase-dead allele; pApe1 and mApe1, precursor and mature (vacuolar) forms of Ape1; *, nonspecific band.

Figure 2.1 (Continued)

(C) Model of the subunit associations within the Atg1 complex based on data in (B) and Figure A1.1. Also indicated are the Atg11-binding domain (11BD) on Atg19 and the receptor-binding domain (RBD) on Atg11.

(D) Logarithmically growing cells with indicated genotypes were treated with rapamycin (Rap.) or mock treated prior to immunoprecipitation (IP) analysis as in (B), with one notable exception: SDS-PAGE was done for a longer time to resolve Atg1 from its autophosphorylated form (Atg1-P), as visualized by immunoblotting (IB). Autophosphorylation (% autophos.) was calculated as percent of total signal contributed by the upper band. See Figure A1.1E for statistical analysis.

(E–G) Extracts derived from logarithmically growing cells with indicated genotypes were immunoprecipitated (IP) as in (B) and then incubated with myelin basic protein (MBP) and ATPγ^{32}P. Kinase reactions were performed in triplicate (one of which is shown) and terminated with loading buffer prior to sample analysis by autoradiography and immunoblotting (IB). Signal from autoradiographs was quantified by densitometry and reported as the average of three reactions, in arbitrary units relative to the wild-type reaction set at 100. See Figure A1.1 for statistical analysis.

See also Figure A1.1.

observations arguing that Atg1 is part of a multi-subunit complex in which Atg11 bridges the core kinase subcomplex (comprising Atg1 and Atg13) with Atg19-bound pApe1 (Figure 2.1B; Figure A1.1B). First, in the absence of Atg11, Atg1 and Atg13 formed a subcomplex devoid of the other components. Second, in the absence of Atg19, Atg1-Atg13 and Atg11 formed a ternary complex devoid of pApe1. Third, in the absence of Atg13, Atg1 interacted only weakly with Atg11 (Figure A1.1C) and, hence, Atg19-pApe1. The existence of the multi-subunit Atg1 kinase complex containing pApe1 described here (Figure 2.1C) has apparently escaped notice in past biochemical studies of immunoprecipitated Atg1, possibly because the Ape1 aggregate is large enough to be sterically excluded from sepharose beads (Inada et al., 2002), and, in the presence of physiological salts, is cleared from cell extracts by centrifugation (>5000 × *g*) (Scott et al., 2001).

2.2.2 Atg1 activity is controlled by Atg19-bound targets

The second key prediction of our hypothesis is that Atg1 kinase is turned on in nourished cells by binding to pApe1 targets. In vivo, Atg1 kinase activation causes autophosphorylation resulting in the appearance of a slower-migrating form of Atg1 on SDS polyacrylamide gels (Figure A1.1D) (Yeh et al., 2010). In wild-type cells a fraction of Atg1 was autophosphorylated (Figure 2.1D; Figure A1.1D) and, as predicted, cells lacking either pApe1, Atg19, or Atg11 had a significantly reduced level of autophosphorylated Atg1 (Figure 2.1D). Notably, Atg1 autophosphorylation could be induced in *ape1*Δ*, atg19*Δ*,* and *atg11*Δ cells following treatment with rapamycin, an inhibitor of Tor kinase signaling that mimics starvation (Kamada et al., 2000; Kim et al., 2001; Scott et al., 2001). These data provide strong support for our hypothesis that pApe1-Atg19 complexes control Atg1 activity in nourished cells and confirm that these factors

are dispensable for the canonical pathway of Atg1 activation that occurs via repression of Tor kinase signaling.

To verify that that Atg19-bound targets increase Atg1's catalytic activity, we incubated affinity-purified Atg1 with myelin basic protein (MBP) and ATPγ^{32}P (Kamada et al., 2000). MBP was robustly phosphorylated upon incubation with wild-type Atg1, but not *kd*-Atg1 or *ad*-Atg1 (Figure A1.1E). Consistent with our hypothesis, Atg1 catalytic activity was dependent on Atg11 and Atg19 (Figure 2.1E). More precisely, we disrupted the Atg11-Atg19 interaction using either Atg11 lacking the Receptor-Binding Domain (RBD) (Figure A1.1F) (Yorimitsu and Klionsky, 2005), which is dispensable for the Atg1-Atg11 interaction (Figure A1.1G), or a mutant version of Atg19 that is unable to bind Atg11 (Atg19Δ11BD) (Figure A1.1H) (Shintani et al., 2002) and observed a strong decrease in Atg1 catalytic activity (Figures 2.1F and 2.1G). We also noted that Atg1 activity was only partially dependent on pApe1 (Figure 2.1E) and this might reflect Atg19's ability to recognize other protein aggregates in the absence of pApe1 (Lynch-Day and Klionsky, 2010). In sum, our data demonstrate that "basal" Atg1 activity in nourished cells is in fact dictated by a chain of interactions between the Atg1-Atg13 subcomplex, Atg11, and Atg19-bound targets.

2.2.3 Atg1 activation by Atg19-bound targets drives autophagosome membrane elongation during nutrient-rich conditions

The mechanistic role of Atg1 kinase activity during autophagy has primarily been studied in the context of the formation of the large (600-900nm) autophagosomes induced by starvation, where it has been shown that Atg1 kinase activity and phosphorylation of Atg9 are required for

expansion of the autophagosome membrane (Papinski et al., 2014; Suzuki et al., 2013). Though the kinase activity of Atg1 is also essential for the trafficking of pApe1 to the vacuole (Kijanska et al., 2010; Papinski et al., 2014), the precise step at which Atg1 kinase activity is required during selective autophagy has not been clarified. In particular, it has not been determined whether Atg1 kinase activity is similarly necessary to promote membrane elongation during formation of the much smaller (~150nm) autophagosomes that enwrap pApe1 aggregates, or if it is strictly required for a later step in autophagy progression (Kraft et al., 2012).

To test the hypothesis that Atg1 kinase activation by pApe1 aggregates is required for elongation of selective autophagosome membranes, we first studied the intracellular localization of Atg2, a protein that localizes to the growing rim of cup-shaped autophagosome membranes (Suzuki et al., 2013). In starved cells, localization of Atg2 to the site of autophagosome formation requires Atg1 kinase activity (Papinski et al., 2014). In nourished cells, Atg2-GFP targeting to pApe1 aggregates results in a punctum of fluorescence (Shintani and Klionsky, 2004) and we found that the proportion of mCherry-Ape1 puncta that colocalized with Atg2-GFP puncta was significantly decreased in cells lacking Atg1 or expressing *kd*-Atg1 or *ad*-Atg1 (Figure 2.2A), whereas mCherry-Ape1 puncta formation was unchanged (Figure A1.2A). These data argue that autoactivated Atg1 molecules are required to initiate membrane expansion during selective autophagy.

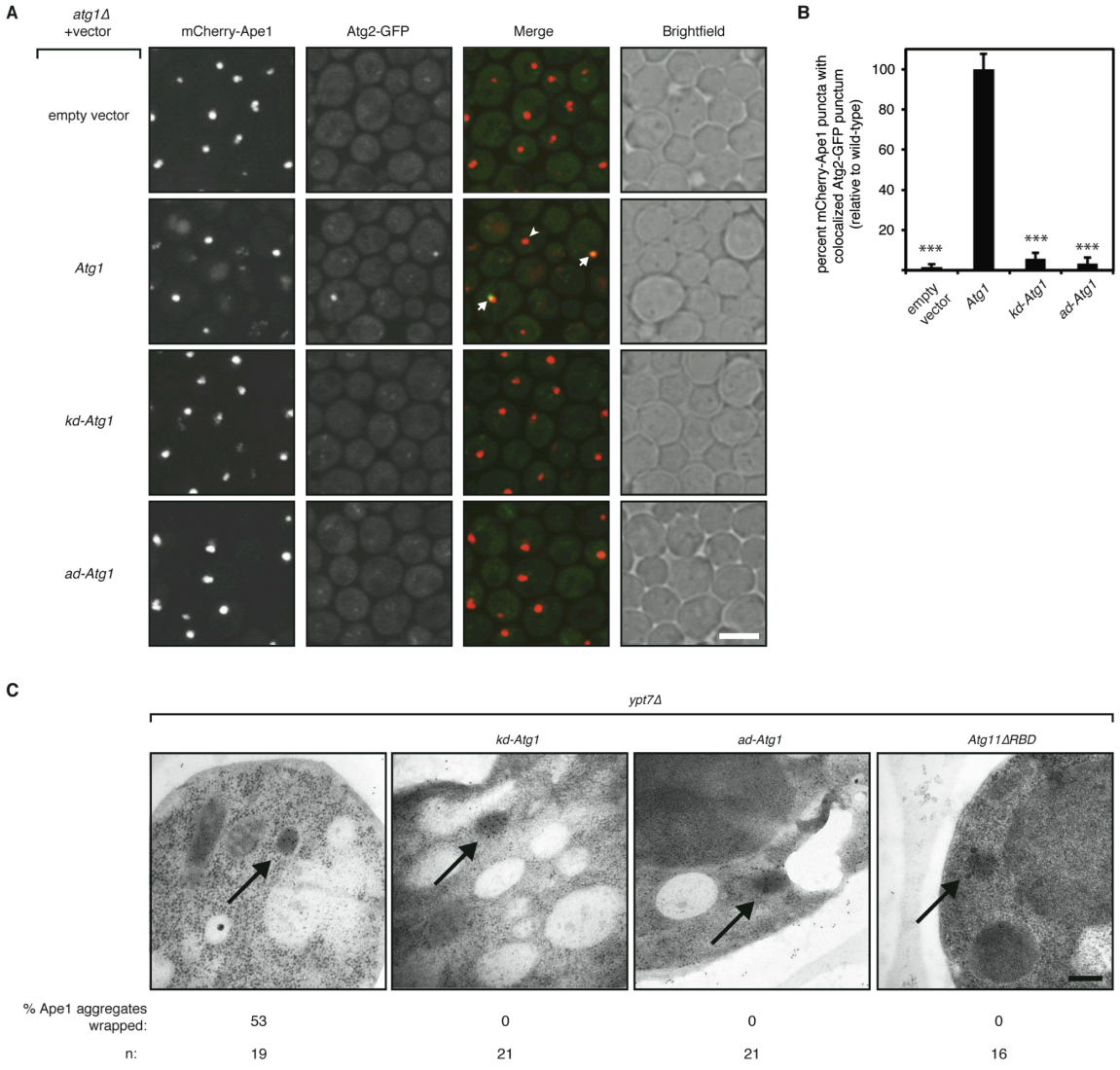

Figure 2.2. Atg1 Kinase Activation in Nourished Cells Is Required for Autophagosome Membrane Elongation around Ape1 Aggregates

(A) Representative images (maximum intensity projections) of logarithmically growing *atg17*Δ *atg1*Δ cells expressing mCherry-Ape1 and Atg2-GFP from their endogenous loci and carrying an empty vector or vector expressing the indicated Atg1 allele. White arrow indicates colocalized mCherry-Ape1 and Atg2-GFP puncta; white arrowhead indicates a lone mCherry-Ape1 punctum. Note that only wild-type Atg1 cells have vacuolar mCherry fluorescence because Atg1 kinase activity is required for pApe1 vacuolar delivery. Scale bar, 5 mm. *kd,* kinase-dead allele; *ad,* autoactivation-dead allele.

Figure 2.2 (Continued)

(B) Image analysis of strains shown in (A) from three independent experiments (>1,000 mCherry-Ape1 puncta per strain per experiment analyzed). Bar graphs report percent mCherry-Ape1 puncta with colocalized Atg2-GFP puncta as the mean and standard deviation (error bars) relative to cells expressing wild-type Atg1 allele. Raw mean percentage of mCherry-Ape1 puncta with colocalized Atg2-GFP puncta in wild-type cells was 3.6%. p values derived from Tukey's post test are reported only for comparisons between each mutant and wild-type. ***$p < 0.0001$.

(C) Representative transmission electron micrographs of logarithmically growing *ypt7*Δ cells expressing the indicated mutant alleles from their endogenous genomic loci. Black arrows indicate immunogold-labeled Ape1 aggregates. Percentage of Ape1 aggregates (out of n number analyzed) surrounded by autophagosome membranes is indicated. Scale bar, 200 nm.

See also Figure A1.2.

As an orthogonal means of examining the role of Atg1 activation on autophagosome membrane expansion in cells, we used transmission electron microscopy (TEM) and immunogold labeling of pApe1 aggregates. To visualize fully-extended autophagosome membranes, which have a short half-life in wild-type cells (Geng et al., 2008), we used the *ypt7*Δ background, in which autophagosomes cannot fuse with the vacuole (Sawa-Makarska et al., 2014). We found that cells expressing wild-type Atg1 exhibited Ape1 clusters that were frequently surrounded by electron-lucent structures that are indicative of double-membrane-bound autophagosomes (Figure 2.2C; Figure A1.2B). These structures were never observed in cells expressing Atg11ΔRBD, confirming that they are indeed representative of selective autophagosomes (Figure 2.2C; Figure A1.2B). In cells expressing *kd*-Atg1 or *ad*-Atg1, we never observed autophagosome membranes around pApe1 aggregates (Figure 2.2C; Figure A1.2B). Collectively, these data show that Atg1 kinase activation is required in nourished cells for the membrane expansion step during selective autophagosome formation.

2.2.4 A novel chemical genetics approach for studying Atg1 kinase regulation in vitro

The most rigorous test of our hypothesis necessitates biochemical reconstitution of Atg1 kinase activation by autophagy targets. Biochemical reconstitution of the minimal Atg1-Atg13 subcomplex, however, has been elusive. Therefore, we developed a chemical genetics approach that detects Atg1 activity in cell extracts and is amenable to mechanistic dissection by genetic analysis, as well as biochemical reconstitution with pure components. Specifically, we replaced the bulky 'gatekeeper residue' in the ATP-binding pocket of Atg1 with a glycine residue (Blethrow et al., 2004) (Figure A1.3A) to create a functional ATP-analog-sensitive allele of Atg1 (*as*-Atg1) (Figure A1.3B). To selectively monitor *as*-Atg1 activity in cell extracts, we utilized an

unnatural, bulky ATP derivative (N^6-PhEt-ATPγS) that is inaccessible to wild-type kinases (Figure 2.3A) but allows for thiophosphorylation of *as*-kinase substrates (Allen et al., 2007). As Atg1 is expressed at a low level (Geng et al., 2008), we improved detection of its kinase activity in two ways. First, as the endogenous nucleoside diphosphate kinase Ynk1 rapidly consumes ATP analogs (Figure A1.3C), we used a *ynk1*Δ genetic background to allow for longer labeling times. Second, we expressed from its endogenous locus a mutant version of Atg13 (*8SA*) that stabilizes Atg13's interaction with Atg1 (Kamada et al., 2010), which led to more robust substrate labeling (Figure A1.3D).

We grew cells expressing *as*-Atg1 from its endogenous locus in rich medium and prepared extracts to which we added N^6-PhEt-ATPγS. Following incubation, extracts were alkylated and analyzed by immunoblotting with an anti-thiophosphate ester antibody (Figure 2.3A). The extract containing *as*-Atg1 yielded a stereotyped banding pattern that was absent from the control wild-type extract (Figure 2.3B). The two most prominent bands had the expected molecular weights of Atg1 and Atg13, which are known Atg1 substrates (Joo et al., 2011; Yeh et al., 2010). To verify these assignments, we epitope-tagged each protein and observed the expected size increases (Figure 2.3B). We also verified that *as*-Atg1 thiophosphorylated the two remaining known Atg1 substrates: Atg2 and Atg9 (Papinski et al., 2014). By analogy to mammalian ULK1, which phosphorylates Beclin1 (Atg6 homolog) (Russell et al., 2013), we confirmed that *as*-Atg1 phosphorylated Atg6 (Figure 2.3C). Lastly, we confirmed that

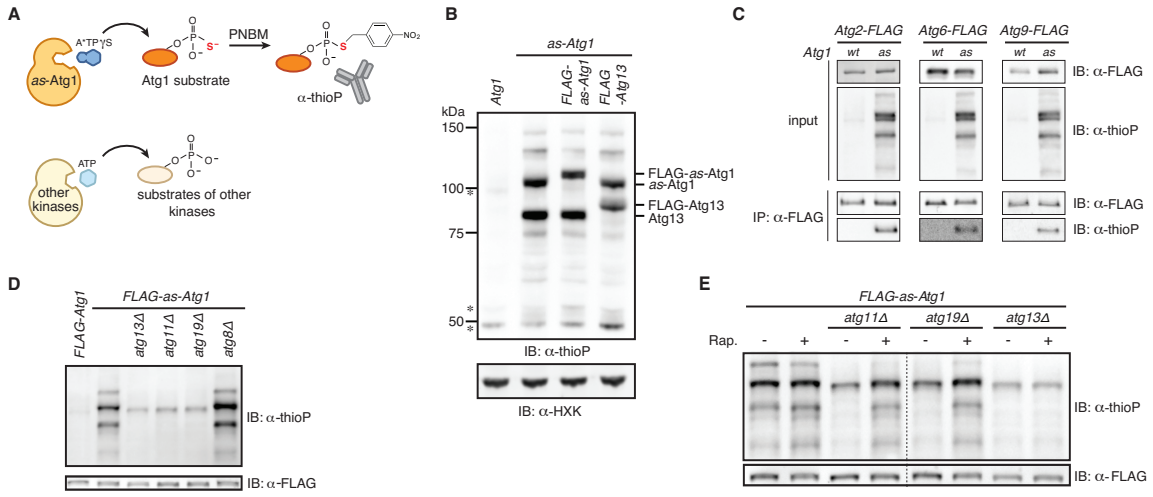

Figure 2.3. A Chemical Genetic Assay for Atg1 Kinase Activity

(A) Schematic of the chemical genetic strategy for monitoring Atg1-dependent thiophosphorylation. Analog-sensitive (as) Atg1 can accept A*TPγS, an N^6-substituted ATPγS analog, to thiophosphorylate its substrates, while other kinases reject the analog. Following alkylation with paranitrobenzyl mesylate (PNBM), labeled substrates are immunodetected with anti-thiophosphate ester (thioP) antibody.

(B) Extracts derived from logarithmically growing cells with indicated genotypes were treated as diagrammed in (A) and analyzed by SDS-PAGE (gel system 1; see section 2.4.2 for details) and immunoblotting (IB) with indicated antibodies. HXK, hexokinase; *, nonspecific band.

(C) The indicated extracts were treated as diagrammed in (A) and subjected to immunoprecipitation (IP) with anti-FLAG agarose resin. Eluates and extract (input) samples were resolved by SDS-PAGE (gel system 2; see section 2.4.2 for details) followed by immunoblotting (IB) with indicated antibodies. *wt,* wild-type.

(D) Extracts derived from logarithmically growing cells with indicated genotypes were treated as diagrammed in (A) in triplicate (one of which is shown) and analyzed by SDS-PAGE (gel system 2) and immunoblotting (IB). For quantitation and statistics, see Figure A1.3F.

(E) Logarithmically growing cells with indicated genotypes were treated with rapamycin (Rap.) or mock treated prior to analysis as in part (D). Dotted line indicates splicing of gel-image data from the same gel. For quantitation and statistics, see Figure A1.3G.

See also Figure A1.3.

thiophosphorylation of Atg6 and Atg9 was dependent on their recruitment to the site of autophagosome formation in vivo (Figure A1.3E) (Backues et al., 2015; Obara et al., 2006). Taken together, these data demonstrate that our cell-free system recapitulates the known substrate specificities of Atg1.

Our extracts were prepared from nourished cells in which Atg1 activity should come specifically from kinase molecules that are part of a multi-subunit complex containing Atg13, Atg11, and Atg19-bound aggregates. Consistent with this notion, Atg1 activity in vitro was severely diminished in *atg13*Δ, *atg11*Δ, and *atg19*Δ extracts. Both Atg1 and Atg19 have Atg8-binding sites but Atg8 was not essential for maintaining Atg1 kinase activity in extracts (Figure 2.3D). Critically, pre-treatment of cells with rapamycin restored Atg1-mediated phosphorylation to *atg11*Δ and *atg19*Δ extracts (Figure 2.3E). By contrast, rapamycin didn't restore Atg1 activity in *atg13*Δ extracts reflecting the essential role of Atg13 in all forms of autophagy (Figure 2.3E). Collectively, these data show that our cell-free assay recapitulates the known genetic and pharmacological requirements for studying Atg1 kinase activation by both Atg19-bound targets and starvation signals.

2.2.5 Biochemical reconstitution of Atg1 activation with purified Atg11 and Atg19-bound targets

To biochemically dissect the mechanism of Atg1 activation by Atg19-bound targets, we first successfully restored Atg1 kinase activity to *atg11*Δ extracts by supplementing them with purified Atg11 (Figure 2.4A and Figure A1.4A). Two lines of evidence argue that the activity of purified Atg11 depends on its interactions with Atg19 endogenous to the extract. First, Atg11

failed to restore robust Atg1 kinase activity to *atg11*Δ *atg19*Δ extracts (Figure 2.4A). Second, purified Atg11ΔRBD did not activate Atg1 in *atg11*Δ extracts (Figure 2.4B) but exerted a dominant negative effect on Atg1 kinase activation by purified Atg11 (Figure A1.4B), consistent with its ability to bind Atg1 independent of Atg19-bound targets. Activation of Atg1 by purified Atg11 required autoactivation of Atg1, as Atg11 failed to stimulate the activity of *ad*-Atg1 (Figure A1.4C).

Next, we purified Atg19 from yeast extracts and used it to restore Atg1 kinase activity to an *atg11Δatg19*Δ extract provided that we also added purified Atg11 (Figures 2.4C, 2.4D, A1.4D, A1.4E). Mass spectrometric analysis revealed that purified Atg19 was in fact a complex containing pApe1 and several other target proteins known to be delivered to the vacuole via their association with Atg19-pApe1 (Kageyama et al., 2009; Suzuki et al., 2011; Yuga et al., 2011) (Figures A1.4F-A1.4I). The ability of the purified Atg19 complex to activate Atg1 was dependent on the presence of pApe1 in the complex, consistent with the primacy of the pApe1 aggregate in directing Atg19-mediated selective autophagy under nutrient-rich conditions (Shintani and Klionsky, 2004) (Figure 2.4C, 2.4D, A1.4E). Similarly, a mutant version of Atg19 lacking a coiled coil domain required for the Atg19-pApe1 interaction (Shintani et al., 2002) (Figure A1.4J) was also unable to support Atg1 kinase activity in extracts (Figure A1.4K). Lastly, Atg19Δ11BD, which still bound the same cohort of target proteins (Figure A1.4G), was unable to activate Atg1 (Figure 2.4D, A1.4E). In sum, these data demonstrate that Atg19-bound aggregates use Atg11 as a scaffold protein to turn on the Atg1 kinase switch.

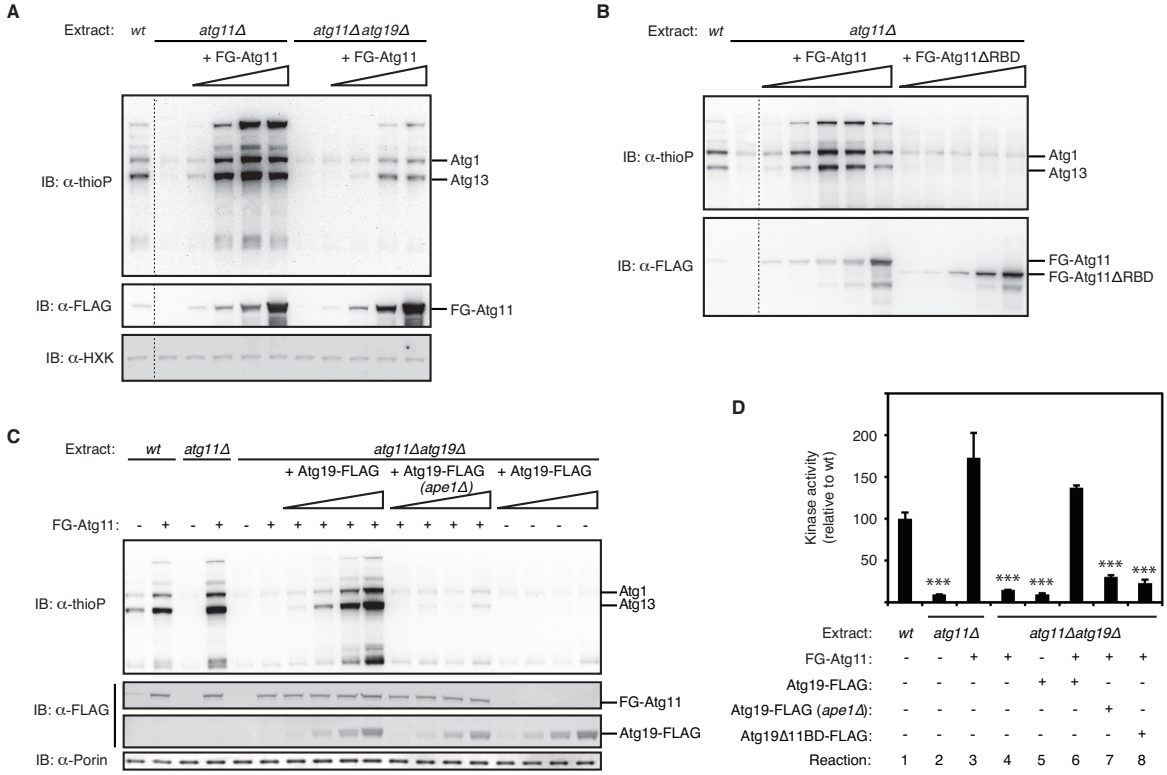

Figure 2.4. Activation of Atg1 Kinase by Purified Atg19-Target Complexes and Atg11

(A) The indicated *as-Atg1* deletion extracts were either preincubated with increasing amounts (indicated by wedge) of FLAG-GFP-Atg11 (FG-Atg11) or mock preincubated prior to analysis of Atg1 kinase activity (see section 2.4.2 for details). Immunoblotting (IB) with indicated antibodies was used to control for protein add-back and any gel loading differences. *wt,* wild-type extract derived from *as-ATG1 FLAG-GFP-ATG11* (expressed from endogenous locus); HXK, hexokinase. Dotted line indicates splicing of gel-image data from the same gel.

(B) Similar to (A) except *as-ATG1 atg11*Δ extract was preincubated with either full-length FLAG-GFP-Atg11 or FLAG-GFP-Atg11ΔRBD or mock pre-incubated. *wt,* wild-type extract derived from *as-ATG1 FLAG-GFP-ATG11* (expressed from endogenous locus). Dotted line indicates splicing of gel image data from the same gel.

Figure 2.4 (Continued)

(C) Similar to (A) except FLAG-GFP-Atg11 was added at the optimal concentration along with increasing amounts of affinity-purified Atg19, as indicated. (ape1Δ) indicates Atg19-FLAG was purified from *ape1*Δ cells (n.b. this purified material did not restore Atg1 activation suggesting that functional Atg19-pApe1 complexes were not reconstituted in situ.). *wt,* wild-type extract derived from *as-ATG1 FLAG-GFP-ATG11* (expressed from endogenous locus). Immunoblotting (IB) against porin (a mitochondrial protein) was used to control for any gel loading differences.

(D) Similar to (C), except done in triplicate with all proteins added at their optimal concentrations. Bar graphs show the mean kinase activity and standard deviation (error bars), relative to wild-type reaction set to 100. p values derived from Tukey's post test for the comparisons between indicated reactions and reaction 1 are shown. ***$p < 0.0001$.

See also Figure A1.4.

2.2.6 Damaged peroxisomes activate Atg1 dependent on Atg11 and the pexophagy receptor Atg36

Protein aggregates represent only one class of selective autophagy targets. To test if organelles targeted for destruction by selective autophagy also activate Atg1, we examined the effect of peroxisome damage on Atg1 activation. Wild-type cells growing in rich media have low autophagic turnover of peroxisomes, but cells lacking Pex1, a AAA+ protein required for protein import into the peroxisome matrix, induce selective autophagy of peroxisomes (pexophagy) mediated by Atg11 and the autophagy receptor Atg36 (Nuttall et al., 2014). To facilitate detection of any Atg1 activation due to peroxisome damage, we induced pexophagy, either by *PEX1* gene deletion or by engineered degradation of Pex1 using an auxin-inducible degron (Nishimura et al., 2009; Nuttall et al., 2014), in the *atg19*Δ genetic background, which abolished Atg1 activation by Atg19-bound targets (Figures 2.5A and A1.5A). Analysis of MBP phosphorylation by affinity-purified Atg1 revealed that the presence of damaged peroxisomes increased Atg1 kinase activity in a manner wholly dependent on Atg11 and Atg36 but independent of Atg8 (Figures 2.5A and A1.5A). As the final test of our starting hypothesis, we biochemically reconstituted Atg1 activation by damaged peroxisomes using an adaptation of our cell-free kinase assay. Mixing of a cell extract containing inactive *as*-Atg1 with an extract from cells that accumulate damaged peroxisomes (Figure A1.5B) resulted in kinase activation dependent on Atg36 (Figure 2.5B). Taken together, these data argue that Atg36-bound damaged peroxisomes use Atg11 to signal activation of the Atg1 kinase.

.

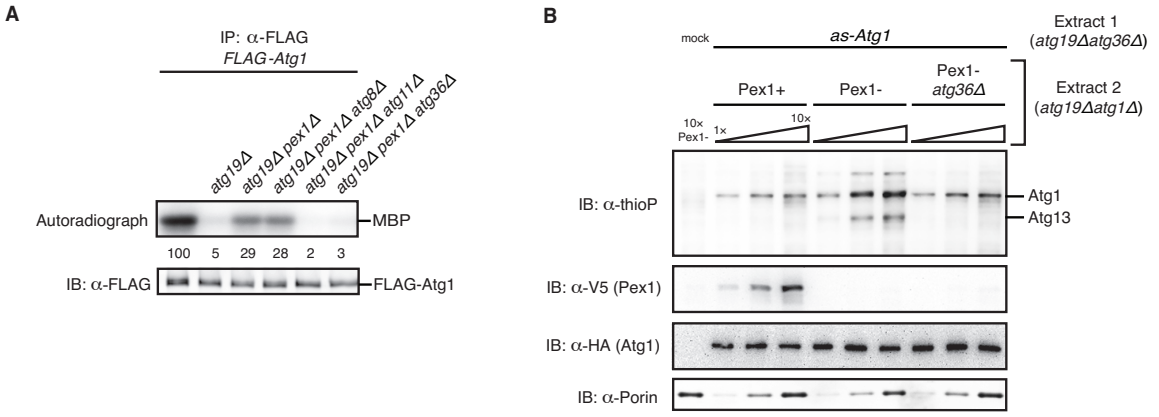

Figure 2.5. Activation of Atg1 by Damaged Peroxisomes

(A) Myelin basic protein (MBP) phosphorylation by FLAG-Atg1 immunoprecipitated (IP) from the indicated extracts (all in the *atg18*Δ genetic background to prevent potential destruction of target-bound Atg1 complexes by pexophagy) was carried out as in Figures 2.1E–2.1G. See Figure A1.5A for statistical analysis.

(B) Increasing amounts of the indicated extracts derived from the *atg19*Δ*atg1*Δ genetic background were preincubated with *HA-as-ATG1 atg19*Δ*atg36*Δ extract, or mock buffer, before analysis of kinase activity as in Figure 2.4A. Immunoblotting (IB) with indicated antibodies was used to control for auxin-induced degradation of Pex1-V5 (see Figure A1.5B) and any gel loading differences.

See also Figure A1.5.

2.3 Discussion

Atg1 kinase activity is essential for selective autophagy of pApe1 aggregates and damaged peroxisomes in nourished cells and, yet, nutrient-sensing pathways repress Atg1 kinase activity under these conditions in order to block non-selective autophagy. How Atg1 overcomes this restriction to promote basal autophagy under nutrient-rich conditions has been a long-standing question. One possibility is that less-catalytically-active Atg1 molecules suffice for the formation of selective autophagosomes. An alternative model is that pApe1 aggregates and damaged peroxisomes activate Atg1 molecules that are target-bound to locally override global Atg1 kinase repression by nutrient-sensing pathways. Here we have presented in vivo and biochemical reconstitution evidence that strongly support the latter model. Our work reveals that disparate autophagic cues (absence of nutrients versus target presence) achieve their objectives (non-selective recycling of cytoplasm versus selective cytoplasmic targeting) using the same signaling currency (Atg1 kinase activation) (Figure 2.6).

The definitional role of autophagy receptors is to connect their targets to Atg8 family proteins on the autophagosome membrane (Schreiber and Peter, 2014). Our work provides an explanation for the conservation of receptor interactions with Atg11 family of proteins: target-bound receptors interact with Atg11 to cause Atg1 kinase activation, a sine qua non for selective autophagy in nourished cells. Interestingly, Atg11 interaction with Atg19 and Atg36 is dependent on receptor phosphorylation by Hrr25 (a homolog of mammalian casein kinase 1δ)

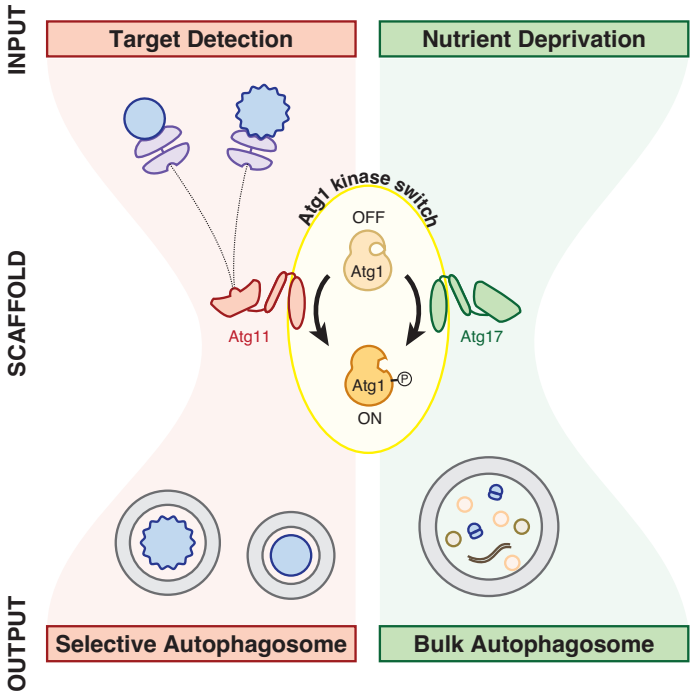

Figure 2.6. Unified Model for Atg1 Activation by Signals for Selective and Bulk Autophagy

Autophagy induction is regulated by a bowtie signaling topology with Atg1 kinase activation at its center. Atg11 and Atg17 serve as scaffold proteins required for Atg1 kinase activation by targets and nutrient depletion, respectively. Note that it remains unclear whether Atg11 and Atg17 form mutually exclusive complexes with Atg1. Atg13 and its regulation by upstream kinases are excluded for simplicity. See text for more details.

(Pfaffenwimmer et al., 2014; Tanaka et al., 2014). This raises the intriguing possibility that selective autophagy can be programmed by physiological or developmental stimuli using the signaling logic of a kinase cascade (activation of a receptor-specific kinase leading to Atg1 kinase activation). Lastly, we note that not all autophagy receptors interact with Atg11 family of proteins. As a case in point, a recent yeast study showed that Cue5 is a receptor for ubiquitinated protein aggregates that does not interact with Atg11 (Lu et al., 2014). Autophagic clearance of Cue5-bound targets was dependent on starvation and we rationalize this as a dependence on starvation cues for Atg1 kinase activation. To conclude, the minimal function of autophagy receptors is to tether their targets to the autophagosome membrane but some receptors additionally interact with scaffold proteins to turn on the autophagy kinase.

How might a scaffolding mechanism for Atg1 kinase activation by selective autophagy targets work? One potential clue is that Atg1 activation by Atg19-bound targets is apparently dependent on autophosphorylation of Thr 226 in the activation loop. Since pApe1 aggregates have many Atg19 binding sites, they have the potential to induce clustering of Atg1 and, hence, facilitate kinase activation by autophosphorylation in trans. Beyond simple clustering, allosteric changes in Atg19 caused by pApe1 binding may also be necessary for Atg1 kinase activation. A recent study showed that pApe1 propeptide binding near the N-terminus of Atg19 increased the binding affinity of Atg8 to the C-terminus of Atg19, which is proximal to the Atg11-binding site (Sawa-Makarska et al., 2014). Regardless of these mechanistic possibilities, our finding that Atg11 is at the core of a versatile molecular switch that receives signal inputs from multiple autophagy receptors is an impetus to obtain structural information about this scaffold protein.

The autophagy kinase activation mechanism we uncovered in budding yeast may be relevant to how selective autophagy in metazoans prevents accumulation of neuronal protein aggregates (Hara et al., 2006; Komatsu et al., 2006), eliminates intracellular bacteria (Ogawa et al., 2005), and clears the *C. elegans* embryo of paternal mitochondria (Al Rawi et al., 2011; Sato and Sato, 2011). Intriguingly, two metazoan protein families (represented by FIP200 and Huntingtin in humans) with sequence homology to Atg11 (Lin et al., 2013; Ochaba et al., 2014) were shown to bind both autophagy receptors and ULK1 (Hara et al., 2008; Lin et al., 2013; Nagy et al., 2014; Ochaba et al., 2014; Rui et al., 2015). Creation of an analog-sensitive ULK1 allele by mutation of the conserved gatekeeper residue will enable development of a cell-free system for defining the role of candidate scaffold proteins and determining whether receptor-bound target activation of the autophagy kinase is conserved in humans.

2.4 Methods and Materials

2.4.1 Strain construction and PCRs

Yeast strains and plasmids are listed in Tables A2.1 and A2.2. Deletion strains were constructed in the BY4741 background (mating type **a**) by standard PCR-mediated gene knockout. *3 × FLAG, 6 × FLAG-GFP, 13 × MYC, mCHERRY,* and *3 × HA* cassettes were used to modify gene loci using standard PCR-mediated tagging. The *ATG11* and *PHO8* promoters were replaced with the *TDH3* promoter using standard PCR-mediated promoter replacement. For truncation of the *ATG11* RBD, a stop codon was introduced after codon 881. For truncation of the *ATG19* 11BD, epitope tags were introduced after codon 387. A *3 × V5-AID* cassette provided by A. Amon was used to modify the *PEX1* gene locus. A *3 × GFP* cassette provided by J. Nunnari was used to modify the *ATG2* locus. To introduce *OsTIR1* into the genome, a plasmid containing *OsTIR1* provided by A. Amon was digested with PmeI and transformed into yeast for integration at the *leu2* locus.

Mutagenesis was performed using QuikChange (Stratagene) mutagenesis. For mutation of the *ATG19* ABD, codons 153–191 were deleted. Genomic allelic exchanges were performed using standard *URA3* replacement and 5-FOA counter-selection. Primer sequences for all strain constructions are available upon request.

2.4.2 Cell-free Atg1 kinase assay

Frozen lysate powder was mixed with cold 1 × kinase buffer (150 mM KOAc, 10 mM MgOAc, 0.5 mM EGTA, 5 mM NaCl, 20 mM HEPES-KOH [pH 7.3], 5% glycerol) in equal volume (wt/vol), thawed on ice, and resuspended by pipetting. Extracts were cleared twice at 1,000 × *g*

for 5 min at 4 centigrade. Equal volumes of clarified extract and 2 × kinase mix (1 × kinase buffer, 2 × energy mix [90 mM creatine phosphate, 2.2 mM ATP, 0.45 mg/ml creatine kinase], 0.2 mM N^6-phenylethyl-ATPγS [N^6-PhEt-ATPγS]) were combined and incubated for 1 hr at room temperature. Reactions were quenched with 1/20th volume 0.5 M EDTA. Thiophosphorylated extracts were alkylated with 1/20th volume 50 mM paranitrobenzyl mesylate (PNBM, Abcam) for 1 hr at room temperature, heated in loading buffer, and analyzed by one of two SDS-PAGE systems. Gel system 1 was Novex NuPAGE 4%–12% Bis- Tris SDS-PAGE (Life Technologies). This lower-percentage gel system was ideal for detecting the small shift in Atg1 mobility due to FLAG tagging. Gel system 2 was Novex 4%–20% Tris-Glycine SDS-PAGE (Life Technologies). Thiophosphorylated substrates were identified by immunoblotting with a rabbit anti-thiophosphate ester primary antibody [51-8] (Abcam) and an anti-rabbit HRP-conjugated secondary antibody (Bio-Rad). Blot imaging was done using an AlphaImager Gel Imaging System (Alpha Innotech).

Purified proteins were preincubated with extracts for 30 min at room temperature. FLAG-GFP-Atg11 was incubated at final concentrations of 1.6, 8, 40, and 200 nM in Figure 2.4A and alongside FLAG-GFP-Atg11ΔRBD, at 2, 6.3, 20, 63 and 200 nM in Figure 2.4B. In Figure A1.4B, FLAG-GFP-Atg11 was used at 8 nM and FLAG-GFP-Atg11ΔRBD was used at 8 nM (1 ×) or 80 nM (10 ×). In Figure A1.4C, FLAG-GFP-Atg11 was used at 40 nM. In Figure 2.4C, 0.1, 0.3, 1, and 3 µl of affinity-purified Atg19-target complexes were incubated with 10 µl extracts in 15 µl reactions containing 20 nM FLAG-GFP-Atg11. For Figure 2.4D, 1.5 µl of affinity-purified Atg19-target complexes were incubated with 2.5 µl extracts in 5 µl reactions containing 20 nM FLAG-GFP-Atg11. After preincubation, reactions were pelleted at 20,000 × *g* for 20 min, and pellets were resuspended in kinase buffer containing 1 × energy mix and 0.1 mM

N^6-PhEt-ATPγS before analysis of kinase activity as above. The pelleting step improved the signal-to-noise ratio, but we obtained qualitatively similar results by analyzing the effect of add-backs on kinase activity in total extracts (data not shown).

Peroxisome-containing extracts were prepared from lysate powder by clearing twice for 10 min at 1,000 × *g,* as above. A total of 1, 3, or 10 µl of extracts were preincubated for 30 min at room temperature with 10 µl *atg19*Δ *atg36*Δ *HA-as-ATG1* extract, which had been precleared at 20,000 × *g* for 20 min. Reactions were then pelleted for 20 min at 20,000 × *g* before resuspension and analysis of kinase activity as above.

2.4.3 Immunoprecipitation of Atg1 substrates after kinase reaction

Following the 1 hr room temperature incubation in the kinase assay, each sample was combined with two volumes of 1 × IP buffer (50 mM HEPES-KOH [pH 6.8], 150 mM KOAc, 2 mM MgOAc, 1 mM $CaCl_2$, 15% glycerol) with 1% NP-40. The resulting solution was incubated with 20 µl washed anti-FLAG M2 affinity gel (Sigma) for 3 hr at 4 centigrade. The resin was washed three times with 500 µl 1 × IP buffer with 1% NP-40 and incubated for 30 min on ice with 30 µl 1 mg/ml 3 × FLAG peptide (Sigma) in 1 × IP buffer containing 1% NP-40. When appropriate, the eluted material was alkylated with 2.5 mM PNBM prior to SDS-PAGE and immunoblotting to detect thiophosphorylation.

2.4.4 Yeast cell growth and lysate preparation

Saturated, overnight cultures were diluted 1:100 and grown for 8 hr in YPD media (1% yeast

extract, 2% peptone, 2% dextrose) to mid-log phase. YP5D (1% yeast extract, 2% peptone, 5% dextrose) media was seeded with logarithmically growing cells to achieve a final OD_{600} of ~2.0-3.0 after 9-11 doublings. When indicated, cultures were treated with 0.2 μM rapamycin (LC laboratories) in 90% ethanol/10% Tween-20 for 20 min prior to cell collection. Cells were pelleted at 3,500 × *g* for 22 min, washed with distilled water and pelleted in 50 ml Falcon tubes (3,000 × *g* for 1 min). Washed cell pellets were weighed and resuspended in 1 ml lysis buffer (50 mM HEPES-KOH, pH 6.8, 150 mM KOAc, 2 mM $MgCl_2$, 1 mM $CaCl_2$, 0.2 M sorbitol) per 6 g pellet. Lysis buffer cell suspensions were frozen, drop-wise, in liquid nitrogen and the resulting frozen material was ground in the presence of cOmplete protease inhibitor cocktail (Roche) using a Retsch PM100 ball mill (large scale, 1 liter cultures) or Retsch MM400 ball mill (small scale, 25 OD_{600} units maximum). Frozen yeast lysate powder was stored at -80 centigrade.

To induce Pex1 degradation, cells were grown overnight in YPD medium to OD_{600} of 0.2 before treating them for 7 hr with 500 μM 3-indoleacetic acid (auxin) (Sigma) in DMSO or mock-treating with DMSO alone.

2.4.5 Protein purifications

FLAG-Atg1 complexes: Frozen lysate powder (~3,000 OD_{600} units) was prepared as described for the cell-free kinase assay. After thawing in 10ml 1 × IP buffer with 1% NP-40 and 1 × phosphatase inhibitors (5 mM sodium fluoride, 62.5 mM beta-glycerophosphate, 10 mM sodium vanadate, 50mM sodium pyrophosphate) lysates were cleared twice at 1,000 × *g* at 4 centigrade. Protein G Dynabeads (Invitrogen) were pre-equilibrated with mouse anti-FLAG antibody (Sigma) and added to clarified extract for 3 hr at 4 centigrade. Beads were collected and washed

five times with 1 × IP buffer containing 1% NP-40 and 1 × phosphatase inhibitors. FLAG-Atg1 complexes were eluted on ice with 25 µl 1 mg/ml 3 × FLAG peptide (Sigma) in IP buffer containing 1% NP-40 and 1 × phosphatase inhibitors.

FLAG-GFP-Atg11: Frozen lysate powder (~9,000 OD_{600} units) was prepared from yeast cells cultured and harvested as described for the cell-free kinase assay. After thawing in 15 ml lysis buffer, lysates were cleared twice at 1,000 × *g* before ultracentrifugation at 100,000 × *g* for 30 min to remove cellular membranes. NP-40 was added to 0.075% before incubating with 1 ml anti-FLAG resin (Sigma) for 2 hr at 4 centigrade. After extensive washing in 1 × IP buffer (containing no detergent), FLAG-GFP-Atg11 was eluted on ice with 0.5 ml 1 mg/ml 3 × FLAG peptide in IP buffer. Eluates were cleared at 20,000 × *g,* aliquoted, frozen in liquid nitrogen and stored at -80 centigrade. Protein purity was evaluated by Colloidal blue staining (Invitrogen).

Atg19-FLAG-target complexes: Frozen lysate powder (~7,500 OD_{600} units) was prepared as described for the cell-free kinase assay. After thawing in 30 ml lysis buffer, lysates were cleared twice at 1,000 × *g.* Protein G Dynabeads were pre-equilibrated with mouse anti-FLAG antibody and added to clarified extract for 3 hr at 4 centigrade. After extensive washing with lysis buffer, proteins were eluted by incubation with 150 µl 1 mg/ml 3 × FLAG peptide in IP buffer for 30 min at room temperature, aliquoted, frozen in liquid nitrogen and stored at -80 centigrade. Eluates were analyzed by Colloidal blue staining (Invitrogen).

In Figure A1.4J, frozen lysate powder (50 OD_{600} units) was prepared as described for the cell-free kinase assay. After thawing in 0.5 ml 1 × IP buffer with 1% NP-40 and 1 × phosphatase inhibitors, lysates were cleared twice at 3,000 × *g* at 4 centigrade. Protein G Dynabeads (Invitrogen) were pre-equilibrated with mouse anti-Myc antibody (9E10, Sigma) and added to

clarified extract for 2 hr at 4 centigrade. Beads were collected, washed three times in 1 × IP buffer with 1% NP-40 and 1 × phosphatase inhibitors, and boiled in sample buffer.

2.4.6 Alkaline phosphatase assays

Alkaline phosphatase assays were performed as described (Noda et al., 1995). Specifically, saturated overnight cultures were diluted to 0.2 OD_{600} in 5 ml YPD media and grown for 4 hr. Cells were pelleted, washed and resuspended in 5 mL SD-N media (0.17% yeast nitrogen base, 2% glucose). Cells were starved for 4 hr, after which 1 OD_{600} unit was collected, washed, and resuspended in 1 mL cold 145 mM NaCl with 1 mM PMSF. Cells were pelleted and resuspended in ALP lysis buffer (1 M PIPES-KOH, pH 6.8, 0.5% Triton X-100, 50 mM KCl, 100 mM KOAc, 10 mM $ZnSO_4$). Cells were lysed by vortexing with glass beads three times for 1 min with 1-min ice rests in between. Lysate was clarified at 15,000 × *g* for 5 min at 4 centigrade. 50 µl lysate, 50 µl ALP lysis buffer and 400 µl substrate solution (250 mM Tris-HCl, pH 8.5, 0.4% Triton X-100, 10 mM $MgSO_4$, 10 mM $ZnSO_4$, 1.25 mM PNPP [para-nitrophenylphosphate]) were incubated at 37 centigrade for 3-15 min, which lie in the linear range of the assay. Samples were quenched with 500 µl 1 M glycine-KOH, pH 11.0 and their absorbance at 400 nm recorded and normalized by protein concentration as determined by BCA protein assay (Pierce).

2.4.7 Thin layer chromatography

Extracts from wild-type and *ynk1*Δ cells were prepared as described for kinase extracts and diluted 1:10 in 1 × kinase buffer containing competitor nucleotides and radiolabeled N^6-PhEt-

ATPγ^{32}P as indicated in Figure A1.3C. Reactions were quenched by the addition of 5 ml 5% formic acid to 2 ml of the reaction mix. Quenched reactions (0.5 ml) were spotted on a PEI cellulose F sheets (EMD Millipore) and resolved in 0.5 M KH_2PO_4, pH 3.5. After drying, the sheet was exposed to a storage phosphor screen (GE Lifesciences) and imaged using a Typhoon TRIO scanner (GE Lifesciences). Signal quantification was performed using Image Quant TL (GE Lifesciences).

2.4.8 Atg1 kinase assay with radiolabeled ATP

Purified Atg1 complexes were incubated with 2 µg/µl myelin basic protein (MBP; Sigma) and ATPγ^{32}P (0.05 µCi/µl; PerkinElmer) in kinase buffer for 30 min at room temperature. Reactions were terminated by addition of SDS sample buffer, heated, and resolved by SDS-PAGE. After drying, the gel was exposed to a storage phosphor screen, and imaged using a Typhoon Trio scanner. For quantification, triplicate reactions were analyzed using ImageQuant TL (GE Life Sciences) to measure intensities of fixed-width bands following background subtraction by the rolling-ball method.

2.4.9 Transmission electron microscopy

Yeast cultures were prepared for electron microscopy as described previously (Giddings et al., 2001). Briefly, cells were collected in exponential phase in YPD medium by vacuum filtration, cryofixed using a Wohlwend Compact 02 high-pressure freezer. Samples were then freeze-substituted in 0.25% glutaraldehyde and 0.1% uranyl acetate in acetone for embedding in an

embedding kit (HM20, Lowicryl). 70-nm sections were poststained in uranyl acetate and lead citrate. Sections were incubated with rabbit anti-Ape1 diluted 1:1000 or 1:2000, then with 10-nm gold-conjugated anti-rabbit IgG, before imaging at 21,000 × magnification in a transmission electron microscope (FEI CM100, Phillips). Ape1 aggregates were identified for each strain, blind to genotype, as clusters of 3 or more gold particles that colocalized with round electron-dense structures approximately 150 nm in diameter. Brightness and contrast were adjusted equally for all images in Photoshop (Adobe).

2.4.10 Fluorescence microscopy

Cells were grown in synthetic dropout medium to logarithmic phase, concentrated, and imaged at room temperature on a microscope (Axiovert 200M; Carl Zeiss) equipped with a Yokogawa CSU-10 spinning disk and 488 nm and 561 nm lasers (Coherent), using an oil-immersion 63 × objective (NA of 1.4). Images were acquired using a Cascade 512B EM-CCD detector (Photometrics) and the Metamorph 7.8.8 acquisition software (Molecular Devices). Each field of view was imaged as a 7 μm Z-stack with a step-size of 0.2 μm. Images were converted to maximum intensity projections in ImageJ. Images shown in Figure 2.2A were assembled and adjusted for brightness and contrast – equally for all images – in Photoshop (Adobe). Atg2-GFP puncta were identified stringently, using the ImageJ Analyze Particles function, as clusters of 2 or more pixels with pixel intensity greater than or equal to 2800, and examined manually to exclude any dead cells. mCherry-Ape1 puncta were defined as clusters of 3 or more pixels with pixel intensity greater than or equal to 2300, with circularity greater than or equal to 0.70, to exclude dead cells. Colocalization analysis of computationally-identified Atg2-GFP and

mCherry-Ape1 puncta was performed manually using aligned images in Photoshop. 82.5% of all Atg2-GFP puncta colocalized with mCherry-Ape1 puncta in cells expressing wild-type Atg1. Total cells were counted manually.

2.4.11 Mass spectrometry

Affinity-purified FLAG-Atg1 and Atg19-FLAG complexes were prepared in triplicate as described under "Protein purifications" (~3,000 OD_{600} and ~1,500 OD_{600} units, respectively, per replicate per strain genotype) for mass spectrometry analysis by the Thermo Fisher Scientific Center for Multiplexed Proteomics at Harvard Medical School. Sample processing steps included SDS-PAGE purification of proteins followed by alkylation of cysteine and in-gel trypsin digestion. Peptides were extracted from the gel and desalted followed by peptide labeling with Tandem Mass Tag 10-plex reagents (Cargnello et al., 2012). Multiplexed quantitative mass spectrometry data were collected on an Orbitrap Fusion mass spectrometer operating in a MS3 mode using synchronous precursor selection for the MS2 to MS3 fragmentation. MS/MS data were searched against a Uniprot yeast database (February 2014) with both the forward and reverse sequences using the SEQUEST algorithm. Further data processing steps included controlling peptide and protein level false discovery rates, assembling proteins from peptides, and protein quantification from peptides (Weekes et al., 2014). Statistical analysis was performed using a one-way ANOVA and Benjamin Hochberg corrected p values were calculated for each protein. Alpha was set to 0.01 and only proteins with more than one quantified peptide were considered when defining proteins significantly different between preparations.

2.4.12 Other statistical analysis

Statistical analysis was performed using GraphPad Prism. A one-way analysis of variance (ANOVA) was calculated for each data panel with a $p < 0.05$ significance threshold. Post hoc comparisons were conducted using Tukey's test, in which adjusted p values < 0.01 were considered significant. $n \geq 3$ for all experiments.

Chapter 3: Local Control of Peroxisomal Autophagy Receptor Activation by the Peroxisomal AAA-ATPase

Attributions

RAK performed the majority of the experiments. Sarah Ward, a Harvard undergraduate, performed the Hrr25 shutoff experiment shown in Figure 3.4D under supervision of RAK and VD. RAK and VD designed and analyzed the experiments and wrote the text. VD supervised the project.

3.1 Introduction

Many autophagy receptors reside constitutively at the surface of their targets (Kanki et al., 2009; Khaminets et al., 2015; Mochida et al., 2015; Novak et al., 2010; Okamoto et al., 2009; Walter et al., 2014) where their ability to drive target degradation is regulated by post-translational modifications – predominantly phosphorylation (Farré et al., 2013; Matsumoto et al., 2011; Tanaka et al., 2014; Wild et al., 2011). Several kinase-receptor pairs have been identified, however, little is known about how autophagy-inducing stimuli induce receptor phosphorylation by general cytosolic kinases. Fundamentally, it remains unclear if the signaling pathways in control of surface-bound receptor phosphorylation can respond to local cues for receptor activation, as would be necessary for autophagy to perform quality control. In other words: can rare damaged organelles be detected in a sea of otherwise healthy organelles in the cell?

Among known autophagy receptor proteins, the yeast receptor for selective autophagy of peroxisomes (pexophagy), Atg36, presents several experimental advantages for the study of how receptor proteins are regulated by phosphorylation. First, Atg36 phosphoactivation can be induced by shifting cells from oleate- to glucose-containing medium (Dunn et al., 2005; Farré et al., 2013). Second, yeast pexophagy involves only a single autophagy receptor whose activating phosphorylation site and modifying kinase have already been discovered (Tanaka et al., 2014); by contrast, the most intensively studied organelle autophagy target – damaged mitochondria in mammalian cells – is degraded via the actions of five or more receptors whose individual roles have been difficult to parse (Lazarou et al., 2015). Third, unlike the endoplasmic reticulum or mitochondria, the yeast peroxisome is not essential, and can thus be perturbed experimentally with ease. Since receptors share sequence similarities and some are even co-regulated by the same kinase, it is likely that the insights gained from dissecting Atg36's role in pexophagy-

specific regulatory mechanisms will provide general insights into how cytosolic kinases control the activation of autophagy receptors that will be applicable to more complex receptor systems.

Atg36 does not contain a transmembrane domain but is bound, even in the absence of pexophagy signals, to the peroxisome membrane by the integral peroxisome membrane protein (PMP) Pex3 (Motley et al., 2012). Inducing pexophagy by switching cells from oleate- to glucose-containing media causes Atg36 to be phosphorylated at serine 97, which drives Atg36-Atg11 complex formation (Farré et al., 2013), thereby triggering Atg1 kinase activity to drive, in turn, new autophagosome formation (Figure 3.1A) (Kamber et al., 2015). Recently, this phosphorylation event was shown to be catalyzed by a yeast casein kinase homolog, Hrr25 (Tanaka et al., 2014). Despite these advances, arguably the most important question in the field remains unanswered: can Atg36 phosphoactivation as a mechanism be specific for individual peroxisomes in a cellular peroxisome population?

3.2 Results

3.2.1 Atg36 phosphoactivation requires Pex3 and is inhibited by peroxisome-localized factor(s)

We envisioned two broad mechanistic models for Atg36 phosphoactivation by pexophagy signals. First, pexophagy signals might impinge on cytosolic Hrr25 to increase its catalytic activity specifically toward Atg36 or more generally toward other substrates as well (Figure 3.1B). Second, pexophagy signals might impinge on Atg36 to make it a better substrate for Hrr25 phosphorylation (Figure 3.1C), which would most likely occur via relief of a local inhibitory mechanism. Preliminarily, we favored the latter model because it provides a plausible

explanation for how locally-generated pexophagy signals might dictate the fate of individual peroxisomes.

In the two initial tests of the "local-inhibition" model, we assumed that any Atg36 inhibition, regardless of mechanism, i.e. via masking of a buried Hrr25 docking site or phosphorylation motif, would likely be exerted by proteins resident at the peroxisome membrane. Our first test made use of the observation that in cells lacking the PMP targeting factor Pex19, Pex3-containing peroxisomal precursors are still present (Halbach et al., 2009; Lambkin and Rachubinski, 2001), but lack all other PMPs (Hettema et al., 2000) with the exception of Pex22, which, like Pex3, is targeted to peroxisomes independently of Pex19 (Halbach et al., 2009) (Figure 3.2A). Strikingly, deletion of Pex19 caused Atg36 to become significantly phosphorylated (Figure 3.2B; see Figure 3.4B for evidence that gel shift is due to Atg36 phosphorylation). Notably, in cells lacking the peroxisome matrix protein receptor Pex5, which contain PMP-positive peroxisomes that lack matrix proteins (Figure 3.2A) (Subramani, 1996), Atg36 phosphorylation was not induced (Figure 3.2C). As a second test of the local inhibitor model, we replaced endogenous Pex3 with either Pex3 lacking the native transmembrane domain (TMD) (cyto-Pex3), or a chimeric Pex3 with the TMD of a mitochondrial outer membrane protein (mito-Pex3) (Figure 3.2D) and in both cases observed induction of Atg36 phosphoactivation (Figure 3.2E). We noted that simply deleting Pex3, which also causes Atg36 to become localized to the cytosol (Motley et al., 2012), did not cause Atg36 to become phosphorylated (Figure 3.2E), nor did expression of a mutant version of Pex3, Pex3-177, that is unable to recruit Atg36 to peroxisomes (Figure 3.2E) (Motley et al., 2012). Taken

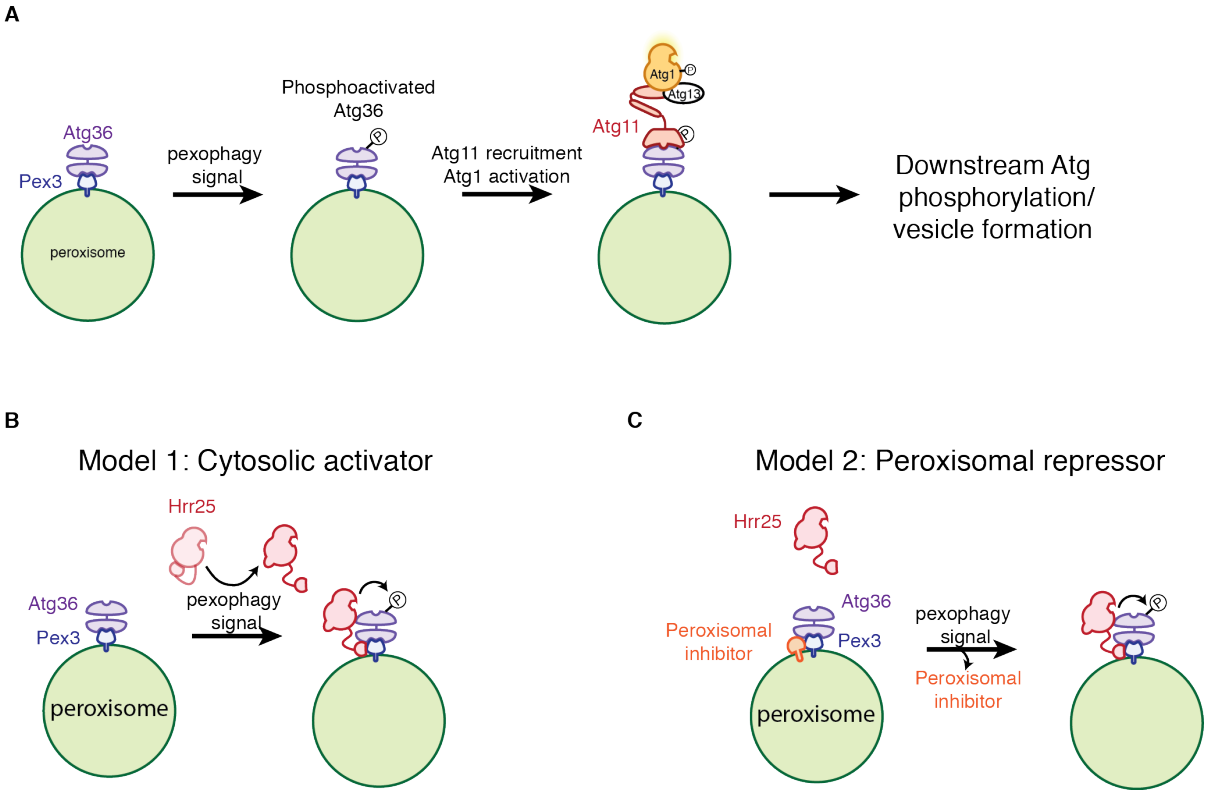

Figure 3.1. Competing Mechanistic Models for Atg36 Phosphoactivation during Pexophagy.

(A) Schematic of Atg36-mediated selective pexophagy in yeast. See text for details.

(B) Model 1 for Atg36 phosphoactivation: Upon receipt of a pexophagy signal, Hrr25 catalytic activity increases (either towards all substrates or Atg36 specifically), causing Atg36 to be phosphorylated and drive pexophagy.

(C) Model 2 for Atg36 phosphoactivation: Pexophagy signals cause Atg36 to become a better substrate for Hrr25 phosphorylation via shedding of an inhibitory molecule. Note that these models are not necessarily mutually exclusive or collectively exhaustive.

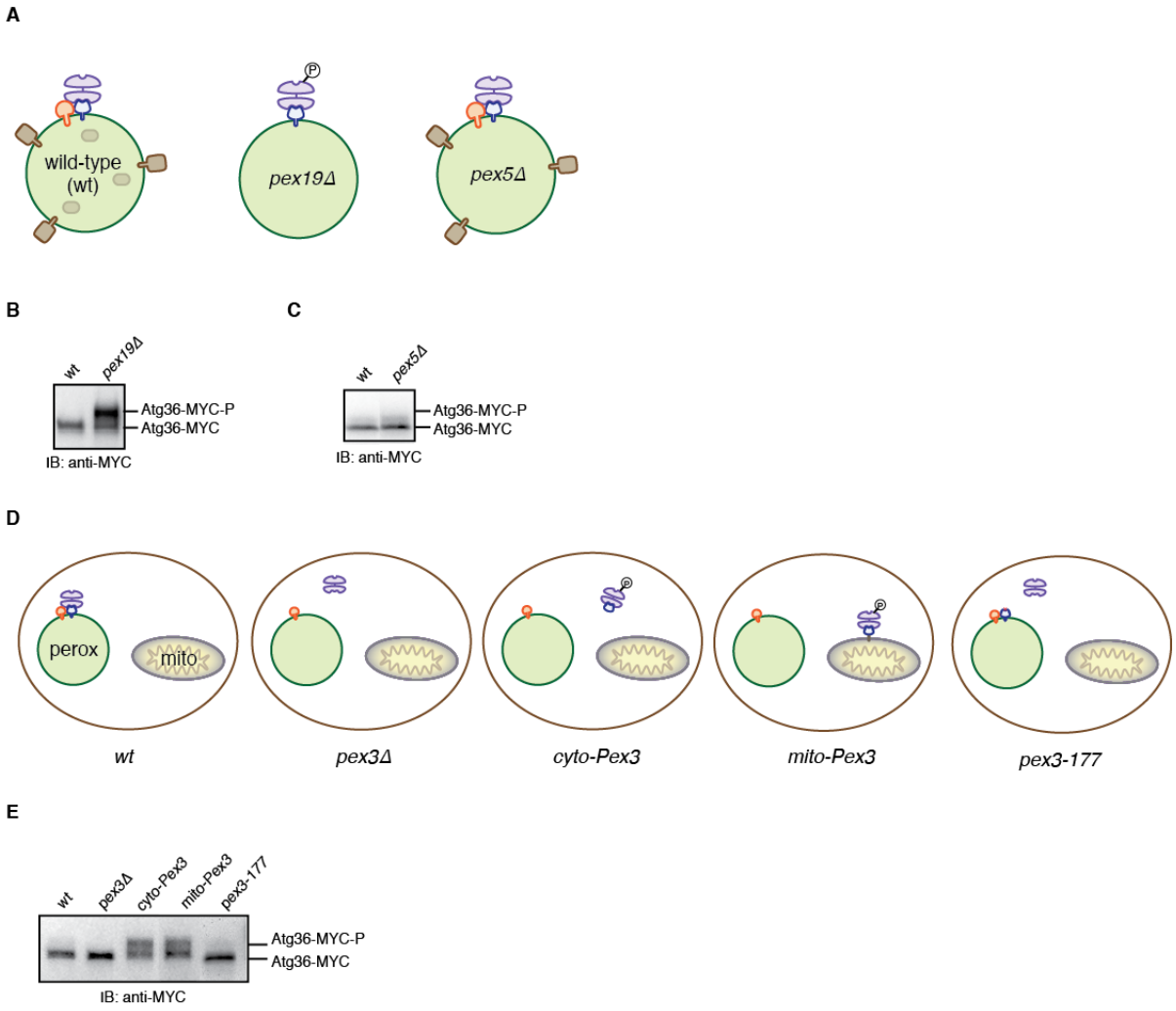

Figure 3.2. Two Tests of a Local Inhibition Model for Atg36 Phosphoregulation.

(A) Schematic of wild-type, *pex19*Δ, and *pex5*Δ peroxisomes. Wild-type peroxisomes contain Pex3 (blue), Atg36 (purple), membrane proteins (brown and orange (putative Pex3-interactor)), and matrix proteins (brown ovals shown in peroxisome lumen). In *pex19*Δ cells, normal peroxisomes do not form, but pre-peroxisomal structures form that contain Pex3 and Atg36. In *pex5*Δ cells, peroxisomes contain the normal complement of membrane proteins but are devoid of matrix proteins. The predicted pattern of Atg36 phosphorylation under a peroxisome-inhibitor model is indicated.

(B and C) Extracts derived from logarithmically growing cells with indicated genotypes were resolved by SDS-PAGE followed by immunoblotting with anti-MYC. Atg36-MYC-P, major phosphorylated species of Atg36-MYC.

Figure 3.2 (Continued)

(D) Schematic illustrating Atg36 (purple) and Pex3 (blue) localization in cells expressing different versions of Pex3. Also shown are a putative peroxisome-membrane Atg36 inhibitor (orange) and the predicted pattern of Atg36 phosphorylation under a peroxisome-inhibitor model. perox, peroxisome; mito, mitochondria.

(E) Extracts derived from logarithmically growing cells with indicated genotypes were resolved by SDS-PAGE followed by immunoblotting with anti-MYC. Cyto-Pex3, Pex3 lacking its transmembrane domain expressed under its endogenous promoter; Mito-Pex3, a chimera of the mitochondrial outer membrane protein Om45 and Pex3 expressed under the Pex3 promoter; Pex3-177; a mutant version of Pex3 unable to interact with Atg36 but which supports normal peroxisome biogenesis; Atg36-MYC-P, major phosphorylated species of Atg36-MYC. Note that cells lacking peroxisome-targeted Pex3 are unable to support normal peroxisome biogenesis but this is not illustrated here.

together, these two tests strongly support the “local-inhibition” model in which one or more PMPs inhibit activation of Atg36 anchored to the peroxisome surface by Pex3.

3.2.2 The Pex3 interactome: identification of candidate Atg36 inhibitors

To identify potential negative regulators of Atg36, we affinity purified Pex3-FLAG complexes, side-by-side with a no tag mock purification, from detergent-solubilized cell extracts that had been cleared at 100,000 × *g* to remove any unsolubilized membranes. SDS-PAGE and silver stain analysis of FLAG-peptide eluates revealed that Pex3 co-immunoprecipitated several proteins, which we identified by mass spectrometry (Figure 3.3A). Among the known binding partners of Pex3, we observed Pex19 (Fang et al., 2004) and Atg36 (Motley et al., 2012). Unexpectedly, we also identified Pex1 and Pex6, which form a heterohexameric AAA-ATPase complex involved in peroxisome biogenesis (Grimm et al., 2012), as well as Pex15, a tail-anchored protein that recruits the Pex1/6 subcomplex to the peroxisome membrane (Birschmann et al., 2003).

3.2.3 Negative regulation of Atg36 phosphorylation and pexophagy by the Pex1/6/15 complex

Pex19 has two signatures of a local Atg36 inhibitor: like Atg36, it is associated with Pex3 and its loss induces Atg36 phosphoactivation. However, we noted by co-IP/IB analysis that loss of Pex19 disrupts the Pex1-Pex3 interaction (Figure 3.3B), but not vice versa (see below). These data, taken together with a recent study showing that Pex19 mediates Pex15 integration into peroxisomes (Chen et al., 2014), suggest a parsimonious explanation in which the absence of Pex19 causes Atg36 phosphoactivation via disruption of Pex1/6/15 targeting to peroxisomes.

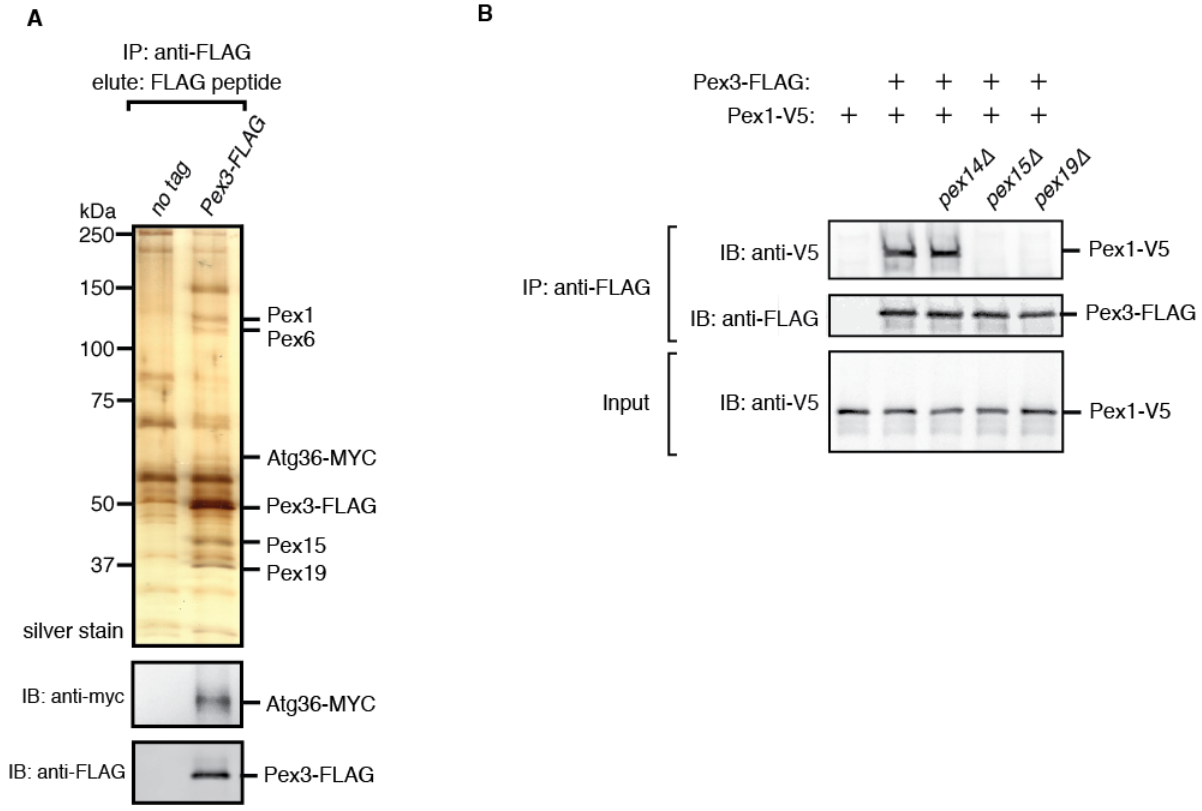

Figure 3.3. Identification of Pex1/6/15 as Novel Pex3-Interacting Proteins

(A) Detergent-solubilized extracts derived from logarithmically growing cells with indicated genotypes (both in the *ATG36-MYC* background*)* were first cleared at 100,000 × *g* and then immunoprecipitated (IP) with anti-FLAG magnetic beads. Eluates were resolved by SDS-PAGE followed by either silver staining or immunoblotting (IB) with indicated antibodies. Selected proteins identified in the Pex3-FLAG eluate by mass spectrometry are indicated based on predicted molecular weight.

(B) The indicated extracts were subjected to immunoprecipitation (IP) with anti-FLAG magnetic beads. Eluates and extract (input) samples were resolved by SDS-PAGE followed by immunoblotting (IB) with indicated antibodies.

To test if Pex1/6/15 is the proximal inhibitor of Atg36 phosphoactivation, we revisited the observation in the literature that single gene deletions of *PEX1/6/15* induce pexophagy by an undefined mechanism associated with an uncharacterized Atg36 modification (Nuttall et al., 2014). First, we confirmed in a side-by-side comparison that loss of Pex1, Pex6, and Pex15 caused Atg36 mobility to decrease on SDS-PAGE (Figure 3.4A). Next, we established that the Atg36 mobility decrease was abolished by lambda phosphatase in a reaction inhibited by phosphatase inhibitors (Figure 3.4B). Atg36 had previously been shown to bind Atg11 when activated following removal of cells from oleate growth conditions (Tanaka et al., 2015). We confirmed that the increased Atg36 phosphorylation we observed in the absence of Pex1 also was accompanied by an increase in Atg11 binding (Figure 3.4C). To test if the Atg36 phosphorylation observed in the absence of Pex1/6/15 is dependent on Hrr25 – which is essential for growth – we tagged Hrr25 with an auxin-inducible-degron (AID) tag that has previously been used to acutely shutoff Hrr25 activity (Tanaka et al., 2014). We also confirmed that auxin-induced degradation of Pex1-AID caused Atg36 to be phosphorylated to a similar extent as observed in *pex1*Δ cells (Figure 3.4D). By combining these two tools, we established that Hrr25 is in fact required for activation of Atg36 upon Pex1 shutoff (Figure 3.4D). Thus, the activation of Atg36 observed in the absence of Pex1 depends on the same kinase that phosophoactivates Atg36 when cells are shifted from growth in an oleate-containing medium – in which peroxisomes are essential for survival – to glucose-containing media in which peroxisomes are superfluous. Pexophagy can be measured by proteolytic processing of Pex11-GFP, a membrane-associated peroxisomal resident (Motley et al., 2012), in the vacuole; by this assay we confirmed that pexophagy in the absence of Pex1 is dependent on Atg36, Atg11 (Nuttall et al., 2014) (Figure 3.4E). We were also able to replace endogenous Hrr25 with an analog-sensitive (as)

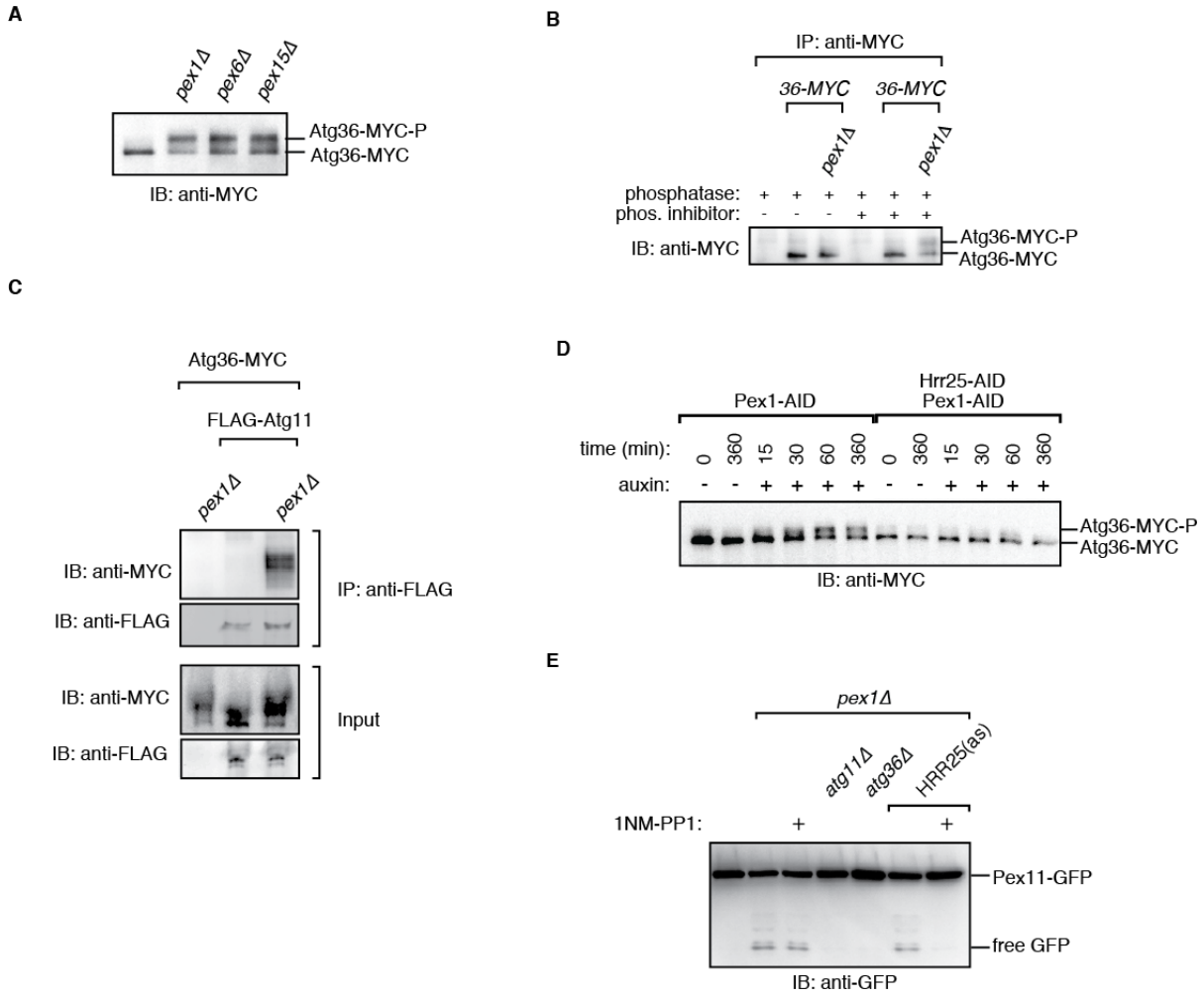

Figure 3.4. Loss of Pex1/6/15 Induces Hrr25-Mediated Phosphoactivation of Atg36 and Peroxisome Degradation

(A) Extracts derived from logarithmically growing cells with indicated genotypes were resolved by SDS-PAGE followed by immunoblotting with anti-MYC. Atg36-MYC-P, major phosphorylated species of Atg36-MYC.

(B) The indicated extracts were subjected to immunoprecipitation (IP) with anti-MYC magnetic beads. After extensive washing, bound material was treated with lambda phosphatase in the presence or absence of phosphatase (phos.) inhibitors, and then resolved by SDS-PAGE followed by immunoblotting (IB) with anti-MYC. See section 3.4.5 for details.

Figure 3.4 (Continued)

(C) The indicated extracts were subjected to immunoprecipitation (IP) with anti-FLAG magnetic beads. Eluates and extract (input) samples were resolved by SDS-PAGE followed by immunoblotting (IB) with indicated antibodies.

(D) Logarithmically growing cells with indicated genotypes were treated with 500μM 3-indoleacetic acid (auxin) in DMSO (+), or DMSO (-) for the indicated time. Cell extracts were resolved by SDS-PAGE followed by immunoblotting with anti-MYC. Atg36-MYC-P, major phosphorylated species of Atg36-MYC; AID, auxin-inducible degron.

(E) Extracts derived from cells with indicated genotypes, expressing Pex11-GFP on a low-copy vector and cultivated for 20h in synthetic defined media containing 20μM 1NM-PP1 in DMSO (+) or DMSO, were resolved by SDS-PAGE followed by immunoblotting with anti-GFP. HRR25(as), analog-sensitive allele of Hrr25 (see section 3.4.1 for details).

version of it in *pex1*Δ cells and block pexophagy using the cell-permeable ATP analog 1NM-PP1 (Figure 3.4E). These preliminary data reveal a surprising point of mechanistic convergence between *pex* mutations that induce pexophagy and pexophagy induced by physiological changes in carbon metabolism.

3.2.4 Reconstitution of Atg36 inhibition by Pex1/6 on the surface of mitochondria

The Pex1/6/15 complex powers the extraction of Pex5 from the peroxisome matrix as part of a multi-step mechanism for importing matrix proteins, which depends on additional Pex components in the peroxisome membrane (Platta et al., 2005). To examine the role of interactions between Pex1/6 and uncharacterized peroxisomal substrates or other possible peroxisomal interacting proteins in Atg36 inhibition, we carried out two tests. First, we analyzed by quantitative mass spectrometry Pex3 immunopurified from *pex1*Δ cells and found no significant depletion of Pex19 (1.2-fold) or any of its less abundant binding partners (Figure 3.5A). By contrast, there was a significant depletion of Pex6 (11.1-fold) and a lesser depletion of Pex15 (1.9-fold) (Figure 3.5A). Second, we tested whether Pex1/6/15 can inhibit Atg36 mislocalized to the mitochondrial outer membrane. To this end, in cells expressing mito-Pex3, we also replaced Pex15 with a Pex15 tail-anchored chimera containing the TMD of Fis1, a tail-anchored resident of the mitochondrial outer membrane (Figure 3.5B). In these cells, we observed repression of Atg36 phosphoactivation (Figures 3.5C and 3.5D) that was lifted if we also shut off Pex1-AID by adding auxin to cells (Figures 3.5C and 3.5D). This repression occurred even in the absence of Pex19 (Figures 3.5C and 3.5D), indicating that Pex19 is not required for Atg36 negative regulation outside of its role in targeting Pex15 to the peroxisome.

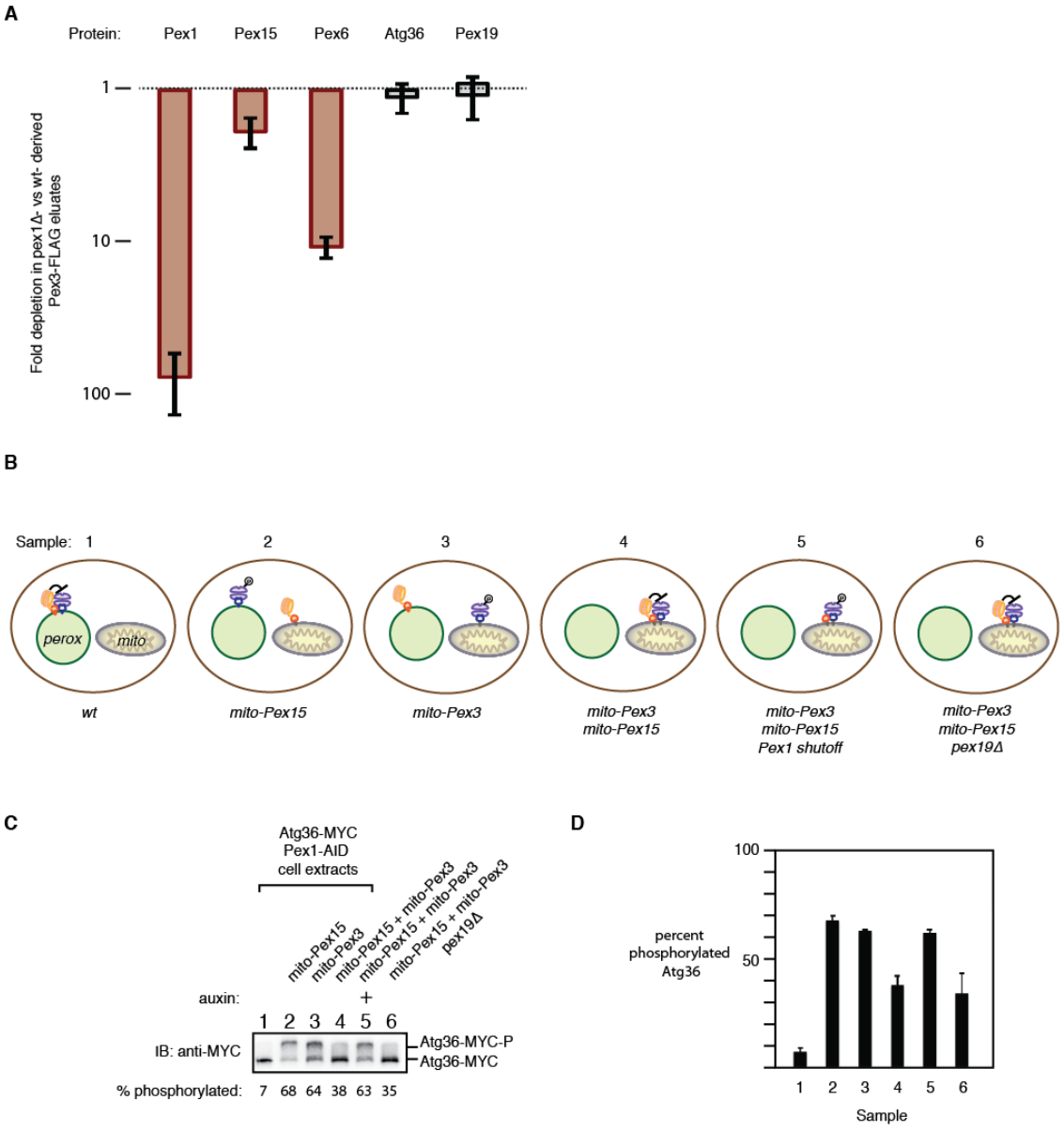

Figure 3.5. Evidence that Pex1/6/15 Inhibit Atg36 Phosphorylation Independently of Other Peroxisomal Proteins.

(A) Quantification of protein abundance in Pex3-FLAG eluates for the three proteins that exhibited significantly different abundances in wild-type (*wt*) and *pex1*Δ samples as well as Atg36 and Pex19. Plotted is the mean ratio of protein abundance (as determined by quantification of 2 or more peptides) in *pex1*Δ- versus wt-derived Pex3-FLAG eluates.

Figure 3.5 (Continued)

(B) Schematic illustrating Atg36 (purple), Pex3 (blue), Pex15 (red-orange), and Pex1/6 (light orange) localization in cells expressing different versions of Pex3 and Pex15. Also shown is the predicted pattern of Atg36 phosphorylation if Pex1/6/15 are sufficient to inhibit Atg36. perox, peroxisome; mito, mitochondria.

(C) Extracts derived from logarithmically growing cells with indicated genotypes were resolved by SDS-PAGE followed by immunoblotting with anti-MYC. Atg36-MYC-P, major phosphorylated species of Atg36-MYC. Samples were treated with 500μM auxin for 2h prior to cell collection where indicated (+). The percentage of Atg36 that was phosphorylated (% phosphorylated) was calculated as percent of total signal contributed by the upper band (average of 3 biological replicates). Numbers above gel corresponds to sample numbers as annotated in (B).

(D) Quantification of (C). Bar graphs show the mean percentage of phosphorylated Atg36 (3 biological replicates) and standard deviation (error bars). Sample number corresponds to annotations in (B).

These data support the idea that Pex3 and the Pex1/6/15 complex are minimally required to control Atg36 phosphoactivation.

3.2.5 Pex1/6 inhibition of Atg36 phosphoactivation requires ATP hydrolysis

The primary described function of the Pex1/6 complex is to use ATP hydrolysis to mechanically extract mono-ubiquitinated Pex5 from the peroxisome membrane. In doing so, this complex drives matrix protein import by recycling the limiting quantity of Pex5 (Platta et al., 2005). This extraction event has also been proposed to serve a quality control function by promoting the destruction of "non-functional," poly-ubiquitinated Pex5 molecules. However, Pex5 is dispensable for both Atg36 inhibition in wild-type cells (Figure 3.2C) and activation in *pex1*Δ cells (Figure 3.6A). Nonetheless, Pex1/6's function as a negative regulator of Atg36 could still depend on its mechanical ability to extract or unfold an unidentified pexophagy regulator or remodel the Pex3-Atg36 complex itself. Thus, to define the mechanism by which Pex1/6 inhibit Atg36 activation, we determined the role of ATP hydrolysis.

In assessing the contribution of Pex1/6 enzymatic activity to repression of Atg36 activation, we noted that most mutations that block the ATP hydrolysis cycle of Pex1/6 also interfere with Pex1/6/15 complex assembly and recruitment to peroxisomes (Ciniawsky et al., 2015; Tamura et al., 2006). Thus, though we established that mutation of a conserved lysine residue in the Walker A (Walk. A) motif or of the arginine finger (RF) of Pex1's D2 domain induces Atg36 phosphoactivation (Figure 3.6B), analysis of these mutants did not allow us to conclude that ATP hydrolysis, per se, is important for Atg36 inhibition because these mutations also lead to Pex1/6/15 dissociation. To resolve this question, we monitored Atg36 phosphoactivation

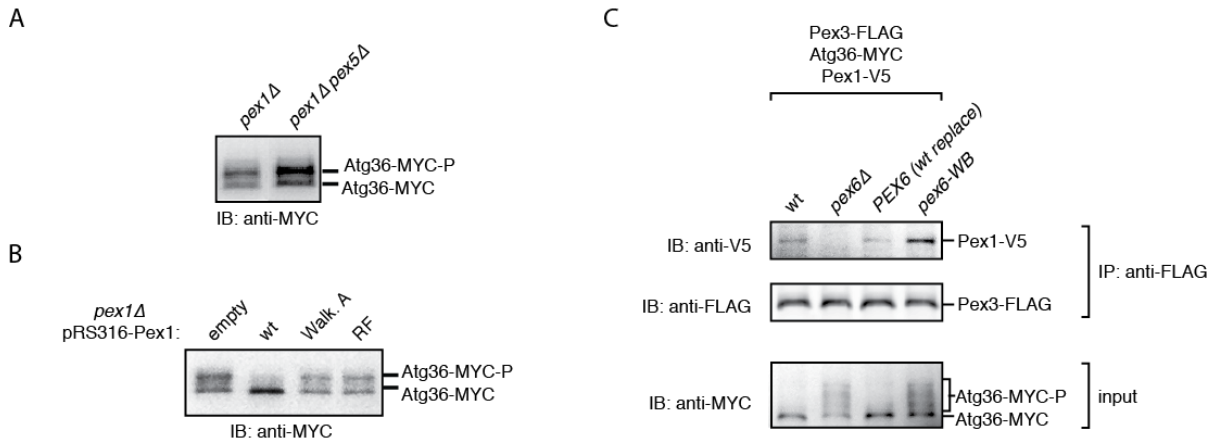

Figure 3.6. Pex1/6 catalytic activity is required for Atg36 inhibition.

(A) Extracts derived from logarithmically growing cells with indicated genotypes were resolved by SDS-PAGE followed by immunoblotting with anti-MYC. Atg36-MYC-P, major phosphorylated species of Atg36-MYC.

(B) Extracts derived from logarithmically growing cells with indicated genotypes were resolved by SDS-PAGE followed by immunoblotting with anti-MYC. Atg36-MYC-P, major phosphorylated species of Atg36-MYC. pRS316 is a low-copy yeast shuttle vector. empty, pRS316 vector with no insert; WT, wild-type *PEX1*; Walk. A, *PEX1* bearing a mutation its Walker A motif (K744E); RF, *PEX1* bearing a mutation its Arginine Finger (R852K).

(C) The indicated extracts were subjected to immunoprecipitation (IP) with anti-FLAG magnetic beads. Eluates and extract (input) samples were resolved by SDS-PAGE followed by immunoblotting (IB) with indicated antibodies. *wt*, wild-type at the *PEX6* locus; *pex6*Δ indicates a genomic deletion of *PEX6* with *URA3* that was replaced with either wild-type *PEX6* (*PEX6 (wt replace))* or a mutant version of *PEX6* bearing a mutation in its Walker B motif (E832Q) (*pex6-WB)*.

in cells expressing a mutant version of Pex6 that was recently shown in in vitro assays to completely abrogate ATP hydrolysis by the Pex1/6 complex, despite its ability to hexamerize with wild-type Pex1 subunits (Ciniawsky et al., 2015) and bind Pex15 (Birschmann et al., 2003). We confirmed that in cells expressing this mutant version of Pex6 (Pex6-WB), Pex1 was still recruited to peroxisomes and formed a complex with Pex3, yet Atg36 was phosphorylated to an extent similar to that observed in the absence of Pex6 (Figure 3.6C). This finding is inconsistent with a "steric hindrance" model for Pex1/6 inhibition of Atg36 phosphorylation and suggest that the ability of Pex1/6 to inhibit Atg36 activation is inseparable from its ability to hydrolyze ATP.

3.3 Discussion

In pursuit of mechanisms by which Atg36 phosphoactivation – and thus, the decision to degrade peroxisomes – is regulated, we first uncovered several new pieces of information about the regulation of Atg36. First, we found that Atg36 is subject to constitutive repression in wild-type cells grown in glucose-containing media. The fact that this repression is relieved when Atg36 is re-targeted to other cellular compartments or when the targeting of other peroxisomal membrane proteins is inhibited demonstrates that the phosphorylation of Atg36 that has been observed during the oleate-glucose shift does not critically depend on components that might be specifically induced under those conditions. Rather, the factors required for Atg36 activation are present at all times; Atg36 activation is not observed because of the existence of mechanisms that constitutively repress it at the peroxisome. By purifying Atg36 in complex with its peroxisome anchor protein, Pex3, we identified novel interacting proteins, three of which (Pex1, Pex6 and Pex15) form a subcomplex that we showed is required for repression of Atg36 phosphorylation and pexophagy.

Our discovery of a novel complex containing Pex3, Atg36, and the Pex1/6/15 complex raises several interesting questions about the regulation of pexophagy. First, how do physiological pexophagy signals feed into this complex to induce Atg36 activation? Recently, numerous perturbations of peroxisome function have been described in multiple model organisms that appear to induce pexophagy, including disruption of Pex5 extraction (Nordgren et al., 2015), aggregation of peroxisome matrix enzymes (Manivannan et al., 2013), oxidative stress (Jin et al., 2016; Zhang et al., 2015), changes in metabolism, and ubiquitination of peroxisome membrane proteins (Kim et al., 2008). An exciting possibility is that pexophagy signals cause partial disassembly of this complex, such that inhibition of Atg36 activation is relieved via loss of Pex1/6/15 from the complex. In this genetic formalism, multiple pexophagy signals would converge on Atg36 as repressors of the Pex1/6/15 repressor. In molecular terms, the assembly of this complex might be differentially affected by various pexophagy signals. For example, modifications of Pex5 that prevent its complete extraction (Nordgren et al., 2015) might put a brake on the ATP hydrolysis cycle of Pex1/6 to inhibit its binding to Pex15, which is known to be affected by the nucleotide state of the cycle (Birschmann et al., 2003; Gardner et al., 2015), and destabilize Pex3's interactions with Pex1/6/15. Alternatively, the accumulation of ubiquitinated Pex5 molecules – or other putative Pex1/6 substrates – at the peroxisome membrane might directly compete for binding to Pex1/6. By simultaneously playing two distinct roles: one in the quality control of membrane proteins, and the other in the regulation of pexophagy, Pex1/6 might integrate information about the status of the peroxisome proteome to enable decision-making about which peroxisomes are damaged and need to be destroyed.

3.4 Methods and Materials

3.4.1 Strain construction and PCRs

Yeast strains and plasmids are listed in Tables A2.1 and A2.2. Deletion strains were constructed in the BY4741 background (mating type **a**) by standard PCR-mediated gene knockout. *3 × FLAG* and *13 × MYC* cassettes were used to modify gene loci using standard PCR-mediated tagging. A *3 × V5-AID* cassette provided by A. Amon was used to modify the *PEX1* and *HRR25* gene loci. To introduce *OsTIR1* into the genome, a plasmid containing *OsTIR1* provided by A. Amon was digested with PmeI and transformed into yeast for integration at the *leu2* locus. The *as-HRR25* yeast strain bearing a gatekeeper mutation (I82G) in *HRR25* at its endogenous locus was provided by C. Shoemaker. *cyto-PEX3-FLAG* was constructed by replacing the endogenous *PEX3* ORF with an allele of *PEX3* lacking codons 2-45. *mito-PEX3-FLAG* was constructed by replacing the endogenous *PEX3* ORF with the product of an overlap extension PCR that fused, in frame, two PCR-generated fragments corresponding to the *OM45* ORF (lacking its stop codon), and codons 46-441 of *PEX3. mito-PEX15* was constructed by modifying the endogenous *PEX15* locus such that the region coding for the TMD and C-terminal region of *PEX15* (codons 331-383) was replaced with the region coding for the TMD of *FIS1* (codons 129-155). To enable selection for integrants bearing the *FIS1* TMD at the *PEX15* locus, a PCR product created by fusing the *FIS1* TMD and the *URA3* selection cassette via overlap extension PCR was transformed into the parent yeast strain.

Mutagenesis was performed using QuikChange (Stratagene) mutagenesis. Unless otherwise indicated, genomic allelic exchanges were performed using standard *URA3* replacement and 5-FOA counter-selection. Primer sequences for all strain constructions are available upon request.

3.4.2 Yeast cell growth and lysate preparation

Saturated, overnight cultures were diluted 1:100 and grown for 8 hr in YPD media (1% yeast extract, 2% peptone, 2% dextrose) to mid-log phase. YP5D (1% yeast extract, 2% peptone, 5% dextrose) media was seeded with logarithmically growing cells to achieve a final OD_{600} of ~2.0-3.0 after 9-11 doublings. Cells were pelleted at 3,500 × *g* for 22 min, washed with distilled water and pelleted in 50 ml Falcon tubes (3,000 × *g* for 1 min). Washed cell pellets were weighed and resuspended in 1 ml lysis buffer (50 mM HEPES-KOH, pH 6.8, 150 mM KOAc, 2 mM $MgCl_2$, 1 mM $CaCl_2$, 0.2 M sorbitol) per 6 g pellet. Lysis buffer cell suspensions were frozen, drop-wise, in liquid nitrogen and the resulting frozen material was ground in the presence of cOmplete protease inhibitor cocktail (Roche) using a Retsch PM100 ball mill (large scale, 1 liter cultures) or Retsch MM400 ball mill (small scale, 25 OD_{600} units maximum). Frozen yeast lysate powder was stored at -80 centigrade.

To induce Pex1 and Hrr25 degradation, cells were treated with 500 μM 3-indoleacetic acid (auxin) (Sigma) in DMSO or mock-treated with DMSO alone. To inhibit Hrr25(as), cells were treated with 20μM 1NM-PP1 (a gift from A. Hansen) for 20h prior to sample collection.

3.4.3 Immunoprecipitation of Pex3-FLAG

For large-scale purification of Pex3-FLAG, frozen lysate powder (4g) was prepared as described above. After thawing in 8 ml HNP buffer (50 mM HEPES-KOH [pH 6.8], 150 mM KOAc, 2 mM MgOAc, 1 mM $CaCl_2$, 15% glycerol, 1% NP-40, 1 × phosphatase inhibitors [5 mM sodium fluoride, 62.5 mM beta-glycerophosphate, 10 mM sodium vanadate, 50mM sodium pyrophosphate]) lysates were cleared twice at 1,000 × *g*. Protein G Dynabeads were pre-

equilibrated with mouse anti-FLAG antibody and added to clarified extract for 3 hr at 4 centigrade. After extensive washing with HNP buffer, proteins were eluted by incubation with 20 µl 1 mg/ml 3 × FLAG peptide in IP buffer (50 mM HEPES-KOH [pH 6.8], 150 mM KOAc, 2 mM MgOAc, 1 mM $CaCl_2$, 15% glycerol) for 30 min on ice, frozen in liquid nitrogen and stored at -80 centigrade. 10% of the eluted material was analyzed by Silver staining (Invitrogen) with the remainder used for quantitative mass spectrometry.

In Figure 3.3B, frozen lysate powder (50 OD_{600} units) was prepared using a Retsch MM400 ball mill. Frozen yeast lysate powder was stored at -80 centigrade. After thawing in 0.5 ml HNP buffer, lysates were cleared twice at 3,000 × *g* at 4 centigrade, then at 20,000 × *g*. Protein G Dynabeads (Invitrogen) were pre-equilibrated with mouse anti-FLAG antibody and added to clarified extract for 3 hr at 4 centigrade. Beads were collected, washed five times in HNP buffer, and boiled in sample buffer.

3.4.4 Mass spectrometry

Affinity-purified Pex3-FLAG complexes were prepared in triplicate as described under Section 3.4.3 for mass spectrometry analysis by the Thermo Fisher Scientific Center for Multiplexed Proteomics at Harvard Medical School. Sample processing steps included SDS-PAGE purification of proteins followed by alkylation of cysteine and in-gel trypsin digestion. Peptides were extracted from the gel and desalted followed by peptide labeling with Tandem Mass Tag 10-plex reagents (Cargnello et al., 2010). Multiplexed quantitative mass spectrometry data were collected on an Orbitrap Fusion mass spectrometer operating in a MS3 mode using synchronous precursor selection for the MS2 to MS3 fragmentation. MS/MS data were searched against a

Uniprot yeast database (February 2014) with both the forward and reverse sequences using the SEQUEST algorithm. Further data processing steps included controlling peptide and protein level false discovery rates, assembling proteins from peptides, and protein quantification from peptides (Weekes et al., 2014). Statistical analysis was performed using a one-way ANOVA and Benjamin Hochberg corrected p values were calculated for each protein.

3.4.5 Phosphatase treatment

Frozen lysate powder (50 OD_{600} units) was prepared using a Retsch MM400 ball mill. Frozen yeast lysate powder was stored at -80 centigrade. After thawing in 0.5 ml HNP buffer, lysates were cleared twice at 3,000 × *g* at 4 centigrade. Protein G Dynabeads (Invitrogen) were pre-equilibrated with mouse anti-MYC (9E10) antibody and added to clarified extract for 2 hr at 4 centigrade. Beads were collected, washed four times in HN (50 mM HEPES-KOH [pH 6.8], 150 mM KOAc, 2 mM MgOAc, 1 mM $CaCl_2$, 15% glycerol, 1% NP-40) buffer, and resuspended in 40µl lambda phosphatase buffer (NEB). Two separate 8-µl aliquots of elutions derived from each strain were treated with 1µl lambda phosphatase (NEB) in 10µl reactions containing, additionally, either 1µl 10 × phosphatase inhibitors or 1µl water for 30 min at room temperature, before the reaction was terminated with equal volume 2 × sample buffer.

Chapter 4: Conclusions

Attributions

RAK wrote the text with input from VD. Small excerpts were published in the journal *Autophagy*: "A molecular switch for selective autophagosome formation." *Autophagy* 11.11 (2015): 2132-2133.

4.1 Summary

Selective autophagy is a cellular quality control process that degrades large unwanted cytoplasmic structures such as protein aggregates and damaged organelles. Defects in the clearance of selective autophagy targets kill post-mitotic cells, such as neurons, that cannot dilute targets during division. Despite the importance of selective autophagy in disease, we have little understanding of how individual selective autophagy events are regulated to prevent the accumulation of a wide variety of toxic subcellular structures while sparing vital structures from destruction.

To discover novel regulatory mechanisms, we focused our studies on two phosphoregulatory events – Atg1 autophosphorylation and receptor phosphorylation – that were previously known to promote selective autophagy. Fundamentally, it was unclear whether these activating phosphorylation events were regulated in such a way as to allow for the logical transmission of information from a target to the autophagy machinery. Using a combination of unbiased characterization of the native protein complexes containing these signaling nodes, in vivo assays, and biochemical reconstitution, we identified two novel regulatory mechanisms that govern 1) Atg1 autophosphorylation and 2) the phosphoactivation of the peroxisomal autophagy receptor. Taken together, the discovery of these mechanisms transforms diffuse questions about selective autophagy regulation into a more defined set of molecular events, and thus prepares the field to answer more targeted questions about the role of selective autophagy in disease.

4.2 Significance for understanding selective autophagy

Centrality of Atg1 in autophagy signaling

Though Atg1 has long been considered the key signaling node in the regulation of non-selective autophagy, whether it plays a similar role in selective autophagy was unclear. Our findings clearly establish that Atg1 activity is responsive to the presence of receptor-bound targets and thus confirm the primacy of Atg1 activation in controlling autophagy initiation. Our characterization of the Atg1 complex revealed that Atg1 is able to be responsive to two types of stimuli – nutrient depletion and target detection – because it engages two distinct scaffold proteins: Atg17 and Atg11, respectively.

Previously, Atg1 kinase activation had been proposed to serve as a "switch" between selective- and non-selective modes of autophagy (Klionsky, 2005; Mizushima, 2010). Our findings argue against this model, as we find that regulated activation of Atg1 is crucial for both types of autophagy. Though it had been suggested that Atg1 might function differently in selective and non-selective autophagy (Abeliovich et al., 2003), we note that our in vitro assay for Atg1-mediated phosphorylation revealed no discernible differences in the pattern of Atg1 substrates whether Atg1 is activated by receptor-bound targets or by rapamycin. While it remains possible that the set of Atg1 phosphorylation sites differs subtly but importantly depending on the scaffold used to activate Atg1, the more parsimonious interpretation of our data is that Atg1 phosphorylates a common set of substrates to drive phagophore synthesis in response to multiple stimuli. Figuring out how these phosphorylation events drive phagophore formation remains a central goal in the field. Notably, dissection of these events, particularly phosphorylation of Atg9 vesicles, which are difficult to purify, should benefit greatly from the cell-free assay for Atg1-mediated phosphorylation we have developed.

An active role for autophagy receptors in autophagosome initiation

Autophagy receptor proteins had previously been characterized as passive tethers that link targets to autophagosomes. Our work clarifies that autophagy receptors play an active role in dictating the site and timing of autophagosome initiation by controlling the activity of Atg1. Our findings are consistent with recent work, published concurrently with ours, showing that autophagy receptors in mammalian cells physically interact with the ULK1 kinase complex (Rui et al., 2015, Lazarou et al., 2015), and provide a mechanistic rationale for multiple observations that the localization of autophagy receptors to the site of autophagosome formation precedes the recruitment of downstream Atg proteins (Suzuki et al., 2007, Itakura et al., 2011).

Local control of receptor activity

Our study of Atg36 phosphorylation provides a molecular basis for the local control of autophagy receptor activation in response to local (i.e. organelle-derived) signals. It remains unclear how Pex1/6 regulation of Atg36 might be used to ensure that only damaged peroxisomes are degraded, but the fact that a complex involved in the quality control of individual proteins has a second function as a regulator of organelle quality control suggests several interesting testable hypotheses. Chief among these is that ubiquitinated Pex5 and other putative ubiquitinated Pex1/6 substrates might compete with Pex3 for binding to Pex1/6; in situations in which peroxisome proteins are extensively damaged and ubiquitinated, Atg36 would be released from Pex1/6 inhibition. This mechanistic model, while speculative, is consistent with three experimental perturbations known to induce pexophagy: 1) overexpression of ubiquitinated peroxisome membrane proteins (Kim et al., 2008), 2) overexpression of a version of Pex5 that

can be bound but not extracted by Pex1/6 (Nordgren et al., 2015), and 3) overexpression of Pex3 (Yamashita et al., 2014).

4.3 Outstanding mechanistic questions

How do receptor-bound targets use Atg11 to activate Atg1?

How, at a molecular level, autophagy receptors use Atg11 to activate Atg1 is an exciting question raised by our work. One possibility, given that Atg1 must autophosphorylate to become fully active, is that receptors clustered on the surface of a target promote Atg1 dimerization and *trans*-autophosphorylation. Appealingly, an enforced dimerization model for Atg1 activation could also explain how binding of Atg17 – which is structurally unrelated to Atg11 but exists as a pre-formed dimer (Ragusa et al., 2012) – activates Atg1. Alternatively, both scaffolds could activate Atg1 using allosteric mechanisms. Testing these speculative models will most likely require structural characterization of Atg1 bound to its activators combined with biochemical analysis.

How does the activity of Pex1/6 inhibit Atg36 activation?

Our discovery of a novel multimeric complex containing Pex3, Atg36, and the peroxisomal AAA-ATPase subcomplex, combined with our observation that Pex1/6 enzymatic activity is required to inhibit Atg36 in rich media – and sufficient to inhibit Atg36 at the mitochondrial outer membrane –, suggest that Pex1/6 might somehow directly inhibit Atg36 activation by Hrr25. An important future goal will be to determine how, at a mechanistic level, this inhibition is exerted. Though our mass spectrometric analysis of Pex3-Atg36 complexes in the absence of Pex1 and our "in vivo" reconstitution of Atg36 regulation at the mitochondrial outer membrane

are consistent with a model in which Pex1/6 inhibit Atg36 activation independent of other factors, it remains possible that Pex1/6 exert this function by acting on a yet-undiscovered Atg36 activating factor. Alternatively, Pex1/6 might act directly on either Pex3 or Atg36, perhaps by unfolding or extracting one or both proteins, to prevent phosphorylation by Hrr25. In either case, it will be critical to both reconstitute this regulation with purified components, and to discover the substrate of Pex1/6 activity.

4.4 Conservation and significance for understanding human diseases

Perhaps the most pressing next step is to test the generality of the mechanisms we uncovered in yeast and to determine the extensibility of our findings to human diseases in which failures in selective autophagy regulation have been implicated.

Receptor activation of Atg1/ULK1

The mammalian homolog of yeast Atg1, ULK1, has also been proposed to exhibit "basal" activity (Rui et al., 2015) that is used to drive commonly-observed "basal" autophagy (Papinski and Kraft, 2016). An important next step will be to test whether the kinase activity of ULK1 in the absence of starvation is in fact controlled by autophagy receptors bound to their targets. Recently-generated mammalian cell lines lacking five partially-redundant autophagy receptors (Lazarou et al., 2015) may be useful in performing such tests. Though Atg11 has long been considered a yeast-specific factor, several proteins in higher eukaryotes with sequence homology to Atg11 have recently been shown to bind both receptors and ULK1 (Li et al., 2014; Lin et al., 2013; Rui et al., 2015). Intriguingly, Huntingtin (mutations in which cause Huntington's disease)

was recently suggested to be a human homologue of Atg11 (Ochaba et al., 2014), heightening the urgency of studying these mechanisms in human cells.

Neurodegenerative diseases

Multiple recent lines of evidence suggest that modulation of selective autophagy is a promising route for the treatment of age-related neurodegenerative diseases (Harris and Rubinsztein, 2011): 1) autophagy targets accumulate in multiple neurodegenerative diseases (Mecocci et al., 1994; Nixon et al., 2005; Wong and Cuervo, 2010); 2) mutations that disrupt autophagy cause neurodegeneration in mice and humans (Hara et al., 2006; Komatsu et al., 2006; Shimura et al., 2000); 3) the efficiency of selective autophagy as a protein targeting mechanism declines with age (Cuervo and Dice, 2000; Donati et al., 2001); and 4) re-activation of autophagy ameliorates neurodegeneration and reverses senescent phenotypes in mice (García-Prat et al., 2016; Ravikumar et al., 2004; Spilman et al., 2010). It remains unclear why selective autophagy fails to eliminate damaged and cytotoxic structures in diseased and aging neurons. Our molecular characterization of the signaling logic in control of selective autophagy reveals several defined molecular events that can now be scrutinized to determine the precise level at which selective autophagy-mediated quality control fails.

Cancer

The role of autophagy in cancer has frequently been likened to a double-edged sword (Apel et al., 2009; Kenific et al., 2010; Kimura et al., 2013); selective autophagy of damaged organelles, including depolarized mitochondria, has been suggested to prevent tumor formation, whereas some cancers have been proposed to rely on non-selective autophagy to survive metabolic stress

(White and DiPaola, 2009). Our findings that Atg1 kinase controls both the rate of selective and non-selective autophagosome formation might inform the design of pharmacological activators and inhibitors of autophagy, many of which are currently being actively investigated as cancer therapeutics.

Zellweger Spectrum disorders and peroxisome quality control

The importance of peroxisome quality for human health is evidenced by the existence of a number of inherited diseases, collectively known as Zellweger Spectrum disorders that involve defects in peroxisome function. Intriguingly, at least one study noted that in cells derived from Zellweger Spectrum patients, peroxisomes can form normally, but are degraded excessively by autophagy (Heikoop et al., 1992). It has remained unclear why mutations in *PEX1* and *PEX6,* among the more than 20 genes involved in peroxisome biogenesis, are by far the most common causes of these diseases (Geisbrecht et al., 1998); our results in yeast suggest it may be worthwhile to test whether hyperactive pexophagy may contribute to Zellweger Syndrome phenotypes.

Only recently, the mammalian protein NBR1 was identified as the pexophagy receptor, providing the first molecular handle for defining the mechanistic details of this process (Deosaran et al., 2013; Walter et al., 2014; Yamashita et al., 2014). However, it remains unclear whether NBR1 is truly a functional ortholog of Atg36. Other autophagy receptors, including p62, have been proposed to play a role in mammalian pexophagy (Kim et al., 2008). Additionally, no phosphorylation sites on NBR1 or p62 that promote interaction with the ULK1 complex have yet been identified. Thus, in determining the generality of our findings regarding the role of Pex1/6

in regulating pexophagy, further basic characterization of the molecular players involved in mammalian pexophagy is paramount.

Appendix 1: Supplementary Figures for Chapter 2

Figure A1.1. Analysis of Protein-Protein Interactions Between Atg1 Complex Subunits by Mass Spectrometry and Coimmunoprecipitation, Related to Figure 2.1.

(A) Extracts derived from logarithmically growing cells with indicated genotypes were immunoprecipitated (IP) with anti-FLAG magnetic beads as in Figure 2.1B. Eluates and extract (input) samples were resolved by SDS-PAGE followed by immunoblotting (IB) with the indicated antibodies. *, non-specific band.

(B) Extracts derived from logarithmically growing cells with indicated genotypes were immunoprecipitated with anti-FLAG magnetic beads. Eluates were analyzed by quantitative mass spectrometry (MS) (see section 2.4.11 for details). Shown is the number (#) of unique tryptic peptides used to quantify each protein abundance. After normalizing the levels of FLAG-Atg1 to correct for input differences between samples, relative abundance of each protein was compared to the amount associated with FLAG-kd-Atg1, which was set to 1. Highlighted in red is the nominal abundance of proteins that were in fact absent from those samples.

(C) Extracts derived from logarithmically growing cells with indicated genotypes (minus indicates absence of corresponding epitope tag; Δ indicates *atg13Δ)* were immunoprecipitated (IP) with anti-FLAG magnetic beads. Eluates and extract (input) samples were resolved by SDS-PAGE followed by immunoblotting (IB) with the indicated antibodies.

(D) Logarithmically growing cells with indicated genotypes were treated with rapamycin (Rap.) or mock treated prior to immunoprecipitation (IP) analysis as in Figure 2.1B with one notable exception: SDS-PAGE was done for a longer time to resolve Atg1 from its autophosphorylated form (Atg1-P), as visualized by immunoblotting (IB). *kd,* kinase-dead allele.

(E) Statistical analysis of data from Figure 2.1D. Plotted data represent mean +/- standard deviation (error bars) for each sample (n=3). Indicated p values are derived from Tukey's post-test. $p < 0.01$ was considered significant.

(F) Myelin basic protein (MBP) phosphorylation by FLAG-Atg1 immunoprecipitated (IP) from indicated extracts was carried out as in Figures 2.1E-G. *kd,* kinase-dead allele; *ad,* autoactivation-dead allele. Statistical analysis is shown on right. Plotted data represent mean +/- standard deviation (error bars) for each sample (n=3). p values derived from Tukey's post-test are reported only for comparisons between each mutant and the wild-type reaction. ***p < 0.0001.

(G) Statistical analysis of data from Figure 2.1E. Plotted data represent mean +/- standard deviation (error bars) for each reaction (n=3). p values derived from Tukey's post-test are reported only for comparisons between each mutant and the wild-type reaction. ***p < 0.0001.

Figure A1.1 (Continued)

(H and I**)** Extracts derived from logarithmically growing cells with indicated genotypes (minus indicates absence of corresponding epitope tag) were immunoprecipitated (IP) with anti-FLAG magnetic beads. Eluates and extract (input) samples were resolved by SDS-PAGE followed by immunoblotting (IB) with the indicated antibodies. *, non-specific band.

(J) The exact same eluates and extract (input) samples shown in Figure 2.1G were resolved by SDS-PAGE followed by immunoblotting (IB) with indicated antibodies. For simplicity, we did not indicate MYC-tagging of Atg19 in Figure 2.1G and we refer the reader to that figure for IP/IB anti-FLAG data that control for any loading differences. *, non-specific band.

(K) Statistical analysis of data from Figure 2.1F. Plotted data represent mean +/- standard deviation (error bars) for each reaction (n=3). p values derived from Tukey's post-test are reported only for comparisons between each mutant and the wild-type reaction. ***$p < 0.0001$.

(L) Statistical analysis of data from Figure 2.1G. Plotted data represent mean +/- standard deviation (error bars) for each reaction (n=3). p values derived from Tukey's post-test are reported only for comparisons between each mutant and the wild-type reaction. ***$p < 0.0001$.

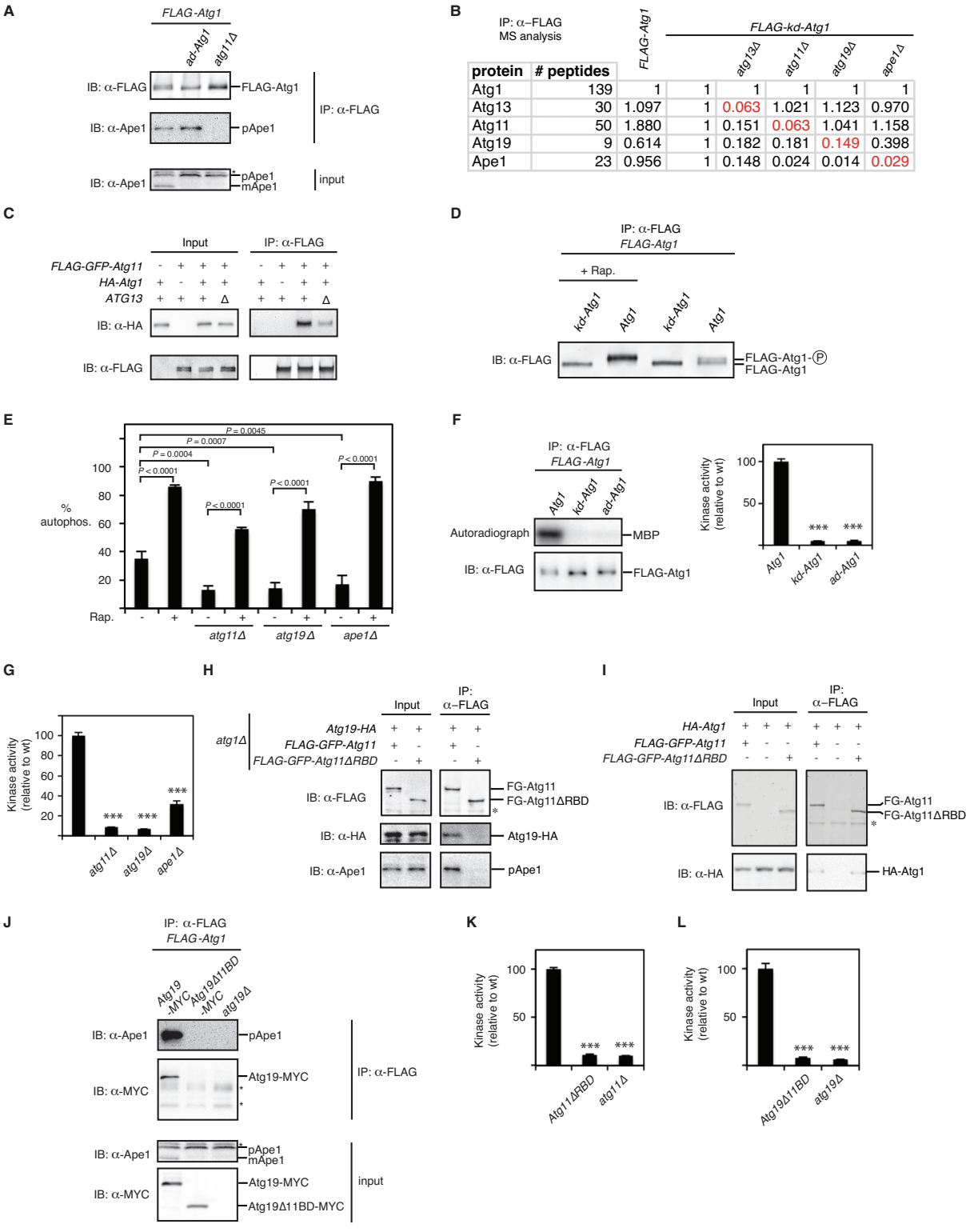

Figure A1.1 (Continued)

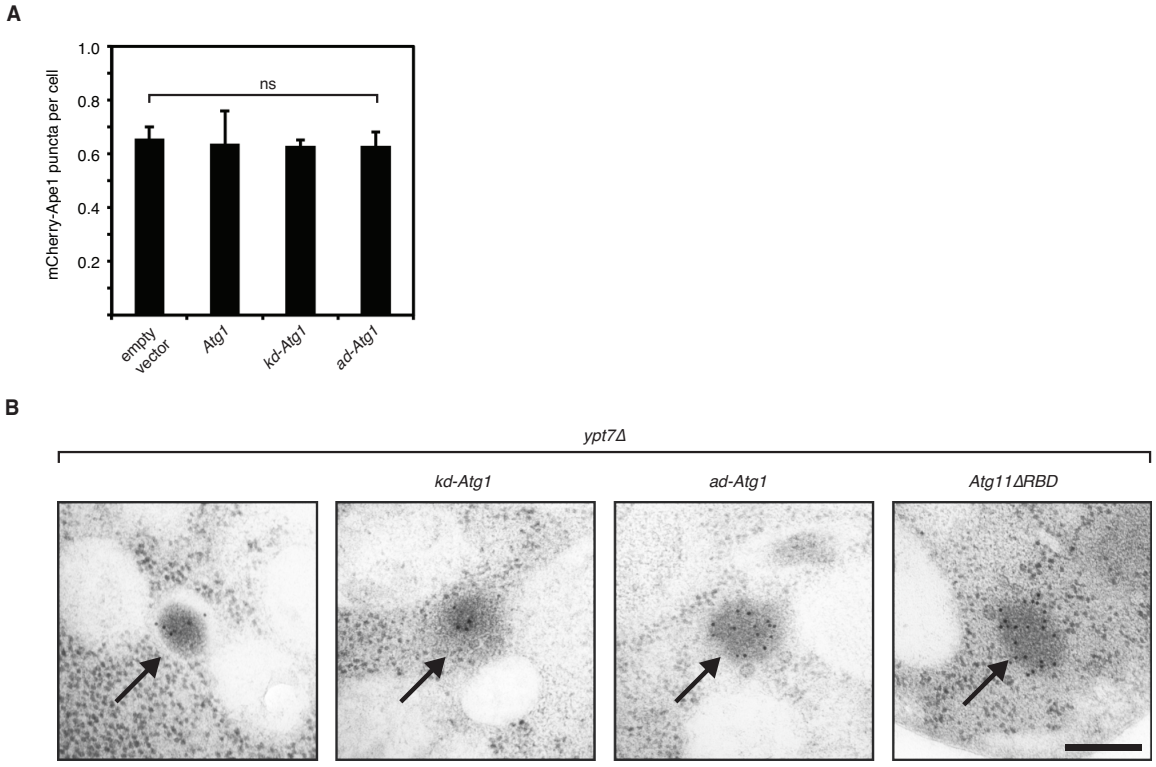

Figure A1.2. Atg1 Kinase Activity and Autoactivation are Required for Selective Autophagosome Membrane Expansion in Nourished Cells, Related to Figure 2.2.

(A) Image analysis of strains shown in Figure 2.2A. Bar graphs report the number of mCherry-Ape1 puncta per cell as the mean and standard deviation (error bars) from three independent experiments (>1500 cells per strain per experiment analyzed). There were no statistically significant differences at the $p < 0.05$ level as determined by one-way ANOVA. ns, not significant.

(B) Additional representative transmission electron micrographs of logarithmically growing *ypt7*Δ cells expressing the indicated mutant alleles from their endogenous genomic loci. Black arrows indicate immunogold-labeled Ape1 aggregates. Scale bar, 200 nm.

Figure A1.3. Development of a Cell-Free Assay for Atg1 Kinase Activity, Related to Figure 2.3.

(A) Sequence alignment of Atg1's "gatekeeper" residue (M102, boxed) with that of previously modified kinases. Red, basic residues; Blue, acidic residues; Green, hydrophobic residues.

(B) Logarithmically growing *atg1*Δ cells carrying the indicated vectors were treated with rapamycin (Rap.) or mock-treated followed by analysis of an alkaline phosphatase reporter of non-selective autophagy (see section 2.4.6 for details). Bar graphs report the mean (n=3) and standard deviation (error bars) of alkaline phosphatase activity in arbitrary units.

(C) Radiolabelled N^6-PhEt-ATPγ^{32}P was incubated for the indicated times in *YNK1* and *ynk1*Δ cell extracts (n.b. both extracts have wild-type Atg1) supplemented with indicated nucleotides. Samples were resolved by thin layer chromatography and visualized by autoradiography. N^6-PhEt-ATPγ^{32}P signal from autoradiograph was quantified by densitometry and is reported below the plate image as a percentage of the starting amount.

(D) Total *as-Atg1* kinase activity of the indicated extracts was measured as described in Figure 2.3 using gel system 2. HXK, hexokinase; *, non-specific bands.

(E) Thiophosphorylation by *as-Atg1* was measured in the total (input) and immunoprecipitated (IP) fractions of the indicated extracts as described in Figure 2.3C. Atg23 is required for Atg9 incorporation into post-Golgi vesicles capable of recruitment to the site of autophagosome formation in the cell (Backues et al., 2014). Atg6 is part of a multi-subunit complex that includes Atg14, a subunit necessary for complex recruitment to the site of autophagosome formation in the cell (Obara et al., 2006).

(F) Statistical analysis of data from Figure 2.3D. Signal from anti-thiophosphate ester (thioP) antibody immunoblots was quantified by densitometry relative to the wild-type reaction set at 100. Plotted data represents mean +/- standard deviation (error bars) for each sample (n=3). Pairwise p values were derived from Tukey's post-test. $p < 0.01$ was considered significant. ***p < 0.0001; ns, not significant.

(G) Statistical analysis of data from Figure 2.3E comparing the effect of rapamycin on Atg1 kinase activity in different backgrounds. Signal from anti-thiophosphate ester (thioP) antibody immunoblots was quantified by densitometry relative to the wild-type reaction set at 100. Plotted data represents mean +/- standard deviation (error bars) for each sample (n=4). Pairwise p values were derived from Tukey's post-test and p values for relevant comparisons are shown. $p < 0.01$ was considered significant. ns, not significant.

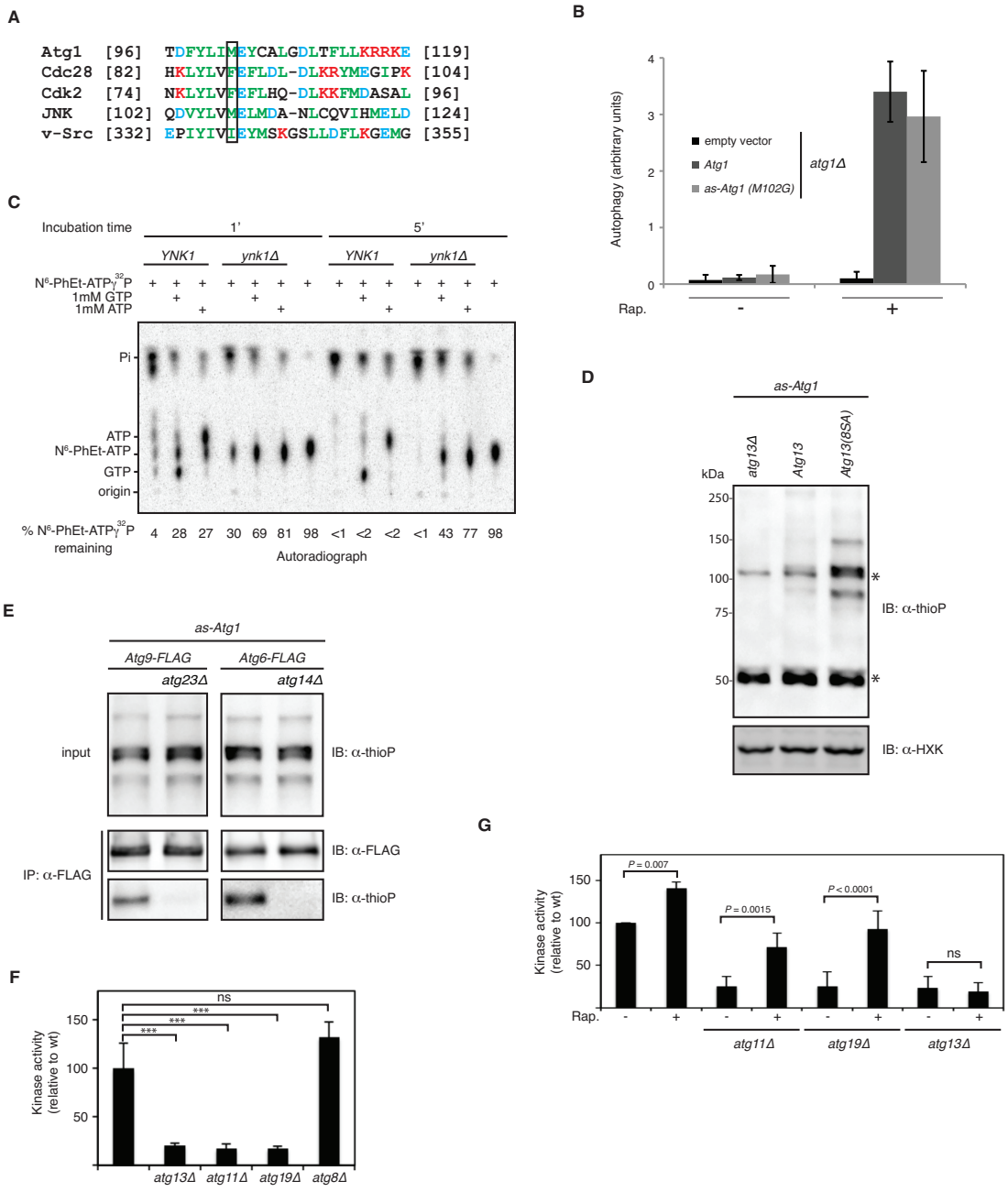

Figure A1.3 (Continued)

Figure A1.4. Characterization of Affinity-Purified Atg11 and Atg19, Related to Figure 2.4.

(A) Purified FLAG-GFP-Atg11 and FLAG-GFP-Atg11ΔRBD (see section 2.4.5 for details) were analyzed by SDS-PAGE followed by Coomassie staining.

(B) *as-Atg1* kinase analysis of the indicated extracts was carried out in triplicate (one set of reactions is shown) as in Figure 2.4A, followed by quantification of kinase activity by densitometry. Plotted data represents mean kinase activity (relative to reaction 1, set to 100) +/- standard deviation (error bars) for each reaction (n=3). Immunoblotting (IB) with anti-porin (a mitochondrial protein) was used to control for any gel-loading differences. p values derived from Tukey's post-test for the comparisons between indicated reactions and reaction 1 are shown. ***$p < 0.0001$.

(C) HA-as-Atg1 extract was pre-incubated with either purified FLAG-GFP-Atg11 (bottom) or mock pre-incubated (top) prior to Atg1 kinase analysis as in Figure 2.4A. Immunoblotting with indicated antibodies was used to control for protein add-back and any gel-loading differences. Dotted lines indicated that all lanes were spliced from the same gel.

(D) Atg19-FLAG was purified from the indicated extracts (see section 2.4.5 for details) and analyzed by SDS-PAGE followed by either Coomassie staining or immunoblotting (IB) with indicated antibodies. Proteins listed to left of Coomassie-stained gel indicate the three most abundant proteins detected by mass spectrometry of material in the indicated gel slice (dotted box).

(E) Source data for Figure 2.4D. Dotted box indicates region of gel that was used for densitometric quantification (n.b. this region excludes the highest molecular weight band because it corresponds to FG-Atg11, which is being added back to certain reactions). Reaction loaded in rightmost lane was incubated without A*TPγS and used to subtract background signal from *bona fide* phosphorylation. Immunoblotting with anti-porin was used to control for any gel-loading differences.

(F) Atg19-FLAG or mutant thereof lacking the Atg11 binding domain (11BD) was purified in triplicate from the indicated extracts (see section 2.4.5 for details) and resolved by SDS-PAGE, followed by SYPRO staining and immunoblotting with the indicated antibodies.

(G) Summary of quantitative mass spectrometry analysis of purified complexes shown in part (F). Proteins whose abundance was significantly different between preparations are indicated. For example, Ape1 is present in both Atg19-FLAG and Atg19Δ11BD-FLAG preparations but its absence from cells apparently enables more Ape4 (a distinct aminopeptidase) to interact with Atg19-FLAG. 289 refers to the number of proteins that were identified in all 3 preparations.

Figure A1.4 (Continued)

(H) List of most abundant proteins in each preparation, ranked by number (#) of quantified peptides, with short description of known function (Func.): SA, selective autophagy; Chap., chaperone; Ribo., ribosome-associated protein; Enz., metabolic enzyme.

(I) Model of subunit associations within the Atg19 complex based on data from mass spectrometry analysis of eluates shown in (F). Bar arrows indicate apparent competition between Ape1 and Ape4 for binding to Atg19. ABD, Ape1-Binding Domain.

(J) Extracts derived from logarithmically-growing cells with indicated genotypes were immunoprecipitated (IP) with anti-MYC magnetic beads. Eluates and extract (input) samples were resolved by SDS-PAGE followed by immunoblotting (IB) with indicated antibodies. *, non-specific band.

(K) The indicated *as-ATG1* extracts were analyzed in triplicate for Atg1 kinase activity as in Figure 2.4A. Statistical analysis shown below. Plotted data represent mean +/- standard deviation (error bars) for each reaction (n=3). Pairwise comparisons derived from Tukey's post-test are reported only for comparisons with Atg19-MYC extract. ***$p < 0.0001$.

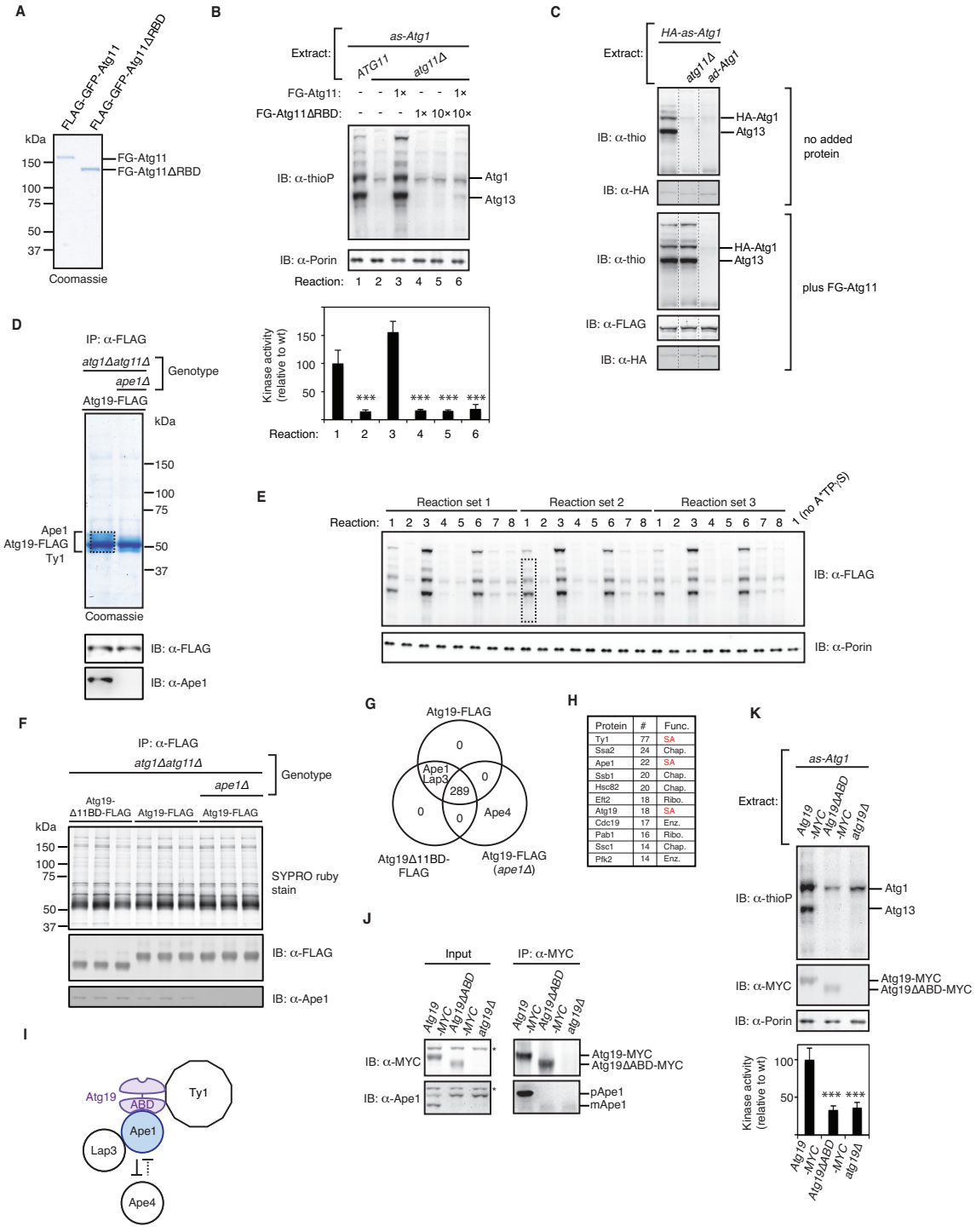

Figure A1.4 (Continued)

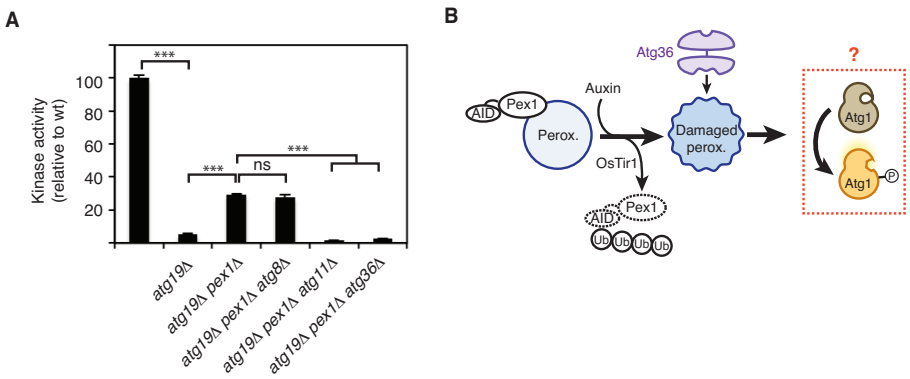

Figure A1.5. Atg1 Activation by Damaged Peroxisomes, Related to Figure 2.5.

(A) Statistical analysis of data from Figure 2.5A. Plotted data represent mean +/- standard deviation (error bars) for each reaction (n=3). p values derived from Tukey's post-test for a subset of pairwise comparisons are shown. ***$p < 0.0001$; ns, not significant.

(B) Schematic showing induction of pexophagy by engineered proteolysis of Pex1. Addition of auxin to cells that express the ubiquitin ligase OsTir1 induces degradation of Pex1-AID (auxin-inducible degron), leading to an undefined damage signal. Presence of Atg36 on damaged peroxisomes enables peroxisome degradation by autophagy, possibly by activating Atg1 (dotted red box). Perox., peroxisome; Ub, ubiquitin.

Appendix 2: Yeast Strains and Plasmids

Table A2.1. List of Yeast Strains

Strain	Genotype	Figure Reference
BY4741	*MATa ura3Δ0 his3Δ1 leu2Δ0 met15Δ0*	background, A1.1C, A1.3C
VDY630	*BY4741 atg1Δ::2×-FLAG-ATG1*	2.1B, 2.1D, 2.1F, A1.1A, A1.1B, A1.1D, A1.1E
VDY2409	*BY4741 atg1Δ::2×-FLAG-ATG1(D211A)*	2.1B, A1.1B, A1.1D, A1.1E
VDY2416	*BY4741 atg1Δ::2×-FLAG-ATG1(D211A) atg13Δ::LEU*	2.1B, A1.1B
VDY2411	*BY4741 atg1Δ::2×-FLAG-ATG1(D211A) atg11Δ::LEU*	2.1B, A1.1B
VDY2412	*BY4741 atg1Δ::2×-FLAG-ATG1(D211A) atg19Δ::LEU*	2.1B, A1.1B
VDY2413	*BY4741 atg1Δ::2×-FLAG-ATG1(D211A) ape1Δ::LEU*	2.1B, A1.1B
VDY2390	*BY4741 atg1Δ::2×-FLAG-ATG1 ape1Δ::LEU*	2.1D
VDY2387	*BY4741 atg1Δ::2×-FLAG-ATG1 atg11Δ::LEU*	2.1D, 2.1F, A1.1A
VDY2388	*BY4741 atg1Δ::2×-FLAG-ATG1 atg19Δ::LEU*	2.1D, 2.1G, A1.1H
VDY635	*BY4741 atg1Δ::2×-FLAG-ATG1 ynk1Δ::KANMX*	2.1E
VDY2249	*BY4741 atg1Δ::2×-FLAG-ATG1 ynk1Δ::KANMX atg11Δ::LEU*	2.1E
VDY2250	*BY4741 atg1Δ::2×-FLAG-ATG1 ynk1Δ::KANMX atg19Δ::URA*	2.1E
VDY2419	*BY4741 atg1Δ::2×-FLAG-ATG1 ynk1Δ::KANMX ape1Δ::URA*	2.1E

Table A2.1 (Continued)

Strain	Genotype	Figure Reference
VDY2577	*BY4741 atg1Δ::2×-FLAG-ATG1 ATG19Δ11BD-13×-MYC::HIS*	2.1G, A1.1H
VDY2585	*BY4741 atg1Δ::HIS atg17::LEU ape1Δ::mCHERRY-APE1 ATG2-3×-GFP::NAT [pRS316]*	2.2A, 2.2B, A1.2A
VDY2588	*BY4741 atg1Δ::HIS atg17::LEU ape1Δ::mCHERRY-APE1 ATG2-3×-GFP::NAT [pVD395]*	2.2A, 2.2B, A1.2A
VDY2589	*BY4741 atg1Δ::HIS atg17::LEU ape1Δ::mCHERRY-APE1 ATG2-3×-GFP::NAT [pVD546]*	2.2A, 2.2B, A1.2A
VDY2590	*BY4741 atg1Δ::HIS atg17::LEU ape1Δ::mCHERRY-APE1 ATG2-3×-GFP::NAT [pVD594]*	2.2A, 2.2B, A1.2A
VDY2552	*BY4741 atg1Δ::2×-FLAG-ATG1 ypt7Δ::URA*	2.2C, A1.2B
VDY2553	*BY4741 atg1Δ::2×-FLAG-ATG1(D211A) ypt7Δ::URA*	2.2C, A1.2B
VDY2554	*BY4741 atg1Δ::2×-FLAG-ATG1(T226A) ypt7Δ::URA*	2.2C, A1.2B
VDY2555	*BY4741 atg1Δ::2×-FLAG-ATG1 ATG11ΔRBD::NAT ypt7Δ::URA*	2.2C, A1.2B
VDY641	*BY4741 ynk1Δ::KANMX atg13Δ::ATG13-8SA*	2.3B
VDY650	*BY4741 atg1Δ::2×-FLAG-ATG1(M102G) ynk1Δ::KANMX atg13Δ::ATG13-8SA*	2.3B
VDY732	*BY4741 atg1Δ::ATG1(M102G) ynk1Δ::KANMX atg13Δ::3×-FLAG-ATG13-8SA*	2.3B
VDY639	*BY4741 atg1Δ::ATG1(M102G) ynk1Δ::KANMX atg13Δ::ATG13-8SA*	2.3B, A1.3D

Table A2.1 (Continued)

Strain	Genotype	Figure Reference
VDY949	*BY4741 ynk1Δ::KANMX atg13Δ::ATG13-8SA ATG2-3×-FLAG::NAT*	2.3C
VDY725	*BY4741 atg1Δ::ATG1(M102G) ynk1Δ::KANMX atg13Δ::ATG13-8SA ATG2-3×-FLAG::NAT*	2.3C
VDY951	*BY4741 ynk1Δ::KANMX atg13Δ::ATG13-8SA ATG9-3×-FLAG::NAT*	2.3C
VDY950	*BY4741 ynk1Δ::KANMX atg13Δ::ATG13-8SA ATG6-3×-FLAG::NAT*	2.3C
VDY727	*BY4741 atg1Δ::ATG1(M102G) ynk1Δ::KANMX atg13Δ::ATG13-8SA ATG9-3×-FLAG::NAT*	2.3C, A1.3E
VDY908	*BY4741 atg1Δ::ATG1(M102G) ynk1Δ::KANMX atg13Δ::ATG13-8SA ATG6-3×-FLAG::NAT*	2.3C, A1.3E
VDY2539	*BY4741 atg1Δ::2×-FLAG-ATG1(M102G) ynk1Δ::KANMX atg13Δ::ATG13-8SA atg8Δ::LEU*	2.3D
VDY649	*BY4741 atg1Δ::2×-FLAG-ATG1 ynk1Δ::KANMX atg13Δ::ATG13-8SA*	2.3D
VDY2147	*BY4741 atg1Δ::2×-FLAG-ATG1(M102G) ynk1Δ::KANMX atg13Δ::ATG13-8SA*	2.3D, 2.3E
VDY773	*BY4741 atg1Δ::2×-FLAG-ATG1(M102G) ynk1Δ::KANMX atg13Δ::ATG13-8SA atg11Δ::NAT*	2.3D, 2.3E
VDY1653	*BY4741 atg1Δ::2×-FLAG-ATG1(M102G) ynk1Δ::KANMX atg13Δ::ATG13-8SA atg19Δ:NAT*	2.3D, 2.3E
VDY646	*BY4741 atg1Δ::2×-FLAG-ATG1(M102G) ynk1Δ::KANMX atg13Δ::URA*	2.3D, 2.3E

Table A2.1 (Continued)

Strain	Genotype	Figure Reference
VDY666	*BY4741 atg1Δ::ATG1(M102G) ynk1Δ::KANMX atg13Δ::ATG13-8SA atg11Δ::NAT*	2.4A, 2.4B, 2.4C, 2.4D, A1.4B, A1.5B
VDY798	*BY4741 atg1Δ::ATG1(M102G) ynk1Δ::KANMX atg13Δ::ATG13-8SA atg11Δ::6×-FLAG-GFP-ATG11*	2.4A, 2.4B, 2.4C, 2.4D, A1.4B, A1.5B
VDY1794	*BY4741 atg1Δ::ATG1(M102G) ynk1Δ::KANMX atg13Δ::ATG13-8SA atg11Δ::NAT atg19Δ::URA*	2.4A, 2.4C, 2.4D, A1.5B
VDY2334	*BY4741 atg1Δ::2×-FLAG-ATG1 ynk1Δ::KANMX atg18Δ::LEU*	2.5A
VDY2529	*BY4741 atg1Δ::2×-FLAG-ATG1 ynk1Δ::KANMX atg18Δ::LEU atg19Δ::URA*	2.5A
VDY2538	*BY4741 atg1Δ::2×-FLAG-ATG1 ynk1Δ::KANMX atg18Δ::LEU atg19Δ::URA pex1Δ::NAT*	2.5A
VDY2573	*BY4741 atg1Δ::2×-FLAG-ATG1 ynk1Δ::KANMX atg18Δ::LEU atg19Δ::URA pex1Δ::NAT atg8Δ::HIS*	2.5A
VDY2574	*BY4741 atg1Δ::2×-FLAG-ATG1 ynk1Δ::KANMX atg18Δ::LEU atg19Δ::URA pex1Δ::NAT atg11Δ::HIS*	2.5A
VDY2575	*BY4741 atg1Δ::2×-FLAG-ATG1 ynk1Δ::KANMX atg18Δ::LEU atg19Δ::URA pex1Δ::NAT atg36::HIS*	2.5A
VDY2370	*BY4741 atg1Δ::2×-HA-ATG1(M102G) ynk1Δ::KANMX atg13Δ::ATG13-8SA atg19Δ::URA atg36Δ::LEU*	2.5B
VDY2379	*BY4741 atg1Δ::NAT atg19Δ::HIS leu2Δ::pGPD-OsTIR1::LEU PEX1-3×-V5-AID::KANMX*	2.5B

Table A2.1 (Continued)

Strain	Genotype	Figure Reference
VDY2380	*BY4741 atg1Δ::NAT atg19Δ::HIS leu2Δ::pGPD-OsTIR1::LEU PEX1-3×-V5-AID::KANMX atg36Δ::URA*	2.5B
VDY2540	*BY4741 atg1Δ::2×-FLAG-ATG1(T226A)*	A1.1A, A1.1E
VDY929	*BY4741 atg11Δ::6×-FLAG-GFP-ATG11*	A1.1C
VDY2584	*BY4741 atg11Δ::6×-FLAG-GFP-ATG11 atg13Δ::LEU*	A1.1C
VDY2423	*BY4741 atg1Δ::URA ynk1Δ::KANMX atg13Δ::ATG13-8SA atg11Δ::6×-FLAG-GFP-ATG11 ATG19-3×-HA::HIS*	A1.1F
VDY2425	*BY4741 atg1Δ::URA ynk1Δ::KANMX atg13Δ::ATG13-8SA atg11Δ::6×-FLAG-GFP-ATG11ΔRBD::NAT ATG19-3×-HA::HIS*	A1.1F
VDY1341	*BY4741 atg1Δ::2×-HA-ATG1(M102G) ynk1Δ::KANMX atg13Δ::ATG13-8SA atg11Δ::6×-FLAG-GFP-ATG11*	A1.1G
VDY1342	*BY4741 atg1Δ::2×-HA-ATG1(M102G) ynk1Δ::KANMX atg13Δ::ATG13-8SA atg11Δ::6×-FLAG-GFP-ATG11ΔRBD::NAT*	A1.1G
VDY1413	*BY4741 atg1Δ::2×-HA-ATG1(M102G) ynk1Δ::KANMX atg13Δ::ATG13-8SA*	A1.1G
VDY564	*BY4741 pho13Δ::MET KANMX::pTDH3-Pho8Δ1-60 atg1Δ::NAT*	A1.3B
VDY585	*BY4741 ynk1Δ::KANMX*	A1.3C
VDY619	*BY4741 atg1Δ::ATG1(M102G) ynk1Δ::KANMX atg13Δ::URA*	A1.3D
VDY611	*BY4741 atg1Δ::ATG1(M102G) ynk1Δ::KANMX*	A1.3D

Table A2.1 (Continued)

Strain	Genotype	Figure Reference
VDY1086	*BY4741 atg1Δ::ATG1(M102G) ynk1Δ::KANMX atg13Δ::ATG13-8SA ATG9-3×-FLAG::NAT atg23Δ::URA*	A1.3E
VDY989	*BY4741 atg1Δ::ATG1(M102G) ynk1Δ::KANMX atg13Δ::ATG13-8SA ATG6-3×-FLAG::NAT atg14Δ::URA*	A1.3E
VDY2420	*BY4741 atg11Δ::NAT::pTDH3-6×-FLAG-GFP-ATG11*	A1.4A
VDy2421	*BY4741 atg11Δ::NAT::pTDH3-6×-FLAG-GFP-ATG11ΔRBD::HIS*	A1.4A
VDY1413	*BY4741 atg1Δ::2×-HA-ATG1(M102G) atg13Δ::ATG13-8SA*	A1.4C
VDY2238	*BY4741 atg1Δ::2×-HA-ATG1(M102G) atg13Δ::ATG13-8SA atg11Δ::LEU*	A1.4C
VDY2218	*BY4741 atg1Δ::2×-HA-ATG1(M102G, T226A) atg13Δ::ATG13-8SA*	A1.4C
VDY2230	*BY4741 atg1Δ::URA ynk1Δ::KANMX atg13Δ::ATG13-8SA atg11Δ::HIS ATG19-3×-FLAG::NAT*	A1.4D, A1.4F
VDY2422	*BY4741 atg1Δ::URA ynk1Δ::KANMX atg13Δ::ATG13-8SA atg11Δ::HIS ATG19-3×-FLAG::NAT ape1Δ::LEU*	A1.4D, A1.4F
VDY2229	*BY4741 atg1Δ::URA ynk1Δ::KANMX atg13Δ::ATG13-8SA atg11Δ::HIS ATG19Δ11BD-3×-FLAG::NAT*	A1.4F
VDY2586	*BY4741 atg1Δ::ATG1(M102G) ynk1Δ::KANMX atg13Δ::ATG13-8SA atg11Δ::6×-FLAG-GFP-ATG11 atg19Δ::ATG19-13×-MYC::HIS*	A1.4J, A1.4K

Table A2.1 (Continued)

Strain	Genotype	Figure Reference
VDY2587	*BY4741 atg1Δ::ATG1(M102G) ynk1Δ::KANMX atg13Δ::ATG13-8SA atg11Δ::6×-FLAG-GFP-ATG11 atg19Δ::ATG19ΔABD-13×-MYC::HIS*	A1.4J, A1.4K
VDY1813	*BY4741 atg1Δ::ATG1(M102G) ynk1Δ::KANMX atg13Δ::ATG13-8SA atg11Δ::6×-FLAG-GFP-ATG11 atg19Δ::URA*	A1.4J, A1.4K
VDY2661	*BY4741 ATG36-13×MYC::HIS PEX3-3×FLAG::NAT*	3.2B, 3.3A, 3.3B
VDY2736	*BY4741 ATG36-13×MYC::HIS PEX3-3×FLAG::NAT pex19Δ::LEU*	3.2B
VDY2603	*BY4741 ATG36-13×MYC::HIS*	3.2C, 3.3A, 3.4A, 3.4B, 3.4E
VDY2725	*BY4741 ATG36-13×MYC::HIS pex5Δ::URA*	3.2C
VDY2738	*BY4741 ATG36-13×MYC::HIS PEX3-3×FLAG::NAT PEX1-3×V5-AID::KAN leu2Δ::pGPD-OsTIR1::LEU*	3.3B, 3.5B, 3.5C, 3.5D, 3.6C
VDY2753	*BY4741 ATG36-13×MYC::HIS PEX3-3×FLAG::NAT PEX1-3×V5-AID::KAN leu2Δ::pGPD-OsTIR1::LEU pex14Δ::URA*	3.3B
VDY2754	*BY4741 ATG36-13×MYC::HIS PEX3-3×FLAG::NAT PEX1-3×V5-AID::KAN leu2Δ::pGPD-OsTIR1::LEU pex15Δ::URA*	3.3B
VDY2755	*BY4741 ATG36-13×MYC::HIS PEX3-3×FLAG::NAT PEX1-3×V5-AID::KAN pex19Δ::LEU*	3.3B
VDY2604	*BY4741 ATG36-13×MYC::HIS pex1Δ::KAN*	3.4A, 3.4B, 3.4C, 3.4E, 3.6A, 3.6B
VDY2726	*BY4741 ATG36-13×MYC::HIS pex6Δ::URA*	3.4A

Table A2.1 (Continued)

Strain	Genotype	Figure Reference
VDY2730	*BY4741 ATG36-13×MYC::HIS pex15Δ::URA*	3.4A
VDY2741	*BY4741 ATG36-13×MYC::HIS atg13Δ::LEU atg11::6×FLAG-GFP-ATG11*	3.4C
VDY2742	*BY4741 ATG36-13×MYC::HIS atg13Δ::LEU atg11::6×FLAG-GFP-ATG11 pex1Δ::KAN*	3.4C
VDY2632	*BY4741 ATG36-13×MYC::HIS PEX1-3×V5-AID::KAN leu2Δ::pGPD-OsTIR1::LEU*	3.4D
VDY2633	*BY4741 ATG36-13×MYC::HIS PEX1-3×V5-AID::KAN HRR25-3×V5-AID::URA leu2Δ::pGPD-OsTIR1::LEU*	3.4D
VDY2757	*BY4741 ATG36-13×MYC::HIS PEX3-3×FLAG::NAT atg11Δ::LEU*	3.4E
VDY2758	*BY4741 ATG36-13×MYC::HIS PEX3-3×FLAG::NAT atg36Δ::LEU*	3.4E
VDY2664	*BY4741 hrr25:HRR25(I82G) pex1Δ::KAN*	3.4E
VDY2682	*BY4741 ATG36-13×MYC::HIS PEX3-3×FLAG::NAT pex8Δ::LEU*	3.5A
VDY2683	*BY4741 ATG36-13×MYC::HIS PEX3-3×FLAG::NAT pex8Δ::LEU pex1Δ::KAN*	3.5A
VDY2781	*BY4741 ATG36-13×MYC::HIS PEX3-3×FLAG::NAT PEX1-3×V5-AID::KAN leu2Δ::pGPD-OsTIR1::LEU pex15::PEX15-FIS1(TMD)::URA*	3.5B, 3.5C, 3.5D
VDY2769	*BY4741 ATG36-13×MYC::HIS pex3::OM45-cytoPEX3-3×FLAG::NAT PEX1-3×V5-AID::KAN leu2Δ::pGPD-OsTIR1::LEU*	3.5B, 3.5C, 3.5D
VDY2784	*BY4741 ATG36-13×MYC::HIS pex3::OM45-cytoPEX3-3×FLAG::NAT PEX1-3×V5-AID::KAN leu2Δ::pGPD-OsTIR1::LEU pex15::PEX15-FIS1(TMD)::URA*	3.5B, 3.5C, 3.5D

Table A2.1 (Continued)

Strain	Genotype	Figure Reference
VDY3091	*BY4741 ATG36-13×MYC::HIS pex3::OM45-cytoPEX3-3×FLAG::NAT PEX1-3×V5-AID::KAN leu2Δ::pGPD-OsTIR1::LEU pex15::PEX15-FIS1(TMD)::URA pex19Δ::HPH*	3.5B, 3.5C, 3.5D
VDY2725	*BY4741 ATG36-13×MYC::HIS pex1Δ::KAN pex5Δ::URA*	3.6A
VDY2817	*BY4741 ATG36-13×MYC::HIS PEX3-3×FLAG::NAT PEX1-3×V5-AID::KAN leu2Δ::pGPD-OsTIR1::LEU pex6Δ::URA*	3.6B
VDY3092	*BY4741 ATG36-13×MYC::HIS PEX3-3×FLAG::NAT PEX1-3×V5-AID::KAN leu2Δ::pGPD-OsTIR1::LEU pex6::PEX6(E832Q)*	3.6B

Table A2.2. List of Plasmids

Plasmids	Experiment
pRS316	2.2A,2.2B, A1.2A, A1.2B, A1.3B, 3.6B
pRS316:ATG1	A1.3B
pRS316:ATG1(M102G)	A1.3B
pRS316:2×-FLAG-ATG1	2.2A,2.2B, A1.2A, A1.2B
pRS316:2×-FLAG-ATG1(D211A)	2.2A,2.2B, A1.2A, A1.2B
pRS316:2×-FLAG-ATG1(T226A)	2.2A,2.2B, A1.2A, A1.2B
pRS316-PEX11-GFP	3.4E
pRS316-PEX1	3.6C
pRS316-PEX1(K744E)	3.6C
pRS316-PEX1(R852K)	3.6C

References

Abeliovich, H., Zhang, C., Dunn, W.A., Shokat, K.M., and Klionsky, D.J. (2003). Chemical genetic analysis of Apg1 reveals a non-kinase role in the induction of autophagy. Mol. Biol. Cell *14*, 477–490.

Allen, J.J., Li, M., Brinkworth, C.S., Paulson, J.L., Wang, D., Hübner, A., Chou, W.-H., Davis, R.J., Burlingame, A.L., Messing, R.O., et al. (2007). A semisynthetic epitope for kinase substrates. Nat. Methods *4*, 511–516.

Aoki, Y., Kanki, T., Hirota, Y., Kurihara, Y., Saigusa, T., Uchiumi, T., and Kang, D. (2011). Phosphorylation of Serine 114 on Atg32 mediates mitophagy. Mol Biol Cell *22*, 3206–3217.

Apel, A., Zentgraf, H., Buchler, M.W., and Herr, I. (2009). Autophagy-A double-edged sword in oncology. Int. J. Cancer *125*, 991–995.

Axe, E.L., Walker, S.A., Manifava, M., Chandra, P., Roderick, H.L., Habermann, A., Griffiths, G., and Ktistakis, N.T. (2008). Autophagosome formation from membrane compartments enriched in phosphatidylinositol 3-phosphate and dynamically connected to the endoplasmic reticulum. J. Cell Biol. *182*, 685–701.

Baba, M., Takeshige, K., Baba, N., and Ohsumi, Y. (1994). Ultrastructural analysis of the autophagic process in yeast: Detection of autophagosomes and their characterization. J. Cell Biol. *124*, 903–913.

Backues, S.K., Orban, D.P., Bernard, A., Singh, K., Cao, Y., and Klionsky, D.J. (2015). Atg23 and Atg27 Act at the Early Stages of Atg9 Trafficking in S. cerevisiae. Traffic *16*, 172–190.

Behrends, C., and Fulda, S. (2012). Receptor proteins in selective autophagy. Int. J. Cell Biol.

Birschmann, I., Stroobants, A.K., van den Berg, M., Schäfer, A., Rosenkranz, K., Kunau, W.-H., and Tabak, H.F. (2003). Pex15p of Saccharomyces cerevisiae provides a molecular basis for recruitment of the AAA peroxin Pex6p to peroxisomal membranes. Mol. Biol. Cell *14*, 2226–2236.

Blethrow, J., Zhang, C., Shokat, K.M., and Weiss, E.L. (2004). Design and use of analog-sensitive protein kinases. Curr. Protoc. Mol. Biol. *Chapter 18*, Unit 18.11.

Cargnello, M., Tcherkezian, J., Dorn, J.F., Huttlin, E.L., Maddox, P.S., Gygi, S.P., and Roux, P.P. (2012). Phosphorylation of the Eukaryotic Translation Initiation Factor 4E-Transporter (4E-

T) by c-Jun N-Terminal Kinase Promotes Stress-Dependent P-Body Assembly. Mol. Cell. Biol. *32*, 4572–4584.

Chen, Y., Pieuchot, L., Loh, R.A., Yang, J., Kari, T.M.A., Wong, J.Y., and Jedd, G. (2014). Hydrophobic handoff for direct delivery of peroxisome tail-anchored proteins. Nat. Commun. *5*, 5790.

Cheong, H., and Klionsky, D.J. (2008). Dual role of Atg1 in regulation of autophagy-specific PAS assembly in Saccharomyces cerevisiae. Autophagy *4*, 724–726.

Ciniawsky, S., Grimm, I., Saffian, D., Girzalsky, W., Erdmann, R., and Wendler, P. (2015). Molecular snapshots of the Pex1/6 AAA+ complex in action. Nat. Commun. *6*, 7331.

Cuervo, A.M., and Dice, J.F. (2000). Age-related decline in chaperone-mediated autophagy. J. Biol. Chem. *275*, 31505–31513.

Deosaran, E., Larsen, K.B., Hua, R., Sargent, G., Wang, Y., Kim, S., Lamark, T., Jauregui, M., Law, K., Lippincott-Schwartz, J., et al. (2013). NBR1 acts as an autophagy receptor for peroxisomes. J. Cell Sci. *126*, 939–952.

Donati, a, Cavallini, G., Paradiso, C., Vittorini, S., Pollera, M., Gori, Z., and Bergamini, E. (2001). Age-related changes in the autophagic proteolysis of rat isolated liver cells: effects of antiaging dietary restrictions. J. Gerontol. A. Biol. Sci. Med. Sci. *56*, B375–B383.

Dowdle, W.E., Nyfeler, B., Nagel, J., Elling, R.A., Liu, S., Triantafellow, E., Menon, S., Wang, Z., Honda, A., Pardee, G., et al. (2014). Selective VPS34 inhibitor blocks autophagy and uncovers a role for NCOA4 in ferritin degradation and iron homeostasis in vivo. Nat. Cell Biol. *16*, 1069–1079.

Dunn, W.A., Cregg, J.M., Kiel, J.A.K.W., van der Klei, I.J., Oku, M., Sakai, Y., Sibirny, A.A., Stasyk, O. V., and Veenhuis, M. (2005). Pexophagy: the selective autophagy of peroxisomes. Autophagy *1*, 75–83.

Eisenberg-Lerner, A., and Kimchi, A. (2009). The paradox of autophagy and its implication in cancer etiology and therapy. Apoptosis *14*, 376–391.

Fang, Y., Morrell, J.C., Jones, J.M., and Gould, S.J. (2004). PEX3 functions as a PEX19 docking factor in the import of class I peroxisomal membrane proteins. J. Cell Biol. *164*, 863–875.

Farré, J.-C., Burkenroad, A., Burnett, S.F., and Subramani, S. (2013). Phosphorylation of mitophagy and pexophagy receptors coordinates their interaction with Atg8 and Atg11. EMBO Rep. *14*, 441–449.

Farré, J.C., Manjithaya, R., Mathewson, R.D., and Subramani, S. (2008). PpAtg30 tags peroxisomes for turnover by selective autophagy. Dev. Cell *14*, 365–376.

García-Prat, L., Martínez-Vicente, M., Perdiguero, E., Ortet, L., Rodríguez-Ubreva, J., Rebollo, E., Ruiz-Bonilla, V., Gutarra, S., Ballestar, E., Serrano, A.L., et al. (2016). Autophagy maintains stemness by preventing senescence. Nature *529*, 37–42.

Gardner, B.M., Chowdhury, S., Lander, G.C., and Martin, A. (2015). The Pex1/Pex6 complex Is a heterohexameric AAA + Motor with alternating and highly coordinated subunits. J. Mol. Biol. *427*, 1375–1388.

Geisbrecht, B. V, Collins, C.S., Reuber, B.E., and Gould, S.J. (1998). Disruption of a PEX1-PEX6 interaction is the most common cause of the neurologic disorders Zellweger syndrome, neonatal adrenoleukodystrophy, and infantile Refsum disease. Proc. Natl. Acad. Sci. U. S. A. *95*, 8630–8635.

Geng, J., Baba, M., Nair, U., and Klionsky, D.J. (2008). Quantitative analysis of autophagy-related protein stoichiometry by fluorescence microscopy. J. Cell Biol. *182*, 129–140.

Giddings, T. H., O'Toole, E. T., Morphew, M., Mastronarde, D. N., McIntosh, J. R., & Winey, M. (2001). Using rapid freeze and freeze-substitution for the preparation of yeast cells for electron microscopy and three-dimensional analysis. Methods Cell Biol. *67*, 27-42.

Grimm, I., Saffian, D., Platta, H.W., and Erdmann, R. (2012). The AAA-type ATPases Pex1p and Pex6p and their role in peroxisomal matrix protein import in Saccharomyces cerevisiae. Biochim. Biophys. Acta - Mol. Cell Res. *1823*, 150–158.

Halbach, A., Rucktächel, R., Rottensteiner, H., and Erdmann, R. (2009). The N-domain of Pex22p can functionally replace the Pex3p N-domain in targeting and peroxisome formation. J. Biol. Chem. *284*, 3906–3916.

Hamasaki, M., and Yoshimori, T. (2010). Where do they come from? Insights into autophagosome formation. FEBS Lett. *584*, 1296–1301.

Hara, T., Nakamura, K., Matsui, M., Yamamoto, A., Nakahara, Y., Suzuki-Migishima, R., Yokoyama, M., Mishima, K., Saito, I., Okano, H., et al. (2006). Suppression of basal autophagy in neural cells causes neurodegenerative disease in mice. Nature *441*, 885–889.

Hara, T., Takamura, A., Kishi, C., Iemura, S.I., Natsume, T., Guan, J.L., and Mizushima, N. (2008). FIP200, a ULK-interacting protein, is required for autophagosome formation in mammalian cells. J. Cell Biol. *181*, 497–510.

Harris, H., and Rubinsztein, D.C. (2011). Control of autophagy as a therapy for neurodegenerative disease. Nat. Rev. Neurol. *8*, 108–117.

Hayashi-Nishino, M., Fujita, N., Noda, T., Yamaguchi, A., Yoshimori, T., and Yamamoto, A. (2009). A subdomain of the endoplasmic reticulum forms a cradle for autophagosome formation. Nat. Cell Biol. *11*, 1433–1437.

He, C., and Klionsky, D.J. (2009). Regulation mechanisms and signaling pathways of autophagy. Annu. Rev. Genet. *43*, 67–93.

Heikoop, J., van, den, Strijland, A., Weijers, P., Just, W., Meijer, A., and Tager, J. (1992). Turnover of peroxisomal vesicles by autophagic proteolysis in cultured fibroblasts from Zellweger patients. Eur J Cell Biol *57*, 165–171.

Hettema, E.H., Girzalsky, W., Berg, M. Van Den, Erdmann, R., Distel, B., van Den Berg, M., Erdmann, R., and Distel, B. (2000). Saccharomyces cerevisiae pex3p and pex19p are required for proper localization and stability of peroxisomal membrane proteins. EMBO J. *19*, 223–233.

Ichimura, Y., Kirisako, T., Takao, T., Satomi, Y., Shimonishi, Y., Ishihara, N., Mizushima, N., Tanida, I., Kominami, E., Ohsumi, M., et al. (2000). A ubiquitin-like system mediates protein lipidation. Nature *408*, 488–492.

Inada, T., Winstall, E., Tarun, S.Z., Yates, J.R., Schieltz, D., and Sachs, A.B. (2002). One-step affinity purification of the yeast ribosome and its associated proteins and mRNAs. RNA *8*, 948–958.

Itakura, E., and Mizushima, N. (2010). Characterization of autophagosome formation site by a hierarchical analysis of mammalian Atg proteins. Autophagy *6*, 764–776.

Itakura, E., Kishi, C., Inoue, K., and Mizushima, N. (2010). Beclin 1 Forms Two Distinct Phosphatidylinositol 3-Kinase Complexes with Mammalian Atg14 and UVRAG. Seikagaku *82*, 327–331.

Itakura, E., Kishi-Itakura, C., and Mizushima, N. (2012). The hairpin-type tail-anchored SNARE syntaxin 17 targets to autophagosomes for fusion with endosomes/lysosomes. Cell *151*, 1256–1269.

Jin, A., Lee, J.N., Kim, M.S., Kwak, S., Kim, S.-J., Song, K., Choe, S.-K., and Park, R. (2016). 2,2′-Dipyridyl Induces Pexophagy. Biochem. Biophys. Res. Commun. *469*, 941–947.

Joo, J.H., Dorsey, F.C., Joshi, A., Hennessy-Walters, K.M., Rose, K.L., McCastlain, K., Zhang, J., Iyengar, R., Jung, C.H., Suen, D.F., et al. (2011). Hsp90-Cdc37 Chaperone Complex Regulates Ulk1- and Atg13-Mediated Mitophagy. Mol. Cell *43*, 572–585.

Juhasz, G., and Neufeld, T.P. (2006). Autophagy: A forty-year search for a missing membrane source. PLoS Biol. *4*, 161–164.

Kabeya, Y. (2000). LC3, a mammalian homologue of yeast Apg8p, is localized in autophagosome membranes after processing. EMBO J. *19*, 5720–5728.

Kabeya, Y., Kamada, Y., Baba, M., Takikawa, H., Sasaki, M., and Ohsumi, Y. (2005). Atg17 functions in cooperation with Atg1 and Atg13 in yeast autophagy. Mol. Biol. Cell *16*, 2544–2553.

Kabeya, Y., Noda, N.N., Fujioka, Y., Suzuki, K., Inagaki, F., and Ohsumi, Y. (2009). Characterization of the Atg17-Atg29-Atg31 complex specifically required for starvation-induced autophagy in Saccharomyces cerevisiae. Biochem. Biophys. Res. Commun. *389*, 612–615.

Kageyama, T., Suzuki, K., and Ohsumi, Y. (2009). Lap3 is a selective target of autophagy in yeast, Saccharomyces cerevisiae. Biochem. Biophys. Res. Commun. *378*, 551–557.

Kamada, Y., Funakoshi, T., Shintani, T., Nagano, K., Ohsumi, M., and Ohsumi, Y. (2000). Tor-mediated induction of autophagy via an Apg1 protein kinase complex. J. Cell Biol. *150*, 1507–1513.

Kamada, Y., Yoshino, K., Kondo, C., Kawamata, T., Oshiro, N., Yonezawa, K., and Ohsumi, Y. (2010). Tor directly controls the Atg1 kinase complex to regulate autophagy. Mol. Cell. Biol. *30*, 1049–1058.

Kamber, R.A., Shoemaker, C.J., and Denic, V. (2015). Receptor-Bound Targets of Selective Autophagy Use a Scaffold Protein to Activate the Atg1 Kinase. Mol. Cell *59*, 372–381.

Kanki, T., Wang, K., Cao, Y., Baba, M., and Klionsky, D.J. (2009). Atg32 Is a Mitochondrial Protein that Confers Selectivity during Mitophagy. Dev. Cell *17*, 98–109.

Kenific, C.M., Thorburn, A., and Debnath, J. (2010). Autophagy and metastasis: Another double-edged sword. Curr. Opin. Cell Biol. *22*, 241–245.

Khaminets, A., Heinrich, T., Mari, M., Huebner, A.K., Akutsu, M., Grumati, P., Liebmann, L., Nietzsche, S., Katona, I., Weis, J., et al. (2015). Regulation of endoplasmic reticulum turnover by FAM134B-mediated selective autophagy. Nature *522*, 359–362.

Kijanska, M., Dohnal, I., Reiter, W., Kaspar, S., Stoffel, I., Ammerer, G., Kraft, C., and Peter, M. (2010). Activation of Atg1 kinase in autophagy by regulated phosphorylation. Autophagy *6*, 1168–1178.

Kim, J., Kamada, Y., Stromhaug, P.E., Guan, J., Hefner-Gravink, A., Baba, M., Scott, S. V., Ohsumi, Y., Dunn, W.A., and Klionsky, D.J. (2001). Cvt9/Gsa9 functions in sequestering selective cytosolic cargo destined for the vacuole. J. Cell Biol. *153*, 381–396.

Kim, P.K., Hailey, D.W., Mullen, R.T., and Lippincott-Schwartz, J. (2008). Ubiquitin signals autophagic degradation of cytosolic proteins and peroxisomes. Proc. Natl. Acad. Sci. U. S. A. *105*, 20567–20574.

Kimura, T., Takabatake, Y., Takahashi, A., and Isaka, Y. (2013). Chloroquine in cancer therapy: A double-edged sword of autophagy. Cancer Res. *73*, 3–7.

Kirkin, V., McEwan, D.G., Novak, I., and Dikic, I. (2009). A Role for Ubiquitin in Selective Autophagy. Mol. Cell *34*, 259–269.

Klionsky, D.J. (2005). The molecular machinery of autophagy: unanswered questions. J. Cell Sci. *118*, 7–18.

Komatsu, M., Waguri, S., Chiba, T., Murata, S., Iwata, J., Tanida, I., Ueno, T., Koike, M., Uchiyama, Y., Kominami, E., et al. (2006). Loss of autophagy in the central nervous system causes neurodegeneration in mice. Nature *441*, 880–884.

Kraft, C., Kijanska, M., Kalie, E., Siergiejuk, E., Lee, S.S., Semplicio, G., Stoffel, I., Brezovich, A., Verma, M., Hansmann, I., et al. (2012). Binding of the Atg1/ULK1 kinase to the ubiquitin-like protein Atg8 regulates autophagy. EMBO J. *31*, 3691–3703.

Lambkin, G.R., and Rachubinski, R.A. (2001). Yarrowia lipolytica cells mutant for the peroxisomal peroxin Pex19p contain structures resembling wild-type peroxisomes. Mol. Biol. Cell *12*, 3353–3364.

Lazarou, M., Sliter, D.A., Kane, L.A., Sarraf, S.A., Wang, C., Burman, J.L., Sideris, D.P., Fogel, A.I., and Youle, R.J. (2015). The ubiquitin kinase PINK1 recruits autophagy receptors to induce mitophagy. Nature *524*, 309–314.

Lazarus, M.B., Novotny, C.J., and Shokat, K.M. (2015). Structure of the Human Autophagy Initiating Kinase ULK1 in Complex with Potent Inhibitors. ACS Chem. Biol. *10*, 257–261.

Li, F., Chung, T., and Vierstra, R.D. (2014). AUTOPHAGY-RELATED11 plays a critical role in general autophagy- and senescence-induced mitophagy in Arabidopsis. Plant Cell *26*, 788–807.

Liang, X.H., Jackson, S., Seaman, M., Brown, K., Kempkes, B., Hibshoosh, H., and Levine, B. (1999). Induction of autophagy and inhibition of tumorigenesis by beclin 1. Nature *402*, 672–676.

Lin, L., Yang, P., Huang, X., Zhang, H., Lu, Q., and Zhang, H. (2013). The scaffold protein EPG-7 links cargo-receptor complexes with the autophagic assembly machinery. J. Cell Biol. *201*, 113–129.

Liu, L., Feng, D., Chen, G., Chen, M., Zheng, Q., Song, P., Ma, Q., Zhu, C., Wang, R., Qi, W., et al. (2012). Mitochondrial outer-membrane protein FUNDC1 mediates hypoxia-induced mitophagy in mammalian cells. Nat Cell Biol *14*, 177–185.

Lu, K., Psakhye, I., and Jentsch, S. (2014). Autophagic clearance of PolyQ proteins mediated by ubiquitin-Atg8 adaptors of the conserved CUET protein family. Cell *158*, 549–563.

Lynch-Day, M.A., and Klionsky, D.J. (2010). The Cvt pathway as a model for selective autophagy. FEBS Lett. *584*, 1359–1366.

Lynch-Day, M.A., Bhandari, D., Menon, S., Huang, J., Cai, H., Bartholomew, C.R., Brumell, J.H., Ferro-Novick, S., and Klionsky, D.J. (2010). Trs85 directs a Ypt1 GEF, TRAPPIII, to the phagophore to promote autophagy. Proc. Natl. Acad. Sci. U. S. A. *107*, 7811–7816.

Mancias, J.D., Wang, X., Gygi, S.P., Harper, J.W., and Kimmelman, A.C. (2014). Quantitative proteomics identifies NCOA4 as the cargo receptor mediating ferritinophagy. Nature *509*, 105–109.

Manivannan, S., De Boer, R., Veenhuis, M., and Van Der Klei, I.J. (2013). Lumenal peroxisomal protein aggregates are removed by concerted fission and autophagy events. Autophagy *9*, 1044–1056.

Matsumoto, G., Wada, K., Okuno, M., Kurosawa, M., and Nukina, N. (2011). Serine 403 phosphorylation of p62/SQSTM1 regulates selective autophagic clearance of ubiquitinated proteins. Mol. Cell *44*, 279–289.

Mecocci, P., MacGarvey, U., and Beal, M.F. (1994). Oxidative damage to mitochondrial DNA is increased in Alzheimer's disease. Ann. Neurol. *36*, 747–751.

Mizushima, N. (2010). The role of the Atg1/ULK1 complex in autophagy regulation. Curr. Opin. Cell Biol. *22*, 132–139.

Mizushima, N., Yamamoto, A., Hatano, M., Kobayashi, Y., Kabey, Y., Suzuki, K., Tokuhis, T., Ohsumi, Y., and Yoshimori, T. (2001). Dissection of autophagosome formation using Apg5-deficient mouse embryonic stem cells. J. Cell Biol. *152*, 657–667.

Mizushima, N., Levine, B., Cuervo, A.M., and Klionsky, D.J. (2008). Autophagy fights disease through cellular self-digestion. Nature *451*, 1069–1075.

Mochida, K., Ohsumi, Y. and Nakatogawa, H. (2014). Hrr25 phosphorylates the autophagic receptor Atg34 to promote vacuolar transport of α-mannosidase under nitrogen starvation conditions. FEBS Lett. *588*, 3862-3869.

Mochida, K., Oikawa, Y., Kimura, Y., Kirisako, H., Hirano, H., Ohsumi, Y., and Nakatogawa, H. (2015). Receptor-mediated selective autophagy degrades the endoplasmic reticulum and the nucleus. Nature *522*, 359–362.

Motley, A.M., Nuttall, J.M., and Hettema, E.H. (2012). Pex3-anchored Atg36 tags peroxisomes for degradation in Saccharomyces cerevisiae. EMBO J. *31*, 2852–2868.

Nagy, P., Kárpáti, M., Varga, Á., Pircs, K., Venkei, Z., Takáts, S., Varga, K., Érdi, B., Hegedus, K., and Juhász, G. (2014). Atg17/FIP200 localizes to perilysosomal Ref(2)P aggregates and promotes autophagy by activation of Atg1 in Drosophila. Autophagy *10*, 453–467.

Nair, U., Jotwani, A., Geng, J., Gammoh, N., Richerson, D., Yen, W.L., Griffith, J., Nag, S., Wang, K., Moss, T., et al. (2011). SNARE proteins are required for macroautophagy. Cell *146*, 290–302.

Nishimura, K., Fukagawa, T., Takisawa, H., Kakimoto, T., and Kanemaki, M. (2009). An auxin-based degron system for the rapid depletion of proteins in nonplant cells. Nat. Methods *6*, 917–922.

Nixon, R.A., Wegiel, J., Kumar, A., Yu, W.H., Peterhoff, C., Cataldo, A., and Cuervo, A.M. (2005). Extensive Involvement of Autophagy in Alzheimer Disease: An Immuno-Electron Microscopy Study. J. Neuropathol. Exp. Neurol. *64*, 113–122.

Noda, N.N., and Inagaki, F. (2015). Mechanisms of Autophagy. Annu. Rev. Biophys. *44*, 101–122.

Noda, N.N., Ohsumi, Y., and Inagaki, F. (2010a). Atg8-family interacting motif crucial for selective autophagy. FEBS Lett. *584*, 1379–1385.

Noda, T., Matsuura, A., Wada, Y., and Ohsumi, Y. (1995). Novel system for monitoring autophagy in the yeast Saccharomyces cerevisiae. Biochem. Biophys. Res. Commun. *210*, 126–132.

Noda, T., Fujita, N., and Yoshimori, T. (2009). The late stages of autophagy: how does the end begin? Cell Death Differ. *16*, 984–990.

Noda, T., Matsunaga, K., Taguchi-Atarashi, N., and Yoshimori, T. (2010b). Regulation of membrane biogenesis in autophagy via PI3P dynamics. Semin. Cell Dev. Biol. *21*, 671–676.

Nordgren, M., Francisco, T., Lismont, C., Hennebel, L., Brees, C., Wang, B., van Veldhoven, P.P., Azevedo, J.E., and Fransen, M. (2015). Export-deficient monoubiquitinated PEX5 triggers peroxisome removal in SV40 large T antigen-transformed mouse embryonic fibroblasts. Autophagy *11*, 1326–1340.

Novak, I., Kirkin, V., McEwan, D.G., Zhang, J., Wild, P., Rozenknop, A., Rogov, V., Löhr, F., Popovic, D., Occhipinti, A., et al. (2010). Nix is a selective autophagy receptor for mitochondrial clearance. EMBO Rep. *11*, 45–51.

Nuttall, J.M., Motley, A.M., and Hettema, E.H. (2014). Deficiency of the exportomer components Pex1, Pex6, and Pex15 causes enhanced pexophagy in Saccharomyces cerevisiae. Autophagy *10*, 835–845.

Obara, K., Sekito, T., and Ohsumi, Y. (2006). Assortment of phosphatidylinositol 3-kinase complexes--Atg14p directs association of complex I to the pre-autophagosomal structure in Saccharomyces cerevisiae. Mol. Biol. Cell *17*, 1527–1539.

Ochaba, J., Lukacsovich, T., Csikos, G., Zheng, S., Margulis, J., Salazar, L., Mao, K., Lau, A.L., Yeung, S.Y., Humbert, S., et al. (2014). Potential function for the Huntingtin protein as a scaffold for selective autophagy. Proc. Natl. Acad. Sci. *111*, 16889–16894.

Ogawa, M., Yoshimori, T., Suzuki, T., Sagara, H., Mizushima, N., and Sasakawa, C. (2005). Escape of intracellular Shigella from autophagy. Science *307*, 727–731.

Okamoto, K., Kondo-Okamoto, N., and Ohsumi, Y. (2009). Mitochondria-Anchored Receptor Atg32 Mediates Degradation of Mitochondria via Selective Autophagy. Dev. Cell *17*, 87–97.

Pankiv, S., Clausen, T.H., Lamark, T., Brech, A., Bruun, J.-A., Outzen, H., Øvervatn, A., Bjørkøy, G., and Johansen, T. (2007). p62/SQSTM1 binds directly to Atg8/LC3 to facilitate degradation of ubiquitinated protein aggregates by autophagy. J. Biol. Chem. *282*, 24131–24145.

Papinski, D., and Kraft, C. (2016). Regulation of Autophagy by Signaling Through the Atg1/ULK1 Complex. J. Mol. Biol. *428*, 1725–1741.

Papinski, D., Schuschnig, M., Reiter, W., Wilhelm, L., Barnes, C.A., Maiolica, A., Hansmann, I., Pfaffenwimmer, T., Kijanska, M., Stoffel, I., et al. (2014). Early Steps in Autophagy Depend on Direct Phosphorylation of Atg9 by the Atg1 Kinase. Mol. Cell *53*, 471–483.

Pfaffenwimmer, T., Reiter, W., Brach, T., Nogellova, V., Papinski, D., Schuschnig, M., Abert, C., Ammerer, G., Martens, S., and Kraft, C. (2014). Hrr25 kinase promotes selective autophagy by phosphorylating the cargo receptor Atg19. EMBO Rep. *15*, 862–870.

Platta, H.W., Grunau, S., Rosenkranz, K., Girzalsky, W., and Erdmann, R. (2005). Functional role of the AAA peroxins in dislocation of the cycling PTS1 receptor back to the cytosol. Nat Cell Biol *7*, 817–822.

Ragusa, M.J., Stanley, R.E., and Hurley, J.H. (2012). Architecture of the atg17 complex as a scaffold for autophagosome biogenesis. Cell *151*, 1501–1512.

Ravikumar, B., Vacher, C., Berger, Z., Davies, J.E., Luo, S., Oroz, L.G., Scaravilli, F., Easton, D.F., Duden, R., O'Kane, C.J., et al. (2004). Inhibition of mTOR induces autophagy and reduces toxicity of polyglutamine expansions in fly and mouse models of Huntington disease. Nat. Genet. *36*, 585–595.

Al Rawi, S., Louvet-Vallée, S., Djeddi, A., Sachse, M., Culetto, E., Hajjar, C., Boyd, L., Legouis, R., and Galy, V. (2011). Postfertilization autophagy of sperm organelles prevents paternal mitochondrial DNA transmission. Sci. (New York, NY) *334*, 1144–1147.

Rogov, V., Dötsch, V., Johansen, T., and Kirkin, V. (2014). Interactions between Autophagy Receptors and Ubiquitin-like Proteins Form the Molecular Basis for Selective Autophagy. Mol. Cell *53*, 167–178.

Rui, Y.-N., Xu, Z., Patel, B., Chen, Z., Chen, D., Tito, A., David, G., Sun, Y., Stimming, E.F., Bellen, H.J., et al. (2015). Huntingtin functions as a scaffold for selective macroautophagy. Nat. Cell Biol. *17*.

Russell, R.C., Tian, Y., Yuan, H., Park, H.W., Chang, Y.-Y., Kim, J., Kim, H., Neufeld, T.P., Dillin, A., and Guan, K.-L. (2013). ULK1 induces autophagy by phosphorylating Beclin-1 and activating VPS34 lipid kinase. Nat. Cell Biol. *15*, 741–750.

Sato, M., and Sato, K. (2011). Degradation of Paternal Mitochondria by Fertilization-Triggered Autophagy in C. elegans Embryos. Science (80-.). *334*, 1141–1144.

Sawa-Makarska, J., Abert, C., Romanov, J., Zens, B., Ibiricu, I., and Martens, S. (2014). Cargo binding to Atg19 unmasks additional Atg8 binding sites to mediate membrane-cargo apposition during selective autophagy. Nat. Cell Biol. *16*, 425–433.

Schreiber, A., and Peter, M. (2014). Substrate recognition in selective autophagy and the ubiquitin-proteasome system. Biochim. Biophys. Acta - Mol. Cell Res. *1843*, 163–181.

Scott, S. V., Baba, M., Ohsumi, Y., and Klionsky, D.J. (1997). Aminopeptidase I is targeted to the vacuole by a nonclassical vesicular mechanism. J. Cell Biol. *138*, 37–44.

Scott, S. V., Guan, J., Hutchins, M.U., Kim, J., and Klionsky, D.J. (2001). Cvt19 is a receptor for the cytoplasm-to-vacuole targeting pathway. Mol. Cell *7*, 1131–1141.

Shimura, H., Hattori, N., Kubo, S.I., Mizuno, Y., Asakawa, S., Minoshima, S., Shimizu, N., Iwai, K., Chiba, T., Tanaka, K., et al. (2000). Familial Parkinson disease gene product, parkin, is a ubiquitin-protein ligase. Nat. Genet. *25*, 302–305.

Shintani, T., and Klionsky, D.J. (2004). Cargo proteins facilitate the formation of transport vesicles in the cytoplasm to vacuole targeting pathway. J. Biol. Chem. *279*, 29889–29894.

Shintani, T., Huang, W.P., Stromhaug, P.E., and Klionsky, D.J. (2002). Mechanism of cargo selection in the cytoplasm to vacuole targeting pathway. Dev. Cell *3*, 825–837.

Shoji-Kawata, S., Sumpter, R., Leveno, M., Campbell, G.R., Zou, Z., Kinch, L., Wilkins, A.D., Sun, Q., Pallauf, K., MacDuff, D., et al. (2013). Identification of a candidate therapeutic autophagy-inducing peptide. Nature *494*, 201–206.

Singh, R., Kaushik, S., Wang, Y., Xiang, Y., Novak, I., Komatsu, M., Tanaka, K., Cuervo, A.M., and Czaja, M.J. (2009). Autophagy regulates lipid metabolism. Nature *458*, 1131–1135.

Spilman, P., Podlutskaya, N., Hart, M.J., Debnath, J., Gorostiza, O., Bredesen, D., Richardson, A., Strong, R., and Galvan, V. (2010). Inhibition of mTOR by rapamycin abolishes cognitive deficits and reduces amyloid-?? levels in a mouse model of alzheimer's disease. PLoS One *5*.

Stephan, J.S., Yeh, Y.-Y., Ramachandran, V., Deminoff, S.J., and Herman, P.K. (2009). The Tor and PKA signaling pathways independently target the Atg1/Atg13 protein kinase complex to control autophagy. Proc. Natl. Acad. Sci. U. S. A. *106*, 17049–17054.

Stolz, A., Ernst, A., and Dikic, I. (2014). Cargo recognition and trafficking in selective autophagy. Nat Cell Biol *16*, 495–501.

Subramani, S. (1996). Protein translocation into peroxisomes. J. Biol. Chem. *271*, 32483–32486.

Suzuki, K., Kirisako, T., Kamada, Y., Mizushima, N., Noda, T., and Ohsumi, Y. (2001). The pre-autophagosomal structure organized by concerted functions of APG genes is essential for autophagosome formation. EMBO J. *20*, 5971–5981.

Suzuki, K., Kubota, Y., Sekito, T., and Ohsumi, Y. (2007). Hierarchy of Atg proteins in pre-autophagosomal structure organization. Genes to Cells *12*, 209–218.

Suzuki, K., Morimoto, M., Kondo, C., and Ohsumi, Y. (2011). Selective Autophagy Regulates Insertional Mutagenesis by the Ty1 Retrotransposon in Saccharomyces cerevisiae. Dev. Cell *21*, 358–365.

Suzuki, K., Akioka, M., Kondo-Kakuta, C., Yamamoto, H., and Ohsumi, Y. (2013). Fine mapping of autophagy-related proteins during autophagosome formation in Saccharomyces cerevisiae. J. Cell Sci. *126*, 2534–2544.

Takáts, S., Pircs, K., Nagy, P., Varga, Á., Kárpáti, M., Hegedűs, K., Kramer, H., Kovács, A.L., Sass, M., and Juhász, G. (2014). Interaction of the HOPS complex with Syntaxin 17 mediates autophagosome clearance in Drosophila. Mol. Biol. Cell *25*, 1338–1354.

Tamura, S., Yasutake, S., Matsumoto, N., and Fujiki, Y. (2006). Dynamic and functional assembly of the AAA peroxins, Pex1p and Pex6p, and their membrane receptor Pex26p. J. Biol. Chem. *281*, 27693–27704.

Tanaka, C., Tan, L.J., Mochida, K., Kirisako, H., Koizumi, M., Asai, E., Sakoh-Nakatogawa, M., Ohsumi, Y., and Nakatogawa, H. (2014). Hrr25 triggers selective autophagy-related pathways by phosphorylating receptor proteins. J. Cell Biol. *207*, 91–105.

Tooze, S.A. (2013). Current views on the source of the autophagosome membrane. Essays Biochem *55*, 29–38.

Walter, K.M., Schonenberger, M.J., Trotzmuller, M., Horn, M., Elsasser, H.P., Moser, A.B., Lucas, M.S., Schwarz, T., Gerber, P. a., Faust, P.L., et al. (2014). Hif-2a Promotes degradation of mammalian peroxisomes by selective autophagy. Cell Metab. *20*, 882–897.

Watanabe, Yasunori, Watanabe, Y., Noda, N. N., Kumeta, H., Suzuki, K., Ohsumi, Y., & Inagaki, F. (2010). Selective Transport of α-Mannosidase by Autophagic Pathways Structural Basis for Cargo Recognition by Atg19 And Atg34. J. Biol. Chem. *285*, 30026-30033.

Weekes, M.P., Tomasec, P., Huttlin, E.L., Fielding, C.A., Nusinow, D., Stanton, R.J., Wang, E.C.Y., Aicheler, R., Murrell, I., Wilkinson, G.W.G., et al. (2014). Quantitative temporal viromics: An approach to investigate host-pathogen interaction. Cell *157*, 1460–1472.

White, E., and DiPaola, R.S. (2009). The double-edged sword of autophagy modulation in cancer. Clin. Cancer Res. *15*, 5308–5316.

Wickner, S., Maurizi, M.R., and Gottesman, S. (1999). Posttranslational quality control: folding, refolding, and degrading proteins. Sci. (New York, NY) *286*, 1888–1893.

Wild, P., Farhan, H., McEwan, D.G., Wagner, S., Rogov, V. V, Brady, N.R., Richter, B., Korac, J., Waidmann, O., Choudhary, C., et al. (2011). Phosphorylation of the autophagy receptor optineurin restricts Salmonella growth. Science *333*, 228–233.

Wong, E., and Cuervo, A.M. (2010). Autophagy gone awry in neurodegenerative diseases. Nat. Neurosci. *13*, 805–811.

Yamamoto, H., Kakuta, S., Watanabe, T.M., Kitamura, A., Sekito, T., Kondo-Kakuta, C., Ichikawa, R., Kinjo, M., and Ohsumi, Y. (2012). Atg9 vesicles are an important membrane source during early steps of autophagosome formation. J. Cell Biol. *198*, 219–233.

Yamashita, S. ichi, Abe, K., Tatemichi, Y., and Fujiki, Y. (2014). The membrane peroxin PEX3 induces peroxisome-ubiquitination-linked pexophagy. Autophagy *10*, 1549–1564.

Yeh, Y.Y., Wrasman, K., and Herman, P.K. (2010). Autophosphorylation within the Atg1 activation loop is required for both kinase activity and the induction of autophagy in Saccharomyces cerevisiae. Genetics *185*, 871–882.

Yorimitsu, T., and Klionsky, D.J. (2005). Atg11 links cargo to the vesicle-forming machinery in the cytoplasm to vacuole targeting pathway. Mol. Biol. Cell *16*, 1593–1605.

Yuga, M., Gomi, K., Klionsky, D.J., and Shintani, T. (2011). Aspartyl aminopeptidase is imported from the cytoplasm to the vacuole by selective autophagy in Saccharomyces cerevisiae. J. Biol. Chem. *286*, 13704–13713.

Zhang, J., Tripathi, D.N., Jing, J., Alexander, A., Kim, J., Powell, R.T., Dere, R., Tait-Mulder, J., Lee, J.-H., Paull, T.T., et al. (2015). ATM functions at the peroxisome to induce pexophagy in response to ROS. Nat Cell Biol *17*, 1259–1269.

Zhang, Y., Yan, L., Zhou, Z., Yang, P., Tian, E., Zhang, K., Zhao, Y., Li, Z., Song, B., Han, J., et al. (2009). SEPA-1 Mediates the Specific Recognition and Degradation of P Granule Components by Autophagy in C. elegans. Cell *136*, 308–321.